博士論文

Theory of quantum dynamical properties of molecules
(分子の量子動力学的性質に関する理論的研究)

Department of Basic Science,

Graduate School of Arts and Sciences,
The University of Tokyo

Shin-ichi Koda
甲田 信一

Contents

Chapter 1

General introduction

1.1 Dynamical properties of molecules as a subject of theoretical chemistry

Since the establishment of quantum mechanics, theoretical treatments of chemistry have been rapidly developed. For example, quantum chemistry gives practical ways to solve the Schrödinger equation approximately. One of the most basic approximation among them is the Born-Oppenheimer approximation. Under this approximation [1], position of nuclei in the Schrödinger equation is fixed at a given configuration and the equation is to be solved only with respect to the degrees of freedom of electrons. In the picture under the Born-Oppenheimer approximation, nuclei are considered to be in a force field created by electrons. Therefore, a local minimum of the potential energy of the force field can be regarded as a stable structure of the molecule under consideration. Finding stable structures of given molecules and their energies has been a main problem in quantum chemistry. Even now, seeking to investigate lager systems more precisely, this stream still continues. Although theoretical studies about the static properties of molecules mentioned above is of great importance, it is difficult for these studies to describe dynamical properties of the system. Considering that many significant phenomena in chemistry including chemical reactions and transfer of charge and energy is dynamical, it is also necessary to develop theoretical frameworks for studies on dynamical properties of molecules.

Targets of theoretical chemistry therefore have expanded from the static properties of molecules to dynamical properties. One of the theoretical methods that has been developed most is molecular dynamics (MD) simulations. Both MD simulation with *ab initio* potential energy and that with empirical potential energy have been carried out intensively in many areas ranging from elementary processes in basic chemical reactions to complex reactions in biochemistry, medial chemistry and other chemistries. However, there are certain realms where MD simulations cannot work well. For example, it is

difficult for MD simulations to estimate quantum effects of nuclei because MD simulations are based on the assumption that nuclei obey classical mechanics. This may cause problems in the case where light nuclei like protons are involved. Another example is the dynamics where many electronic states are involved. This is because, in general, MD simulations are based on one potential energy surface of an electronic state and cannot treat electronic transition well.

This thesis therefore aims at developing theoretical methods for these realms and shows some examples of their applications. Firstly, this thesis treats semiclassical dynamics as one of the methods to include quantum effects into MD simulations. Secondly, excitation energy transfer in light-harvesting dendrimers is studied as an example of the dynamical process where many electronic excited states are involved. Next section briefly reviews backgrounds of these subjects and presents purposes of this thesis in these subjects.

1.2   Semiclassical dynamics

As is mentioned above, dynamics of nuclei has been treated classical mechanically in most MD simulations and quantum nature of nuclei has been ignored. This is because computational cost of precise quantum dynamics of nuclei is impossibly high, which exponentially increases with respect to the number of degree of freedom. Hence, approximation methods are required to study quantum dynamics of nuclei. Semiclassical dynamics, one of the subjects in this thesis, is an approximation method for quantum dynamics of nuclei. In semiclassical dynamics, various quantum quantities are approximated by physical quantities of classical mechanics (such approximation is called semiclassical approximation). Because classical dynamics is not a dynamics of distribution functions like wave functions but a dynamics of mass points, semiclassical approximation greatly reduces the computational cost. In addition, because this approximation is valid when mass of objects consisting of the system is not very light, semiclassical dynamics is usually applied to dynamics of nuclei to estimate nuclei's quantum effects.

This thesis particularly studies semiclassically approximated propagators (semiclassical propagators) [2, 3]. A propagator of a given quantum system is the operator that maps a wave function at time 0 to the wave function at time t and is usually denoted as $e^{-it\hat{H}/\hbar}$ or $\hat{K}(t)$. Semiclassical propagators therefore propagate wave functions using only classical mechanics. Until now, many types of semiclassical propagator have been proposed [4–6]. Unfortunately, these semiclassical propagators have been derived originally in independent and complicated manners. As a result, relation among these semiclassical propagators has been not clear for several decades. We therefore aims at understanding these semiclassical propagators in a unified way.

For this purpose, we show that various semiclassical propagators can be derived systematically based on a normal quantum mechanical method. We firstly generalize the coherent-state path integral, which is one of the representations of quantum dynamics. For the generalization, we add arbitrary parameters to the path integral. After presenting a propagator by the generalized path integral and approximately evaluating the integral by the steepest descent method, we show that various semiclassical propagators can be derived systematically by choosing the arbitrary parameters properly. Owing to the unified derivation, a common theoretical ground among these semiclassical propagators is established.

1.3 Excitation energy transfer in light-harvesting dendrimers

This thesis also discusses excitation energy transfer (EET) in light-harvesting dendrimers [7, 8]. Dendrimers are molecules with repetitively branched structure. This unique structure gives dendrimers various functions. For example, light-harvesting dendrimers (see Fig. 1.1), in which many pigment molecules are embedded in their peripheral parts, absorb photons of light at the peripheral parts and efficiently transfer it to their core molecules, which are bonded to the root of the light-harvesting dendrimers. This function is called antenna effect and is expected to be applied in artificial photosynthetic systems and solar cells. One of the curious properties of EET in light-harvesting dendrimers is that the yield of the EET highly depends on their geometric structure, or morphology, which has been shown experimentally [9–11]. This suggests that the morphology of dendrimers plays certain roles for the function of dendrimers; in other words, there may be a mechanism enhancing EET originated from the morphology. This thesis therefore focuses on the relation between morphology and function of light-harvesting dendrimers.

We here review the general mechanism of EET in a molecular aggregate [12]. The EET in a molecular aggregate is generally explained as a relaxation process of excitation energy among many electronic excited states. While each pigment molecule consisting of a molecular aggregate has its own electronic excited states, the excited states of these pigment molecules interact each other in the aggregate and form many electronic excited states of whole of the aggregate. Excitation energy absorbed by the aggregate is transferred from excited states of higher energies to those of lower energies in a relaxation process. In this process, excitation energy is spatially transferred from the region where the former states locate to the region where the latter states locate. Therefore, in order to realize high yield of EET, there should be the gradient of energy descending toward the destination of the EET. If there is no or weak energy gradient, it takes extra times
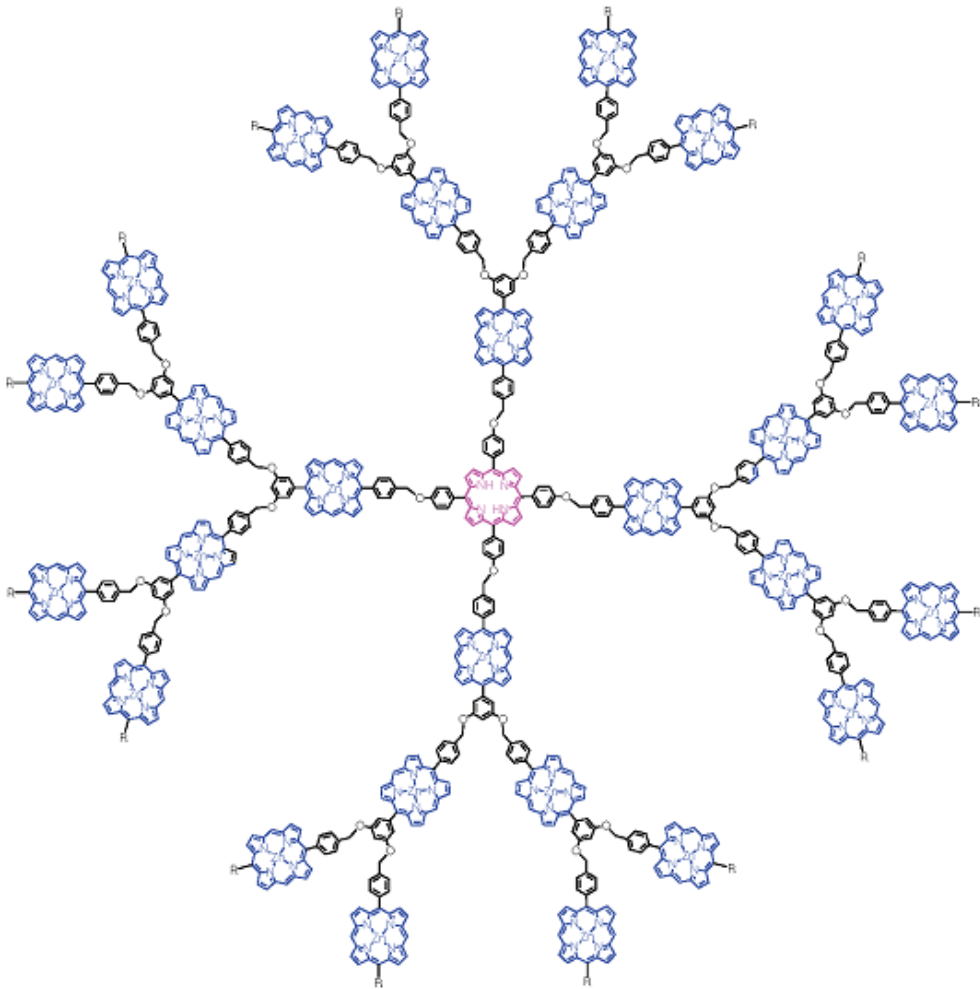
Figure 1.1: An example of light-harvesting dendrimers. From Ref. [7].

to reach the destination while excitation energy wanders and, as a result, electronic excitation may be quenched before EET is finished.

Taking the background reviewed above in to consideration, this thesis aims at seeking a possibility that the repetitively branched morphology of light-harvesting dendrimers enhances the EET in them by creating the energy gradient descending toward their core parts.

In this thesis, we use a Frenkel exciton Hamiltonian [12] to investigate the spatial locations and energy levels of electronic excited states in light-harvesting dendrimers. The Frenkel exciton Hamiltonian is a simple model Hamiltonian for EET and is represented as

$$\hat{H} = \sum_i E_i |i\rangle\langle i| + \sum_{i,j \ (i \neq j)} J_{ij} |i\rangle\langle j| \ . \tag{1.1}$$

$|i\rangle$ is a quantum state where only the ith pigment molecule in the aggregate is excited and rest of the pigment molecules are at their own ground state, E_i is energy gap between the ground state and the excited state of the ith molecule and J_{ij} is interaction energy between the ith and the jth molecules. By setting these parameters properly and diagonalizing the Hamiltonian, the spatial locations and energy levels of excited states can be roughly estimated. In general, these properties of excited states highly depend on the connectivity of the network linked by non-zero (or significantly large) J_{ij}. The relation between the connectivity and the properties of excited states may provide some insights on the role of morphology on EET in a given molecular aggregate.

In this thesis, we define a Frenkel exciton Hamiltonian as shown in Fig. 1.2. Nodes in Fig. 1.2 correspond to the excited states of pigment molecules $|i\rangle$ and edges present non-zero interaction between two pigment molecules J_{ij}. In order to focus only on the morphology of the network, we set all E_i to be identical. Note that the core molecule, which is usually bonded to the root of the dendrimer, is excluded from the model system. The core molecule usually has lower energy level and therefore collect excitation energy in the relaxation process. However, because the purpose of this thesis is clarifying whether the repetitive branched structure of dendrimers itself has the ability to collect excitation energy, we exclude the core molecule so that we can distinguish the ability originated from the structure, form the ability of the core molecule.

Although the energy landscape can be obtained through the diagonalization of the model Hamiltonian, it is still difficult to describe how the morphology forms the energy landscape because the shape of the repetitively branched structure is rather complicated. Hence, for the later analysis about the role of the morphology, the Hamiltonian should be simplified as much as possible. Fortunately, in the studies on dendrimers (in other areas) [13–15], it has been shown that a model system defined on a dendritic network like Fig. 1.2 can be equivalently transformed into a set of one-dimensional systems as shown in Fig. 1.3. We refer to such equivalent transformation as linear chain (LC) decomposition.
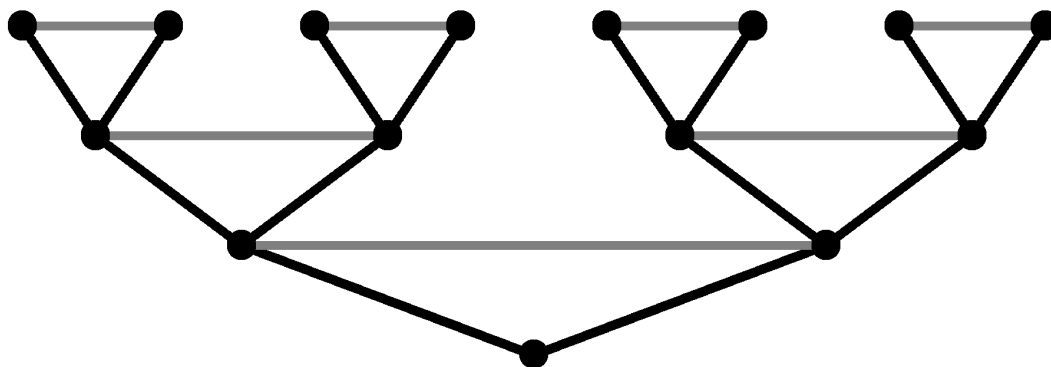
Figure 1.2: The network of interactions in the model Hamiltonian.
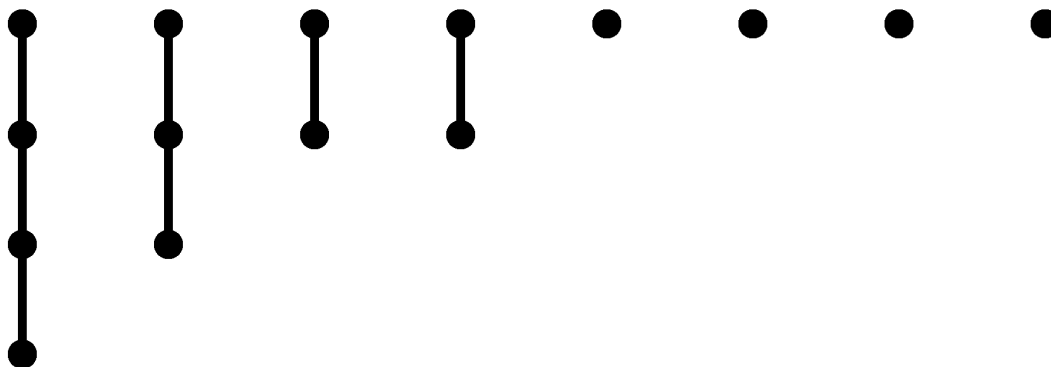
Figure 1.3: A set of simple networks, which visualizes the Hamiltonian that is equivalent to the original Hamiltonian.

LC decomposition means that the motion in a dendritic system is equivalent to just a superposition of several one-dimensional modes of motion. In the literatures [13–15], properties of their dendritic systems are well explained using the simple picture of LC decomposition. In this thesis, we also apply the LC decomposition to the analysis of the energy landscape originated from the morphology of light-harvesting dendrimers.

The problem of the LC decomposition, however, is that conditions for LC decomposability of a given dendritic system has not been known. The literatures introduced above [13–15] use a special model system for their studies and they do not give general

6

conditions for LC decomposability. In the present thesis, we therefore seek the general conditions. We show in Chapter 3 that LC decomposition is feasible when the network and the Hamiltonian on it have certain symmetry (details of the symmetry are shown in Chapter 3). Even though the repetitive brunchings make the morphology of dendrimers complicated, they also give the dendrimers rich symmetry on the other hand. Owing to this rich symmetry, the dendritic systems becomes capable of the simplification.

In Chapter 4, we next investigate in detail the role of morphology of dendrimers on EET with the model Hamiltonian introduced above and show a possibility that the symmetry of dendrimers enhances EET by creating unidirectional energy gradient descending from the peripheral part to the inner part of each light-harvesting dendrimer. To do so, we first numerically show that excited states of higher energies are located at the peripheral part and those of lower energies are located at the inner part. To our knowledge, this work is the first theoretical study showing the possibility that light-harvesting dendrimers can collect excitation energy at their inner parts even if they do not have core molecules. Because we set the model Hamiltonian so that one can focus only on the role of the morphology of interaction energy's network as mentioned above, this result of numerical calculation suggests that the ability to collect excitation is originated from the dendritic morphology of the network.

We also investigate the reason why the ability to collect excitation arise. In Chapter 4, we propose two mechanisms that create the energy gradient based on the simple picture of LC decomposition. We show that energy gradient is formed both in each linear chain (one-dimensional system) and among these linear chains. For example, the latter is explained as follows: the inter-chain energy gradient is formed because the longer one-dimensional systems are, the lower energy levels they have and the more inner part they can spatially reach.

To sum up, through the discussion in Part II, it is found that the simple one-dimensional modes are formed owing to the symmetry of light-harvesting dendrimers and the one-dimensional modes with various length create the energy gradient descending toward the inner part. This is the role of morphology on EET in light-harvesting dendrimers found in this thesis. The EET is possibly enhanced by this symmetry-origin energy gradient.

1.4　Organization of this thesis

This thesis is organized as follows. This thesis is divided into two part. Part I is for the subject on the semiclassical dynamics and Part II is devoted to the subject on the EET in light-harvesting dendrimers. Chapter 2 in Part I presents the systematic derivation of various semiclassical propagators. In Part II, Chapter 3 shows the general

theory to simplify linear operators defined on dendritic networks and Chapter 4 discusses the relation between morphology and function with respect to EET in light-harvesting dendrimers. In Chapter 4, two mechanisms that create the energy gradient are proposed base on the theory in Chapter 3. Finally, Chapter 5 concludes this thesis. Each chapter is written so that it can be read independently.

Reference

[1] M. Born and R. Oppenheimer, Ann. Phys. **389**, 457 (1927).

[2] W. H. Miller, J. Phys. Chem. A **105**, 2942 (2001).

[3] K. G. Kay, Annu. Rev. Phys. Chem. **56**, 255 (2005).

[4] J. V. Vleck, Proc. Natl. Acad. Sci. **14**, 178 (1928).

[5] E. J. Heller, J. Chem. Phys. **62**, 1544 (1975).

[6] M. F. Herman and E. Kluk, Chem. Phys. **91**, 27 (1984).

[7] W.-S. Li and T. Aida, Chem. Rev. **109**, 6047 (2009).

[8] D. Astruc, E. Boisselier, and C. Ornelas, Chem. Rev. **110**, 1857 (2010).

[9] C. Devadoss, P. Bharathi, and J. S. Moore, J. Am. Chem. Soc. **118**, 9635 (1996).

[10] D.-L. Jiang and T. Aida, J. Am. Chem. Soc. **120**, 10895 (1998).

[11] M. Kimura, T. Shiba, T. Muto, K. Hanabusa, and H. Shirai, Macromolecules **32**, 8237 (1999).

[12] L. Valkunas, D. Abramavicius, and T. Mančal, *Molecular Excitation Dynamics and Relaxation*, Wiley, Weinheim, 2013.

[13] C. Cai and Z. Y. Chen, Macromolecules **30**, 5104 (1997).

[14] M. Galiceanu and A. Blumen, J. Chem. Phys. **127**, 134904 (2007).

[15] M. Galiceanu, J. Phys. A Math. Theor. **43**, 305002 (2010).

Part I

Theory for time propagation in quantum systems

Chapter 2

A generalization of the coherent state path integrals and systematic derivation of semiclassical propagators

Abstract

The coherent path integral is generalized such that the identity operator represented in a complete (actually overcomplete) set of the coherent states with the "time-variable" exponents are inserted in between two consecutive short-time propagators. Since such a complete set of any given exponent can constitute the identity operator, the exponent may be varied from time to time without loss of generality as long as it is set common to all the Gaussians. However, a finite truncation of the coherent state expansion should result in different values of the propagator depending on the choice of the exponents. Furthermore, approximation methodology to treat with the exact propagator can also depend on this choice, and thereby many different semiclassical propagators may emerge from these combinations. Indeed, we show that the well-known semiclassical propagators such as those of Van Vleck, Herman-Kluk, Heller's thawed Gaussian, and many more can be derived in a systematic manner, which enables to comprehend these semiclassical propagators from a unified point of view. We are particularly interested in a generalized form of the Herman-Kluk propagator, since the relative accuracy of this propagator has been well established by Kay, and since, nevertheless, its derivation was not necessarily clear. Thus generalized Herman-Kluk propagator replaces the classical Hamiltonian with a Gaussian averaged quantum Hamiltonian, generating non-Newtonian trajectories. We perform a numerical test to assess the quality of such a family of the generalized Herman-Kluk propagators, and find the original Herman-Kluk

gives an accurate result. The reason why this has come about is also discussed.

2.1   Introduction

Semiclassical mechanics has been one of the major methods to study the dynamics of systems containing heavy elements like nuclei in a molecule. It is known to be quite useful not only as a numerically efficient method but as a theoretical means to analyze the profound relationship between quantum and classical mechanics. There are many traditional pathways to correlate quantum theory to classical counterpart such as those through Hamilton-Jacobi equation (WKB), phase space mechanics (Wigner distribution function), and so on. Among the wide variety of semiclassical methodologies, the semiclassical kernel has played one of the central roles, since it works on the quantum-mechanical propagator rather than the time-propagation of the individual wavefunctions. The so-called Van-Vleck determinant figured out in 1928 [1] had set a theoretical foundation of such notion before the systematic approximation to the Feynman kernel started much later [2]. The Feynman kernel is characterized parametrically with the initial and final positions (either in configuration space, phase-space, or mixed spaces), and consequently its semiclassical approximation is reduced to a cumbersome root-search procedure seeking for classical paths to tie the two such boundary positions. Also, the primitive semiclassical approximation is suffered from divergence at every caustic, at which the relevant Van-Vleck determinant gives zero.

A major remedy to these difficulties has been made by the so-called initial value representation to the semiclassical propagator, which is now commonly terms as SC-IVR [3–8]. SC-IVRs are represented with a classical trajectory starting from a given initial position and initial momentum, and therefore the root search is avoided. At the same time, the divergence at caustics is all converted to "zero".

Another major development in semiclassical representation of a wavefunction has been achieved by an extensive introduction of the Gaussian function, which has particular advantage in visualization and numerical calculations of the transition probabilities, since it gives a continuous distribution of the amplitudes rather than a set of points and yet is well localized in both the position and momentum spaces mimicking a "classical particle" in quantum mechanics. Heller proposed fascinating methods which propagate the coherent states including the thawed Gaussian approximation (having a variable Gaussian exponent in time) [4] and the frozen Gaussian approximation (FGA) (of fixed Gaussian exponent) [5]. Herman and Kluk attempted to reformulate the frozen Gaussian approximation in terms of the VV propagator [7], which is now known as Herman-Kluk (HK) propagator. In his series of extensive studies on semiclassical mechanics [10, 11] [9], Kay compared various versions of SC-IVR proposed by that time

14

and numerically found that the HK propagator gave the most accurate results among the competitors. Since then, the HK propagator has established itself as one of the most popular semiclassical methods [12–16],

However, the derivation of the HK propagator is still subject to more rigorous argument and verification even to date [17–26]. The original derivation was made as follows [7]. Herman and Kluk obtained the HK propagator by "sandwiching" the VV propagator in between two identity operators, which are in turn represented in terms of the complete (actually over-complete) set of coherent states. Then they applied the stationary phase approximation in a rather artificial manner. Besides, Kay derived a more general HK propagator, allowing that the coherent states at the initial and final time may have different Gaussian exponents from each other [9]. Since these ways of derivation resorted to the VV propagator, a false impression that the HK propagator should serve as an approximation to the VV propagator itself and consequently must be worse in its accuracy have emerged without a theoretical evidence. Then, Grossmann and Xavier attempted to derive the HK propagator from the coherent state path integral without use of the VV propagator [17]. Unfortunately, however, Baranger et al. saw some mathematical flaws in the derivation in ref. [17] and showed that the correct mathematical procedure should result in a representation like a propagator for the thawed Gaussian rather than the frozen Gaussian [18, 19]. They were also led to a conclusion that the HK propagator is not a semiclassical propagator in a canonical sense that $\hbar \to 0$ in quantum mechanics. Grossmann and Herman claimed in reply that although no mathematical flaw was made in their derivation, some misconception might have been conducted with respect to the theoretical structure of the HK propagator. Meanwhile, Hu et al. [21], Miller [22,23], Child and Shalashilin [24] and Kay [25] derived the HK propagator independently, but any one of them does not seem to be sufficiently general nor simple enough.

In this chapter, we also apply the coherent path integrals to study semiclassical propagators with one step further ahead. We here relax a set of the coherent states, which is to be inserted as an identity operator in between two consecutive short-time propagators, such that the individual sets (or the identity operators) may have different Gaussian exponents from time to tome. Since the complete (actually overcomplete) set of the coherent states of any exponents can constitute an identity operator, they may vary from time to time without loss of generality. But, of course, computational results with use of a finite truncation of the coherent state expansion should depend on the choice of the exponents. Furthermore, approximation methodology to treat with the exact propagator can give different functional forms depend on the choice of the exponent, and thereby many different semiclassical propagators may emerge from these combinations. Indeed, on the basis of the general representation obtained, we will show

in a systematic manner that the well-known semiclassical propagators such as those of Van Vleck, Herman-Kluk, Heller's thawed Gaussian, and many more can be derived and that they can be comprehended from a unified point of view.

Among others, we are particularly interested in a generalized form of the Herman-Kluk propagator, since the relative accuracy of this propagator has been well established by Kay, and since, nevertheless, its derivation was not necessarily clear before. The generalized Herman-Kluk propagator we derive replaces the classical Hamiltonian with a Gaussian averaged quantum Hamiltonian. In contrast to the Heller frozen Gaussian approximation, in which the Gaussian averaged Hamiltonian appears in the phase factor to integrate the action integral along a classical trajectory [5], our generalized Herman-Kluk propagator requires to generate non-Newtonian paths in terms of the Gaussian averaged Hamiltonian. Besides, we perform a numerical test for such a family of the generalized Herman-Kluk propagators, finding that the original Herman-Kluk version gives an accurate result. We study from the unified point of view why the HK propagator is so good.

This chapter is organized as follows. In Sec. 2.2, we derive a general expression of semiclassical propagator. Various SC-IVRs are derived in Sec. 2.3 as special cases of the propagator derived in Sec. 2.2. Sec. 2.4 is devoted to numerical comparison among the generalized HK propagators along with qualitative discussion for the results. Sec. 2.5 concludes this chapter with some remarks.

2.2 Generalization of the coherent state path integrals

In this section, we derive a general expression of the initial value representation of the semiclassical propagator by (i) representing the quantum mechanical propagator in terms the coherent state path integral (CSPI) and (ii) approximating it with the steepest descent method (SDM). We will mostly follow the theoretical development achieved by Baranger et al. [18] except for the following two important aspects. One is that we allow the Gaussian exponents of the coherent states to arbitrarily change from time to time. This procedure does not make any difference if a complete set of the coherent states is used, but a numerous semiclassical versions of the kernel can emerge from different choices of the exponent. The other deviation from the Baranger formalism is a different choice of the integration variables in the steepest descent approximation applied to the CSPI.

2.2.1 Coherent state path integrals with tunable Gaussian width

We first represent the propagator in terms of coherent path integrals (CSPI) with the standard definition of the coherent state $|\mathbf{\Gamma}, \mathbf{q}, \mathbf{p}\rangle$ as

$$\langle \mathbf{x}|\mathbf{\Gamma}, \mathbf{q}, \mathbf{p}\rangle = \frac{\det(\mathbf{\Gamma}_{\mathrm{r}})^{1/4}}{(\pi\hbar)^{D/4}} \exp\left[-\frac{1}{2\hbar}(\mathbf{x}-\mathbf{q})^{\mathrm{T}}\mathbf{\Gamma}(\mathbf{x}-\mathbf{q}) + \frac{i}{\hbar}\mathbf{p}^{\mathrm{T}}(\mathbf{x}-\mathbf{q})\right], \qquad (2.1)$$

where

$$\mathbf{\Gamma}_{\mathrm{r}} = (\mathbf{\Gamma} + \mathbf{\Gamma}^{*})/2 .$$

$\mathbf{q}$ and $\mathbf{p}$ are D-dimensional real vectors corresponding to coordinate and momentum. Theses coherent states are adopted to the resolution of identity such that

$$\hat{\mathbf{1}} = \int \frac{d\mathbf{q}d\mathbf{p}}{(2\pi\hbar)^{D}}|\mathbf{\Gamma}, \mathbf{q}, \mathbf{p}\rangle\langle\mathbf{\Gamma}, \mathbf{q}, \mathbf{p}|, \qquad (2.2)$$

which will be inserted into the Trotter decomposition. $\mathbf{\Gamma}$ is a $D \times D$ complex symmetric matrix representing the width of the coherent states. The real part of eigen values of $\mathbf{\Gamma}$ should be taken to be positive. This definition of the coherent states is slightly different from that used by Baranger et al. [18] in that the phase part in Eq. (2.1) includes $-\frac{i}{2\hbar}\mathbf{p}^{\mathrm{T}}\mathbf{q}$. In this chapter, $\mathbf{\Gamma}$ is explicitly labeled as a parameter of the coherent states because it can be allowed to be different from time to time at a place of the insertion of the unity operator Eq. (2.2). Recall that as long as the complete set can be prepared, the unity operator does not depend on the choice of the width $\mathbf{\Gamma}$. For simplicity we often use the following abbreviation

$$|g\rangle = |\mathbf{\Gamma}, \mathbf{q}, \mathbf{p}\rangle . \qquad (2.3)$$

With use of the new variables $\mathbf{Q}$ and $\mathbf{Q}^{*}$ defined as

$$\mathbf{Q} = \frac{\mathbf{q} + i\mathbf{\Gamma}^{-1}\mathbf{p}}{\sqrt{2}}, \quad \mathbf{Q}^{*} = \frac{\mathbf{q} - i\mathbf{\Gamma}^{*-1}\mathbf{p}}{\sqrt{2}}, \qquad (2.4)$$

the coherent states are represented as

$$\begin{aligned}\langle \mathbf{x}|g\rangle &= \frac{\det(\mathbf{\Gamma}_{\mathrm{r}})^{1/4}}{(\pi\hbar)^{D/4}} \exp\left[-\frac{1}{2\hbar}(\mathbf{x}-\sqrt{2}\mathbf{Q})^{\mathrm{T}}\mathbf{\Gamma}(\mathbf{x}-\sqrt{2}\mathbf{Q}) \right. \\ &\left. \qquad\qquad +\frac{1}{4\hbar}(\mathbf{Q}-\mathbf{Q}^{*})^{\mathrm{T}}\mathbf{\Xi}_{\mathrm{r}}\mathbf{\Gamma}^{-1}\mathbf{\Xi}_{\mathrm{r}}(\mathbf{Q}-\mathbf{Q}^{*})\right], \end{aligned} \qquad (2.5)$$

where

$$\mathbf{\Xi}_{\mathrm{r}} = 2(\mathbf{\Gamma}^{-1} + \mathbf{\Gamma}^{*-1})^{-1} . \qquad (2.6)$$

Now we represent the propagator for the system with Hamiltonian $\hat{H}(t)$ in terms of these coherent states. First we Trotter-decompose the finite time quantum propagator of the system $K(\mathbf{x}, t, \mathbf{x}', 0)$ as

$$K(\mathbf{x}, t, \mathbf{x}', 0) \approx \langle \mathbf{x}| \prod_{k=0}^{N-1} \exp\left(-\frac{i\Delta t\hat{H}(t_{k})}{\hbar} \right)|\mathbf{x}'\rangle, \qquad (2.7)$$

17

with a large integer N and

$$\Delta t = t/N, \quad t_k = k\Delta t \quad (k = 0, 1, \ldots, N). \tag{2.8}$$

Inserting the identity operator of the form of Eq. (2.2), we see Eq. (2.7) become

$$
\begin{aligned}
K(\mathbf{x}, t, \mathbf{x}', 0) &= \int \prod_{k=0}^{N-1} \frac{d\mathbf{q}_k d\mathbf{p}_k}{(2\pi\hbar)^D} \\
&\quad \times \langle \mathbf{x} | g_N \rangle \prod_{k=0}^{N-1} \left\{ \langle g_{k+1} | \exp\left(-\frac{i\Delta t \hat{H}(t_k)}{\hbar} \right) | g_k \rangle \right\} \langle g_0 | \mathbf{x}' \rangle.
\end{aligned} \tag{2.9}
$$

The transition matrix elements $\langle g_{k+1} | \exp(-\frac{i\Delta t \hat{H}(t_k)}{\hbar}) | g_k \rangle$ in this expression can be estimated approximately as

$$
\begin{aligned}
\langle g_{k+1} | \exp\left[-\frac{i\Delta t \hat{H}(t_k)}{\hbar} \right] | g_k \rangle &\approx \langle g_{k+1} | \left(\hat{\mathbf{1}} - \frac{i\Delta t \hat{H}(t_k)}{\hbar} \right) | g_k \rangle \\
&= \langle g_{k+1} | g_k \rangle \left(1 - \frac{i\Delta t \langle g_{k+1} | \hat{H}(t_k) | g_k \rangle}{\hbar \langle g_{k+1} | g_k \rangle} \right) \\
&\approx \langle g_{k+1} | g_k \rangle \exp\left[-\frac{i\Delta t}{\hbar} \bar{H}_{k+1,k} \right],
\end{aligned} \tag{2.10}
$$

where

$$\bar{H}_{k+1,k} = \bar{H}(\mathbf{Q}_{k+1}^*, \mathbf{Q}_k) = \frac{\langle g_{k+1} | \hat{H}(t_k) | g_k \rangle}{\langle g_{k+1} | g_k \rangle}. \tag{2.11}$$

It is important to notice that $\bar{H}_{k+1,k}$ depends only on $\mathbf{Q}_{k+1}^*$ and $\mathbf{Q}_k$. The quality of this approximation should depend on the choice of the magnitude of $\Delta t/\hbar$, on which we will discuss later. The overlap integral between the two neighboring coherent state can be readily given as

$$
\begin{aligned}
\langle g_{k+1} | g_k \rangle &= \frac{\det(\mathbf{\Gamma}_{\mathrm{r}k+1})^{1/4} \det(\mathbf{\Gamma}_{\mathrm{r}k})^{1/4}}{\det(\mathbf{\Gamma}_{k+1,k})^{1/2}} \\
&\quad \times \exp\left[-\frac{1}{2\hbar} (\mathbf{Q}_{k+1}^* - \mathbf{Q}_k)^{\mathrm{T}} \mathbf{\Xi}_{k+1,k} (\mathbf{Q}_{k+1}^* - \mathbf{Q}_k) \right. \\
&\quad + \frac{1}{4\hbar} (\mathbf{Q}_{k+1} - \mathbf{Q}_{k+1}^*)^{\mathrm{T}} \mathbf{\Xi}_{\mathrm{r}k+1} \mathbf{\Gamma}_{k+1}^{*-1} \mathbf{\Xi}_{\mathrm{r}k+1} (\mathbf{Q}_{k+1} - \mathbf{Q}_{k+1}^*) \\
&\quad \left. + \frac{1}{4\hbar} (\mathbf{Q}_k - \mathbf{Q}_k^*)^{\mathrm{T}} \mathbf{\Xi}_{\mathrm{r}k} \mathbf{\Gamma}_k^{-1} \mathbf{\Xi}_{\mathrm{r}k} (\mathbf{Q}_k - \mathbf{Q}_k^*) \right]
\end{aligned} \tag{2.12}
$$

with the matrices denoted as

$$
\begin{aligned}
\mathbf{\Gamma}_{k+1,k} &= (\mathbf{\Gamma}_{k+1}^* + \mathbf{\Gamma}_k)/2 \tag{2.13} \\
\mathbf{\Xi}_{k+1,k} &= 2(\mathbf{\Gamma}_{k+1}^{*-1} + \mathbf{\Gamma}_k^{-1})^{-1}. \tag{2.14}
\end{aligned}
$$

After all, the propagator is expressed as

$$
\begin{aligned}
K(\mathbf{x}, t, \mathbf{x}', 0) &= \int \prod_{k=0}^{N-1} \frac{d\mathbf{q}_k d\mathbf{p}_k}{(2\pi\hbar)^D} \left\{ \frac{\det(\mathbf{\Gamma}_{\mathrm{r}k+1})^{1/4} \det(\mathbf{\Gamma}_{\mathrm{r}k})^{1/4}}{\det(\mathbf{\Gamma}_{k+1,k})^{1/2}} \right\} \\
&\quad \times \frac{\det(\mathbf{\Gamma}_{\mathrm{r}N})^{1/4} \det(\mathbf{\Gamma}_{\mathrm{r}0})^{1/4}}{(\pi\hbar)^{D/2}} \exp\left[\frac{1}{\hbar} \phi_N \right],
\end{aligned} \tag{2.15}
$$

where

$$
\begin{aligned}
\phi_N = \ & -\frac{1}{2}(\mathbf{x} - \sqrt{2}\mathbf{Q}_N)^{\mathrm{T}}\boldsymbol{\Gamma}_N(\mathbf{x} - \sqrt{2}\mathbf{Q}_N) - \frac{1}{2}(\mathbf{x}' - \sqrt{2}\mathbf{Q}_0^*)^{\mathrm{T}}\boldsymbol{\Gamma}_0^*(\mathbf{x}' - \sqrt{2}\mathbf{Q}_0^*) \\
& + \frac{1}{2}(\mathbf{Q}_N - \mathbf{Q}_N^*)^{\mathrm{T}}\boldsymbol{\Xi}_{\mathrm{r}N}(\mathbf{Q}_N - \mathbf{Q}_N^*) \\
& + \sum_{k=0}^{N-1}\left\{\frac{1}{2}(\mathbf{Q}_k - \mathbf{Q}_k^*)^{\mathrm{T}}\boldsymbol{\Xi}_{\mathrm{r}k}(\mathbf{Q}_k - \mathbf{Q}_k^*) - \frac{1}{2}(\mathbf{Q}_{k+1}^* - \mathbf{Q}_k)^{\mathrm{T}}\boldsymbol{\Xi}_{k+1,k}(\mathbf{Q}_{k+1}^* - \mathbf{Q}_k) \right. \\
& \left. -i\Delta t \bar{H}_{k+1,k}\right\}. \tag{2.16}
\end{aligned}
$$

Equations (2.15) and (2.16) are our basic formulae from which to proceed to various levels of approximation.

2.2.2   A critical choice of the integral variables in the steepest descent methods

As a standard procedure in semiclassical mechanics, we apply the steepest descent method (SDM) to the integrals in Eqs. (2.15) and (2.16). We assume that the stationary points are all isolated from one another. Just to remind that $\mathbf{Q}_k$ and $\mathbf{Q}_k^*$ are independent variables, we re-denote them as

$$
\begin{aligned}
\mathbf{u}_k &= \mathbf{Q}_k = \frac{\mathbf{q}_k + i\boldsymbol{\Gamma}_k^{-1}\mathbf{p}_k}{\sqrt{2}}, \tag{2.17} \\
\mathbf{v}_k &= \mathbf{Q}_k^* = \frac{\mathbf{q}_k - i\boldsymbol{\Gamma}_k^{*-1}\mathbf{p}_k}{\sqrt{2}}. \tag{2.18}
\end{aligned}
$$

Then, with the Jacobian determinant due to the variable transformation, the phase-space integrations are written as

$$
\int d\mathbf{q}_k d\mathbf{p}_k = \int d\mathbf{u}_k d\mathbf{v}_k \det(i\boldsymbol{\Xi}_k) . \tag{2.19}
$$

We assume that there are appropriate integral contours in the $\mathbf{u}_k$ and $\mathbf{v}_k$ spaces that make sense even in the limit of $|\mathbf{u}_k|, |\mathbf{v}_k| \to \infty$. However, it suffices for us to concentrate on the stationary points in the present context.

Much more serious problem to evaluate the kernel of Eq. (2.15) and Eq. (2.16) with SDM is the choice of the integration variables. Baranger et al. chose those to obtain their semiclassical IVR propagator [18] such that

$$
\int d\mathbf{u}_N d\mathbf{v}_N \ldots d\mathbf{u}_1 d\mathbf{v}_1. \tag{2.20}
$$

They estimated $\langle z''|\hat{K}(t)|z'\rangle$ with the coherent state path integrals and then evaluated $\langle x|\hat{K}(t)|z'\rangle$ by performing SDM to the integral $\int d^2 z'' \langle x|z''\rangle \langle z''|\hat{K}(t)|z'\rangle/\pi$ with use of the choice of the integration variables, which are equivalent to the choice of Eq. (2.20).

It seems to us that this is one of the origins of the difficulty they encountered afterward. Therefore we instead choose

$$\int d\mathbf{v}_N d\mathbf{u}_{N-1} d\mathbf{v}_{N-1} \dots d\mathbf{u}_1 d\mathbf{v}_1 d\mathbf{u}_0, \tag{2.21}$$

which will lead us to a correct formula as will be outlined below. The detailed mathematical manipulations for SDM are essentially the same as those taken by Baranger et al.'s except that ours include $\mathbf{\Gamma}$, which can vary from one sliced-time to another. (See the appendix for more details.) The result of our SDM and its continuous limit ($N \to \infty$) is

$$
\begin{aligned}
K(\mathbf{x}, t, \mathbf{x}', 0) &= \int \frac{d\mathbf{u}_f d\mathbf{v}_i}{(2\pi\hbar)^D} \; i^D \det(\mathbf{\Xi}_{\mathrm{rt}})^{1/2} \det(\mathbf{\Xi}_{\mathrm{r0}})^{1/2} \det(\mathbf{\Gamma}_{\mathrm{rt}})^{1/4} \det(\mathbf{\Gamma}_{\mathrm{r0}})^{-1/4} \\
&\quad \times \det(\mathbf{\Gamma}_t^*)^{-1/2} \det(\mathbf{\Gamma}_0^*)^{1/2} \det(\mathbf{U_u})^{-1/2} \\
&\quad \times \exp\left[\frac{i}{\hbar} \int_0^t d\tau \phi(\tau)\right] \langle\mathbf{x}|g_t\rangle\langle g_0|\mathbf{x}'\rangle,
\end{aligned}
\tag{2.22}
$$

where

$$\phi(t) = \frac{1}{2}(\mathbf{u}_t - \mathbf{v}_t)^{\mathrm{T}}\mathbf{\Xi}_{\mathrm{rt}}(\mathbf{\Gamma}_t^{-1}\frac{\partial \bar{H}_t}{\partial \mathbf{u}} - \mathbf{\Gamma}_t^{*-1}\frac{\partial \bar{H}_t}{\partial \mathbf{v}}) - \bar{H}_t + \frac{\hbar}{2}\mathrm{Tr}\left(\mathbf{\Xi}_{\mathrm{rt}}^{-1}\frac{\partial^2 \bar{H}_t}{\partial\mathbf{u}\partial\mathbf{v}}\right)$$

and $\mathbf{u}_t$ and $\mathbf{v}_t$ are the solution of the coupled ordinary differential equations

$$\dot{\mathbf{u}}_t - \frac{1}{2}\dot{\mathbf{\Gamma}}_t^{-1}\mathbf{\Xi}_{\mathrm{rt}}(\mathbf{u}_t - \mathbf{v}_t) = -i\mathbf{\Xi}_{\mathrm{rt}}^{-1}\frac{\partial \bar{H}_t}{\partial \mathbf{v}} \tag{2.23}$$

$$\dot{\mathbf{v}}_t + \frac{1}{2}\dot{\mathbf{\Gamma}}_t^{*-1}\mathbf{\Xi}_{\mathrm{rt}}(\mathbf{u}_t - \mathbf{v}_t) = i\mathbf{\Xi}_{\mathrm{rt}}^{-1}\frac{\partial \bar{H}_t}{\partial \mathbf{u}} \tag{2.24}$$

$$\mathbf{v}(0) = \mathbf{v}_i, \quad \mathbf{u}(t) = \mathbf{u}_f. \tag{2.25}$$

$\mathbf{U_u}, \mathbf{U_v}, \mathbf{V_u}, \mathbf{V_v}$ are matrices defined by

$$\begin{pmatrix} \mathbf{U_u} & \mathbf{U_v} \\ \mathbf{V_u} & \mathbf{V_v} \end{pmatrix} = \begin{pmatrix} \frac{\partial \mathbf{u}(t)}{\partial \mathbf{u}_i} & \frac{\partial \mathbf{u}(t)}{\partial \mathbf{v}_i} \\ \frac{\partial \mathbf{v}(t)}{\partial \mathbf{u}_i} & \frac{\partial \mathbf{v}(t)}{\partial \mathbf{v}_i} \end{pmatrix}, \tag{2.26}$$

where $\mathbf{u}(t)$ and $\mathbf{v}(t)$ are the solutions of Eq. (2.23) and Eq. (2.24) with the initial conditions

$$\mathbf{u}(0) = \mathbf{u}_i, \quad \mathbf{v}(0) = \mathbf{v}_i \tag{2.27}$$

and $\mathbf{u}_i$ is chosen to satisfy the condition Eq. (2.25).

Two features are noteworthy in the present result: (i) By not performing SDM with respect to $\mathbf{u}_N$ and $\mathbf{v}_0$, $\mathbf{x}$ or $\mathbf{x}'$ do not appear in the boundary conditions for either Eq. (2.23) or Eq. (2.24). (ii) The boundary conditions mentioned above are the combination of the initial and final condition. Thus, this propagator is not yet an initial value representation.

2.2.3 To the initial value representation

To transform the expression of Eq. (2.22) to a semiclassical initial value representation (SC-IVR), we further change the variables $\mathbf{u}_f$ and $\mathbf{v}_i$ in terms of the initial coordinates and momenta. First, we choose the integral route of $\int d\mathbf{u}_f d\mathbf{v}_i$ as follows

$$\mathbf{u}_f = \mathbf{u}(t, \mathbf{q}_0, \mathbf{p}_0), \quad \mathbf{v}_i = \mathbf{v}(0, \mathbf{q}_0, \mathbf{p}_0) \quad (\mathbf{q}_0, \mathbf{p}_0 \in \mathbb{R}^D), \tag{2.28}$$

where $\mathbf{u}(t, \mathbf{q}_0, \mathbf{p}_0)$ and $\mathbf{v}(t, \mathbf{q}_0, \mathbf{p}_0)$ is the solutions of Eq. (2.23) and Eq. (2.24) with the initial conditions

$$\mathbf{u}(0) = \frac{\mathbf{q}_0 + i\mathbf{\Gamma}_0^{-1}\mathbf{p}_0}{\sqrt{2}}, \quad \mathbf{v}(0) = \mathbf{u}^*(0) = \frac{\mathbf{q}_0 - i\mathbf{\Gamma}_0^{*-1}\mathbf{p}_0}{\sqrt{2}}. \tag{2.29}$$

Due to the fact that $\mathbf{v}(t) = \mathbf{u}^*(t)$ at any time if the relation $\mathbf{v}(0) = \mathbf{u}^*(0)$ is satisfied, this can be easily shown by Eq. (2.23) and Eq. (2.24). Thus we may define real vectors $\mathbf{q}(t)$ and $\mathbf{p}(t)$ as

$$\mathbf{q}(t) = \frac{\mathbf{\Gamma}_{rt}^{-1}(\mathbf{\Gamma}_t\mathbf{u}(t) + \mathbf{\Gamma}_t^*\mathbf{v}(t))}{\sqrt{2}}, \quad \mathbf{p}(t) = \frac{\mathbf{\Xi}_{rt}(\mathbf{u}(t) - \mathbf{v}(t))}{i\sqrt{2}}, \tag{2.30}$$

which is equivalent to

$$\frac{\mathbf{q}(t) + i\mathbf{\Gamma}_t^{-1}\mathbf{p}(t)}{\sqrt{2}} = \mathbf{u}(t), \quad \frac{\mathbf{q}(t) - i\mathbf{\Gamma}_t^{*-1}\mathbf{p}(t)}{\sqrt{2}} = \mathbf{v}(t). \tag{2.31}$$

Next, we rewrite Eq. (2.22) by changing the integral variables $\mathbf{u}_f$ and $\mathbf{v}_i$ to $\mathbf{q}_0$ and $\mathbf{p}_0$ and represent the integrand in terms of $\mathbf{q}(t)$ and $\mathbf{p}(t)$ instead of $\mathbf{u}(t)$ and $\mathbf{v}(t)$. With use of the relations

$$\begin{pmatrix} \frac{\partial}{\partial \mathbf{u}} \\ \frac{\partial}{\partial \mathbf{v}} \end{pmatrix} = \frac{1}{\sqrt{2}} \begin{pmatrix} \mathbf{\Gamma}\mathbf{\Gamma}_r^{-1} & -i\mathbf{\Xi}_r \\ \mathbf{\Gamma}^*\mathbf{\Gamma}_r^{-1} & i\mathbf{\Xi}_r \end{pmatrix} \begin{pmatrix} \frac{\partial}{\partial \mathbf{q}} \\ \frac{\partial}{\partial \mathbf{p}} \end{pmatrix} \tag{2.32}$$

and

$$\mathbf{\Xi}_r = \mathbf{\Gamma}\mathbf{\Gamma}_r^{-1}\mathbf{\Gamma}^* = \mathbf{\Gamma}^*\mathbf{\Gamma}_r^{-1}\mathbf{\Gamma}, \tag{2.33}$$

Eq. (2.23) and Eq. (2.24) turn out to be

$$\dot{\mathbf{q}} = \frac{\partial \bar{H}_t}{\partial \mathbf{p}} \tag{2.34}$$

$$\dot{\mathbf{p}} = -\frac{\partial \bar{H}_t}{\partial \mathbf{q}}. \tag{2.35}$$

Accordingly the phase $\phi(t)$ becomes

$$\phi(t) = \mathbf{p}^{\mathrm{T}}\dot{\mathbf{q}} - \bar{H}_t + \frac{\hbar}{4}\mathrm{Tr}\Big(\mathbf{\Gamma}_{rt}^{-1}\frac{\partial^2 \bar{H}_t}{\partial \mathbf{q}\partial \mathbf{q}} + \mathbf{\Xi}_{rt}\frac{\partial^2 \bar{H}_t}{\partial \mathbf{p}\partial \mathbf{p}} + i(\mathbf{\Gamma}_t - \mathbf{\Gamma}_t^*)\mathbf{\Gamma}_{rt}^{-1}\frac{\partial^2 \bar{H}_t}{\partial \mathbf{q}\partial \mathbf{p}}\Big), \tag{2.36}$$

and $\mathbf{U}_{\mathbf{u}}$ of Eq. (2.26) becomes

$$\mathbf{U}_{\mathbf{u}} = \frac{1}{2}(\mathbf{Q}_{\mathbf{q}} + i\mathbf{\Gamma}_t^{-1}\mathbf{P}_{\mathbf{q}} - i\mathbf{Q}_{\mathbf{p}}\mathbf{\Gamma}_0^* + \mathbf{\Gamma}_t^{-1}\mathbf{P}_{\mathbf{p}}\mathbf{\Gamma}_0^*)\mathbf{\Gamma}_{r0}^{-1}\mathbf{\Gamma}_0, \tag{2.37}$$

where

$$\begin{pmatrix} \mathbf{Q_q} & \mathbf{Q_p} \\ \mathbf{P_q} & \mathbf{P_p} \end{pmatrix} = \begin{pmatrix} \frac{\partial \mathbf{q}(t)}{\partial \mathbf{q}_0} & \frac{\partial \mathbf{q}(t)}{\partial \mathbf{p}_0} \\ \frac{\partial \mathbf{p}(t)}{\partial \mathbf{q}_0} & \frac{\partial \mathbf{p}(t)}{\partial \mathbf{p}_0} \end{pmatrix}. \tag{2.38}$$

Also, $\int d\mathbf{u}_f d\mathbf{v}_i$ becomes

$$\int d\mathbf{u}_f d\mathbf{v}_i = \int d\mathbf{q}_0 d\mathbf{p}_0 \det\left[\frac{1}{2}(\mathbf{Q_q} + i\mathbf{\Gamma}_t^{-1}\mathbf{P_q} - i\mathbf{Q_p}\mathbf{\Gamma}_0^* + \mathbf{\Gamma}_t^{-1}\mathbf{P_p}\mathbf{\Gamma}_0^*)\right]\det(-i\mathbf{\Gamma}_0^{*-1}). \tag{2.39}$$

Correcting these expressions, we can rewrite Eq. (2.22) as

$$K(\mathbf{x}, t, \mathbf{x}', 0) = \int \frac{d\mathbf{q}_0 d\mathbf{p}_0}{(2\pi\hbar)^D} \det\left[\frac{1}{2}(\mathbf{\Gamma}_t\mathbf{Q_q} + i\mathbf{P_q} - i\mathbf{\Gamma}_t\mathbf{Q_p}\mathbf{\Gamma}_0^* + \mathbf{P_p}\mathbf{\Gamma}_0^*)\right]^{1/2} \det(\mathbf{\Gamma}_{\mathrm{r}t}\mathbf{\Gamma}_{\mathrm{r}0})^{-1/4}$$

$$\times \exp\left[\frac{i}{\hbar}\int_0^t d\tau \phi(\tau)\right] \langle \mathbf{x}|\mathbf{\Gamma}_t, \mathbf{q}_t, \mathbf{p}_t\rangle\langle \mathbf{\Gamma}_0, \mathbf{q}_0, \mathbf{p}_0|\mathbf{x}'\rangle. \tag{2.40}$$

This is the main result of this chapter.

At a glance, Eq. (2.40) is similar to the original HK propagator derived by Kay [9]. However, there are two important differences between them. First, in our propagator, the Hamiltonian which determines the classical trajectories is defined as an average over the coherent states

$$\bar{H}_t(\mathbf{q}, \mathbf{p}) = \langle \mathbf{\Gamma}_t, \mathbf{q}, \mathbf{p}|\hat{H}(t)|\mathbf{\Gamma}_t, \mathbf{q}, \mathbf{p}\rangle \tag{2.41}$$

rather than the bare classical Hamiltonian. Second, the new terms have appeared that do not in the original HK propagator, that are

$$\frac{i}{4}\int_0^t d\tau \mathrm{Tr}\left(\mathbf{\Gamma}_{\mathrm{r}\tau}^{-1}\frac{\partial^2 \bar{H}_\tau}{\partial \mathbf{q}\partial \mathbf{q}} + \mathbf{\Xi}_{\mathrm{r}\tau}\frac{\partial^2 \bar{H}_\tau}{\partial \mathbf{p}\partial \mathbf{p}} + i(\mathbf{\Gamma}_\tau - \mathbf{\Gamma}_\tau^*)\mathbf{\Gamma}_{\mathrm{r}\tau}^{-1}\frac{\partial^2 \bar{H}_\tau}{\partial \mathbf{q}\partial \mathbf{p}}\right).$$

The propagator of Baranger et al. [18] has also the similar features to ours. A critical difference though is that the Gaussian exponent of the coherent states can be tuned with time in the present propagator, which allows for a theoretical flexibility leading to various versions of SC-IVR by specifying the choice of $\mathbf{\Gamma}_t$.

2.3   Selected semiclassical propagators as special cases

We show that some of the existing semiclassical propagators are derived as a special case of the kernel of Eq. (2.40). We here consider only the Hamiltonian of canonical form

$$\hat{H} = \frac{1}{2}\hat{\mathbf{p}}^{\mathrm{T}}\mathbf{M}^{-1}\hat{\mathbf{p}} + V(\hat{\mathbf{x}}), \tag{2.42}$$

where $\mathbf{M}$ is real positive matrix. In this case, $\bar{H}_t$ becomes

$$\bar{H}_t = \frac{1}{2}\mathbf{p}^{\mathrm{T}}\mathbf{M}^{-1}\mathbf{p} + \bar{V}_t(\mathbf{q}) + \frac{\hbar}{4}\mathrm{Tr}(\mathbf{M}^{-1}\mathbf{\Xi}_{\mathrm{r}t}), \tag{2.43}$$

where $\bar{V}_t(\mathbf{q})$ is the averaged potential

$$\bar{V}_t(\mathbf{q}) = \langle \mathbf{\Gamma}_t, \mathbf{q}, \mathbf{p}|\hat{V}|\mathbf{\Gamma}_t, \mathbf{q}, \mathbf{p}\rangle, \tag{2.44}$$

and $\phi(t)$ is

$$\phi(t) = \frac{1}{2}\mathbf{p}^{\mathrm{T}}\mathbf{M}^{-1}\mathbf{p} - \bar{V}_t(\mathbf{q}) + \frac{\hbar}{4}\mathrm{Tr}\left(\mathbf{\Gamma}_{\mathrm{rt}}^{-1}\frac{\partial^2 \bar{H}_t}{\partial \mathbf{q}\partial \mathbf{q}}\right). \tag{2.45}$$

It is noteworthy that if V is the quadratic form, $\bar{H}$ and $\phi(t)$ are simply

$$\bar{H} = \frac{1}{2}\mathbf{p}^{\mathrm{T}}\mathbf{M}^{-1}\mathbf{p} + V(\mathbf{q}) + const. , \quad \phi(t) = \frac{1}{2}\mathbf{p}^{\mathrm{T}}\mathbf{M}^{-1}\mathbf{p} - V(\mathbf{q}). \tag{2.46}$$

Thus, $(\mathbf{q}_t, \mathbf{p}_t)$ run along a purely classical trajectory and Eq. (2.40) coincides with the original HK propagator, which is exact when V is quadratic.

2.3.1 HK propagator with averaged Hamiltonian

Consider a choice such that $\mathbf{\Gamma}$ is a real constant matrix. Then, Eq.(2.40) becomes

$$\begin{aligned}
K(\mathbf{x}, t, \mathbf{x}', 0) &= \int \frac{d\mathbf{q}_0 d\mathbf{p}_0}{(2\pi\hbar)^D} \det\left[\frac{1}{2}(\mathbf{Q_q} + i\mathbf{\Gamma}^{-1}\mathbf{P_q} - i\mathbf{Q_p}\mathbf{\Gamma} + \mathbf{\Gamma}^{-1}\mathbf{P_p}\mathbf{\Gamma})\right]^{1/2} \\
&\quad \times \exp\left[\frac{i}{\hbar}\int_0^t d\tau \phi(\tau)\right]\langle\mathbf{x}|\mathbf{\Gamma}, \mathbf{q}_t, \mathbf{p}_t\rangle\langle\mathbf{\Gamma}, \mathbf{q}_0, \mathbf{p}_0|\mathbf{x}'\rangle .
\end{aligned} \tag{2.47}$$

In this particular case, both $\bar{H}$ and $\phi(t)$ become identical, respectively, to those appeared in Baranger's propagator, which has a fixed exponent in the coherent states. Therefore this propagator can be regarded as one of the HK propagators for the averaged Hamiltonian $\bar{H}$.

2.3.2 HK propagator

Take a choice

$$\mathbf{\Gamma}_\tau = \begin{cases} \mathbf{\Gamma}_0 & (\tau = 0) \\ \gamma\mathbf{E} & (0 < \tau < t) \\ \mathbf{\Gamma}_t & (\tau = t), \end{cases} \tag{2.48}$$

where γ is a real constant and $\mathbf{E}$ is the identity matrix, and also consider the limit

$$\gamma \to \infty. \tag{2.49}$$

This choice seems very strange, since the Gaussian width is finite only at the initial and final points, while it is infinite in between. However, this choice is at least mathematically allowed since we are treating with an approximation to the propagator itself but not with the propagation of a wavefunction during this interval. Recall that any information is not to be taken out on the way of propagation except for $\tau = 0$ and $\tau = t$. A physical quantity should be extracted only from $K(\mathbf{x}, t, \mathbf{x}', 0)$ at each t after its construction up to $\tau = t$. We call this propagator as the generalized HK propagator in what follows.

In this limit, $\bar{V}(\mathbf{q})$ and $\boldsymbol{\Gamma}_{\mathrm{rt}}^{-1}\frac{\partial^2 \bar{H}_t}{\partial \mathbf{q} \partial \mathbf{q}}$ become

$$\bar{V}(\mathbf{q}) \to V(\mathbf{q}), \quad \boldsymbol{\Gamma}_{\mathrm{r}\tau}^{-1}\frac{\partial^2 \bar{H}_\tau}{\partial \mathbf{q} \partial \mathbf{q}} \to \mathbf{O} \quad (0 < \tau < t). \tag{2.50}$$

Therefore $\bar{H}$ and $\phi(t)$ are simply

$$\bar{H} = \frac{1}{2}\mathbf{p}^{\mathrm{T}}\mathbf{M}^{-1}\mathbf{p} + V(\mathbf{q}) + const. , \quad \phi(t) = \frac{1}{2}\mathbf{p}^{\mathrm{T}}\mathbf{M}^{-1}\mathbf{p} - V(\mathbf{q}). \tag{2.51}$$

Thus, Eq. (2.40) is reduced to the the original HK propagator.

2.3.3   The Van Vleck IVR propagator

Choose $\boldsymbol{\Gamma}_\tau = \gamma\mathbf{E}$ $(0 \le \tau \le t)$ and take a limit $\gamma \to \infty$. Then, $|\boldsymbol{\Gamma}, \mathbf{q}, \mathbf{p}\rangle$ becomes

$$\frac{\det(\boldsymbol{\Gamma})^{1/4}}{(4\pi\hbar)^{D/4}}|\boldsymbol{\Gamma}, \mathbf{q}, \mathbf{p}\rangle \to |\mathbf{q}\rangle \tag{2.52}$$

and $\bar{H}$ and $\phi(t)$ become purely classical. Therefore Eq. (2.40) becomes

$$K(\mathbf{x}, t, \mathbf{x}', 0) = \int \frac{d\mathbf{q}_0 d\mathbf{p}_0}{(2\pi\hbar i)^{D/2}} \det(\mathbf{Q}_{\mathbf{p}})^{1/2} \exp\left[\frac{i}{\hbar}\int_0^t d\tau \phi(\tau)\right]\langle\mathbf{x}|\mathbf{q}_t\rangle\langle\mathbf{q}_0|\mathbf{x}'\rangle. \tag{2.53}$$

This is the initial value representation of VV propagator.

There is some confusion about the relationship between the HK propagator and VV-IVR propagator, since, as is well known, VV-IVR propagator can be derive from HK propagator, but the HK propagator was originally derived utilizing the VV propagator. Thus there remains an impression the HK propagator belongs to a subclass of VV propagator. However, it has been clarified here that both the HK and VV-IVR propagators can be derived independently from a single framework.

2.3.4   TGA-type propagator

To preserve the identity in Eq. (2.2), the width $\boldsymbol{\Gamma}$ must not have the dependence on $\mathbf{q}$ or $\mathbf{p}$. Nevertheless, let us try see what happens if $\boldsymbol{\Gamma}$ has such a dependence in the final expression Eq. (2.40). Take for instance

$$\boldsymbol{\Gamma}_\tau = \begin{cases} \boldsymbol{\Gamma}_0 & (0 \le \tau < t) \\ (\mathbf{Q}_{\mathbf{q}}^{\mathrm{T}} + i\boldsymbol{\Gamma}_0^{\mathrm{T}}\mathbf{Q}_{\mathbf{p}}^{\mathrm{T}})^{-1}(-i\mathbf{P}_{\mathbf{q}}^{\mathrm{T}} + \boldsymbol{\Gamma}_0^{\mathrm{T}}\mathbf{P}_{\mathbf{p}}^{\mathrm{T}}) & (\tau = t), \end{cases} \tag{2.54}$$

and another choice of the limit $\gamma \to \infty$ in

$$\boldsymbol{\Gamma}_\tau = \begin{cases} \boldsymbol{\Gamma}_0 & (\tau = 0) \\ \gamma\mathbf{E} & (0 < \tau < t) \\ (\mathbf{Q}_{\mathbf{q}}^{\mathrm{T}} + i\boldsymbol{\Gamma}_0^{\mathrm{T}}\mathbf{Q}_{\mathbf{p}}^{\mathrm{T}})^{-1}(-i\mathbf{P}_{\mathbf{q}}^{\mathrm{T}} + \boldsymbol{\Gamma}_0^{\mathrm{T}}\mathbf{P}_{\mathbf{p}}^{\mathrm{T}}) & (\tau = t). \end{cases} \tag{2.55}$$

Then, using the relations

$$\mathbf{Q}_\mathbf{q}^\mathrm{T}\mathbf{P}_\mathbf{p} - \mathbf{P}_\mathbf{q}^\mathrm{T}\mathbf{Q}_\mathbf{p} = \mathbf{E} \tag{2.56}$$

$$\mathbf{Q}_\mathbf{q}^\mathrm{T}\mathbf{P}_\mathbf{q} - \mathbf{P}_\mathbf{q}^\mathrm{T}\mathbf{Q}_\mathbf{q} = \mathbf{O} \tag{2.57}$$

$$\mathbf{Q}_\mathbf{p}^\mathrm{T}\mathbf{P}_\mathbf{p} - \mathbf{P}_\mathbf{p}^\mathrm{T}\mathbf{Q}_\mathbf{p} = \mathbf{O}, \tag{2.58}$$

Eq. (2.40) becomes

$$
\begin{aligned}
K(\mathbf{x}, t, \mathbf{x}', 0) &= \int \frac{d\mathbf{q}_0 d\mathbf{p}_0}{(2\pi\hbar)^D} \det(\mathbf{Q}_\mathbf{q} + i\mathbf{Q}_\mathbf{p}\boldsymbol{\Gamma}_0)^{-1/2} \left(\frac{\det(\boldsymbol{\Gamma}_{\mathrm{r}0})}{\det(\boldsymbol{\Gamma}_{\mathrm{r}t})} \right)^{1/4} \\
&\quad \exp\left[\frac{i}{\hbar} \int_0^t d\tau \phi(\tau) \right] \langle \mathbf{x} | \boldsymbol{\Gamma}_t, \mathbf{q}_t, \mathbf{p}_t \rangle \langle \boldsymbol{\Gamma}_0, \mathbf{q}_0, \mathbf{p}_0 | \mathbf{x}' \rangle.
\end{aligned} \tag{2.59}
$$

$K(\mathbf{x}, t, \mathbf{x}', 0)$ of the former choice is identical to the propagator derived by Baranger et al. The latter is a propagator that expands the initial state in the coherent states and propagates each coherent state by Heller's TGA. We call these propagators as TGA-type propagator in this chapter.

It is a little amazing that in spite of the violation of the $\mathbf{q}, \mathbf{p}$ independence of $\boldsymbol{\Gamma}$, these popular propagators can be derived. This fact can be understood as follows: These TGA-type propagators are originally derived by propagating each initial coherent states independently. Heller derived TGA by propagating one coherent state on the potential function approximated to be quadratic around the center of the coherent state [4]. Baranger et al. derived their propagator by evaluating the value $\langle x | \hat{K}(t) | z \rangle$ for each initial coherent state [18]. Thus, in these propagators, the propagation of each Gaussian is made independently. On the other hand, in the derivation of HK-type propagator, the effect of the neighboring Gaussians are taken into account. In the original and present derivation, SDM is performed with respect to one of the initial variables, corresponding to $\int d\mathbf{u}_0$ in the present framework. Therefore the HK-type propagator takes account of the interaction among the individual Gaussians. It is therefore conceived that to compensate the ignorance between the Gaussians $\boldsymbol{\Gamma}$ in TGA must have the $\mathbf{q}, \mathbf{p}$ dependence.

The thawed Gaussian theory is designed so that each one should satisfy the normalization condition along its path, and it is quite natural that the normalization is violated if they are adopted in a collective set in the path integration. Harabati et al. [27] showed numerically that the TGA-type propagators do not preserve the norm in contrast to the fact that the HK propagators do well. But this claim is not fair to the TGA theory in view of the original spirit [4]. From our point of view, the violation of the norm is obvious because the TGA propagators are attained only violation of the independence of $\boldsymbol{\Gamma}$ with respect to $\mathbf{q}$ and $\mathbf{p}$, which automatically breaks the normalization condition, since under such a circumstance, the operator of Eq. (2.2) to be represented in terms of the coherent states is no longer an identity operator and loses unitarity.

2.4 Numerical studies on the HK propagators

2.4.1 Facts

We examine the accuracy of the generalized HK propagators in this section. As mentioned above, the TGA type propagator has been numerically studied elsewhere [27]. We consider a one-dimensional Hamiltonian as a test system, that is

$$\hat{H} = \frac{\hat{p}^2}{2m} + m\omega^2 \frac{\cosh(\alpha\hat{q}) - 1}{\alpha^2}, \tag{2.60}$$

where α parametrizes the anharmonicity of the system. Since the potential term becomes

$$m\omega^2 \frac{\cosh(\alpha\hat{q}) - 1}{\alpha^2} = \frac{m\omega^2}{2}\hat{q}^2 + \frac{m\omega^2}{4!}\alpha^2\hat{q}^4 + \cdots, \tag{2.61}$$

the potential term approaches $\frac{m\omega^2}{2}\hat{q}^2$ for α to come closer to 0, and the bigger α makes the potential more anharmonic. We set $m = \omega = \hbar = 1$ and carry out the calculation for the system of $\alpha = 0.1$, 0.5, 1.0, and 1.5.

We here compare the following propagators corresponding to the choice of $\mathbf{\Gamma}_\tau$;

$$\mathbf{\Gamma}_\tau = \begin{cases} m\omega\mathbf{E} & (\tau = 0) \\ \beta m\omega\mathbf{E} & (0 < \tau < t) \\ m\omega\mathbf{E} & (\tau = t) \end{cases}, \tag{2.62}$$

where β is a parameter which determines the averaged Hamiltonian. We choose $\beta = 0.5$, $1, 2$, and ∞ for comparison. The propagator of $\beta = \infty$ gives just the original HK propagator and the others are new.

In order to compare the accuracy of the propagators, we propagate an initial coherent wavepacket $\Psi(x, 0) = \langle x|m\omega\mathbf{E}, q_0, p_0\rangle$ semiclassically with these generalized HK propagators and quantum mechanically by the FFT split operator method [28, 29]. We denote these propagated states $\Psi_{SC}(x, t)$ and $\Psi(x, t)$ respectively. As an indicator to monitor the accuracy, we calculate the norm of $\Psi_{SC}(x, t)$

$$N_{SC}(t) = \langle\Psi_{SC}(t)|\Psi_{SC}(t)\rangle \tag{2.63}$$

and an overlap between $\Psi(x, t)$ and the normalized $\Psi_{SC}(x, t)$,

$$S(t) = N_{SC}(t)^{-1/2}\langle\Psi(t)|\Psi_{SC}(t)\rangle. \tag{2.64}$$

The closer $N_{SC}(t)$ and $S(t)$ are to unity, the more accurate we judge the method to be. In all cases, we set $(q_0, p_0) = (0, 1)$, the integration in each generalized HK propagator is done by the Monte Carlo integration procedure with 5,000 trajectories and the calculations are done up to $t = 100$. The results are exhibited in Fig. 2.1.
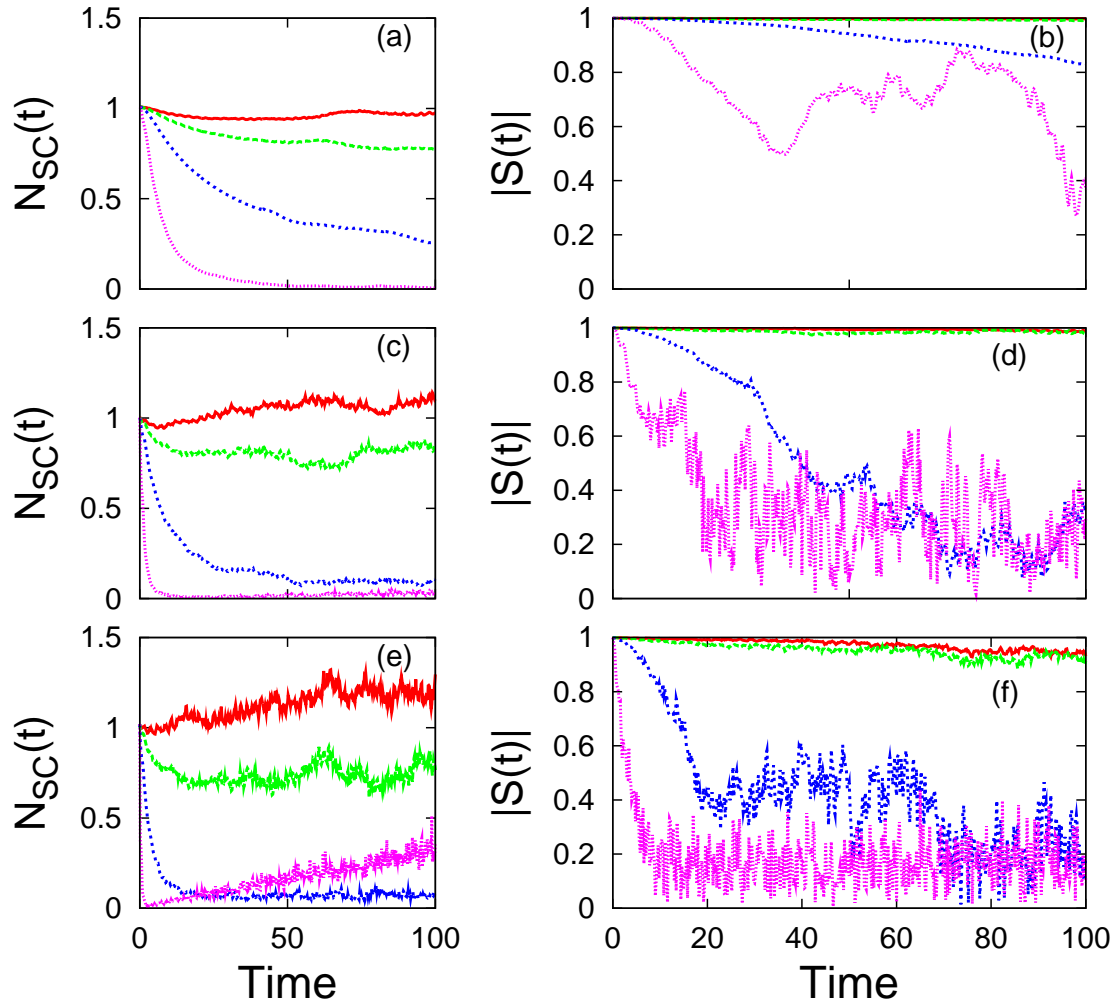
26

Figure 2.1: Comparison of the norm $N_{SC}(t)$ and overlap $S(t)$ calculated with the generalized HK propagators with $\beta = \infty$ (red, solid), $\beta = 2$ (green, dashed), $\beta = 1$ (blue, short dashed), and $\beta = 0.5$ (purple, dotted) for the potential: (a), (b) $\alpha = 0.5$, (c), (d) $\alpha = 1.0$, and (e), (f) $\alpha = 1.5$.

In the case of $\alpha = 0.1$, for which the anharmonicity is small enough, $N_{SC}(t)$ and $S(t)$ for all the generalized HK propagators are nearly 1.0 up to $t = 100$ (not shown). However, for the larger α values ($\alpha = 0.5, 1, 1.5$), the deviation from the exact values becomes evident (Fig. 2.1(a),(c), (e)). In particular, a large deviation is seen in the decay of the norm $N_{SC}(t)$ for $\alpha = 1.5$ and the small β values. Actually, the norm with $\beta = \infty$ shows almost no decay while the norm with $\beta = 0.5$ decays so quickly that it becomes nearly 0. Corresponding to the norm decay, the overlap $S(t)$ detects that it deviate from unity more as β becomes smaller. Besides, very unphysical oscillation is observed in $S(t)$. Thus it is consistently observed that the quality of the propagators in the generalized HK propagators is deteriorated as α becomes larger and β gets smaller. Thus it turns out that the original HK propagator generally provides with the best quality both in the norm and overlap integral. Thus, one may conclude that the averaging of the Hamiltonian over the coherent states does not give additional quantum correction to the original HK propagator.

2.4.2 Discussion

Let us discuss then why the original HK propagator is more accurate than the other generalized counterparts: First of all, we recall that a qualitative and critical difference of the original HK propagator from the other generalized ones lies in that the Gaussian average Hamiltonian is reduced to the purely classical one when $\beta = \infty$ (in the original HK propagator). On the other hands, the "classical paths" generated in the generalized HK propagators tend to deviate from the purely classical ones (the Newtonian trajectories) as β becomes smaller, and the quality of the resultant wavefunctions is more deteriorated. The present results therefore show that the Gaussian averaged Hamiltonian is not likely to aid in taking account of additional quantum effects in the classical region. This seems rather counter intuitive because it almost claims that the use of the classical Hamiltonian in quantum approximation is better than laboriously working with the quantum averaged Hamiltonian. However, we need a little more careful discussion.

In the standard semiclassical theories like the WKB theory, the classical-path representation of semiclassical propagation of wavefunctions and kernels is generally accepted to be (very) good, as long as a system energy is in a classically allowed region, where no quantum tunneling is needed to be considered. This is quite often experienced numerically. In these theories, the stationary phase approximation (SPA) is a standard mathematical tool, which is valid in the limit of $\hbar \to 0$, and the Newtonian paths usually arise in this limit. Recall on the other hand that we have used the steepest descent method (SDM) rather than SPA in our derivation of the coherent-state representation of the kernel. In this conjunction, it is subtle to judge whether the generalized HK

propagators (including the original one) are really a semiclassical approximation in the sense of the small $\hbar$ limit. On the other hand side, the SDM we used is expected to be more accurate for an integral the sharper Gaussians are involved in. Due to the uncertainty relation, however, a sharp distribution in configuration space may result in a broader distribution in the associated momentum space to which we applied SDM too in phase-space path integration, and thereby the assessment of the quality of the steepest descent in the entire phase-space integrals is not simple.

Here enters the Gaussian functions with a critical role in the coherent path integration. As the first example, let us look back at the series of approximation in Eq. (2.10). This is a standard approximation frequently used in the evaluation of the path integrals, which we also did in this work. Equation (2.10) is the source spot from which for the Gaussian averaged Hamiltonian to emerge. Here again we should note that this approximation is not a semiclassical approximation either: The two step approximations in Eq. (2.10) should be deteriorated for a long time interval Δt. For the same reason, a very small choice of $\hbar$ is expected to make the approximation worse. Fortunately, however, an exceptional advantage of the coherent states (Gaussian functions in general) works in Eq. (2.10). Suppose our Hamiltonian is of potential-free, and that the kinetic energy operator $\hat{T} = \sum \hat{p}_i^2/2m_i$, then

$$
\begin{aligned}
\left\langle g \left| \exp\left(c\hat{T} \right) \right| g \right\rangle &= \int dp \left\langle g | p \right\rangle \exp\left(c \sum p_i^2/2m_i \right) \left\langle p | g \right\rangle \\
&\simeq \exp\left[\left\langle g \left| c\hat{T} \right| g \right\rangle \right] = \exp\left(c \sum \bar{p}_i^2/2m_i \right),
\end{aligned}
\tag{2.65}
$$

where at $\bar{p}_i$ is the average position of the coherent state in momentum space and c is an arbitrary constant. The relevant relation has already appeared explicitly in Eq. (2.43). Besides, if the Gaussian is sharply localized in configuration space (corresponding to a large β or more generally a large Γ), it should hold

$$
\left\langle g \left| V \right| g \right\rangle \to V\left(\bar{q} \right),
\tag{2.66}
$$

where $\bar{q}$ is the central position of such a sharp Gaussian. Thus in this sharp Gaussian limit, the approximation in Eq. (2.10) should be more valid without broadening of the momentum space components, irrespective of the smallness of the Planck constant. At the same time, the Gaussian averaged Hamiltonian turns to be the classical counterpart more closely.

The similar argument can apply with more importance to the SDM to achieve Eq. (2.22), which is the central expression of the approximate kernel. The quality of the generalized HK propagators is heavily dependent on this integral. Again we recall that the classical Hamiltonian has resulted as a consequence of the large exponent as exemplified in Eq. (2.43). Thus we may say such that the sharp Gaussian limit on the propagation as in Eqs. (2.48) and (2.49) leads to a reasonable approximation in the

relevant Gaussian integrals and at the same time reduces, consequently, the Gaussian averaged Hamiltonian to the classical counterpart.

2.5 Concluding remarks

In this chapter we have introduced a generalized coherent state path integral. This path integral explicitly considers the time dependence of the width of the coherent states inserted into the time-windows in the Trotter decomposition of the finite-time quantum propagator. On this basis, we have shown that various SC-IVR can be derived by estimating thus obtained general propagator with the steepest descent method, which includes the VV propagator, generalized HK propagators and TGA-type propagators with an appropriate choice of the Gaussian width. A special care has been exercised in choosing the appropriate integral coordinates in the steepest descent method, leaving $\mathbf{x}$ and $\mathbf{x}'$ as the boundary position of the classical trajectory. This choice made a large difference from the previously studied coherent state path integrals [18].

To examine the accuracy of the generalized HK propagators, we have carried out a numerical test. It have been revealed that the original HK propagator, which uses the classical Hamiltonian rather than the counterpart averaged over the coherent states, is the most accurate among the generalized HK propagators. It is argued that the success of the original HK propagator is greatly attributed to the nice characteristics of the Gaussian functions, the sharp one among which readily reduces the averaged Hamiltonian to the classical counterpart.

2.6 Appendix: Derivation of Equation (2.22)

Before deriving Eq. (2.22), we review the procedure of steepest descent method (SDM). Assume $F(\mathbf{x})$ and $G(\mathbf{x})$ are complex analytic functions. Then, SDM approximates $\int d\mathbf{x} G(\mathbf{x}) \exp[-F(\mathbf{x})]$ as

$$\int d\mathbf{x} G(\mathbf{x}) \exp[-F(\mathbf{x})] \approx \sum_j \det \left(\frac{\mathbf{F}''(\mathbf{x}_j)}{2\pi} \right)^{-1/2} G(\mathbf{x}_j) \exp[-F(\mathbf{x}_j)], \qquad (2.67)$$

where $\mathbf{x}_j$ are the stationary points of F, with $\mathbf{x}_j$ satisfying

$$\frac{\partial F}{\partial \mathbf{x}}(\mathbf{x}_j) = \mathbf{O} \qquad (2.68)$$

and $\mathbf{F}''(\mathbf{x})$ is Hessian of $F(\mathbf{x})$.

Now we perform SDM for the integral in Eq. (2.15) with respect to the variables $\mathbf{v}_N, \mathbf{u}_{N-1}, \ldots, \mathbf{v}_1, \mathbf{u}_0$. The procedure below is mostly same as that of Baranger et al. [18],

except that the time dependence of Γ is newly considered. First, to find the stationary point, we differentiate ϕ_N obtaining the following stationary state conditions

$$\frac{\partial \phi_N}{\partial \mathbf{u}_k} = \mathbf{\Xi}_{k+1,k}(\mathbf{v}_{k+1} - \mathbf{u}_k) + \mathbf{\Xi}_{\mathrm{r}k}(\mathbf{u}_k - \mathbf{v}_k) - i\Delta t \frac{\partial \bar{H}_{k+1,k}}{\partial \mathbf{u}_k} = 0 \tag{2.69}$$

$$\frac{\partial \phi_N}{\partial \mathbf{v}_{k+1}} = -\mathbf{\Xi}_{k+1,k}(\mathbf{v}_{k+1} - \mathbf{u}_k) - \mathbf{\Xi}_{\mathrm{r}k+1}(\mathbf{u}_{k+1} - \mathbf{v}_{k+1}) - i\Delta t \frac{\partial \bar{H}_{k+1,k}}{\partial \mathbf{v}_{k+1}} = 0 \tag{2.70}$$

$$(k = 0, 1, \ldots, N-1).$$

The stationary point is obtained by solving these equations with respect to $\mathbf{v}_N, \ldots, \mathbf{v}_1, \mathbf{u}_0$. Note that $\mathbf{u}_N$ and $\mathbf{v}_0$ are parameters which determine $\mathbf{v}_N, \ldots, \mathbf{v}_1, \mathbf{u}_0$. Note also that there is no $\mathbf{x}$ or $\mathbf{x}'$ included in Eqs. (2.69) and (2.70). This is the important advantage of the choice $\mathbf{v}_N, \mathbf{u}_{N-1}, \ldots, \mathbf{v}_1, \mathbf{u}_0$ for SDM. Then we evaluate the Hessian of ϕ_N at the stationary point. The second derivatives of ϕ_N becomes

$$\frac{\partial^2 \phi_N}{\partial \mathbf{u}_k \partial \mathbf{u}_k} = -\mathbf{\Xi}_{k+1,k} + \mathbf{\Xi}_{\mathrm{r}k} - i\Delta t \frac{\partial^2 \bar{H}_{k+1,k}}{\partial \mathbf{u}_k \partial \mathbf{u}_k} \tag{2.71}$$

$$\frac{\partial^2 \phi_N}{\partial \mathbf{u}_k \partial \mathbf{v}_{k+1}} = \mathbf{\Xi}_{k+1,k} - i\Delta t \frac{\partial^2 \bar{H}_{k+1,k}}{\partial \mathbf{u}_k \partial \mathbf{v}_{k+1}} \tag{2.72}$$

$$\frac{\partial^2 \phi_N}{\partial \mathbf{v}_{k+1} \partial \mathbf{u}_k} = \mathbf{\Xi}_{k+1,k} - i\Delta t \frac{\partial^2 \bar{H}_{k+1,k}}{\partial \mathbf{v}_{k+1} \partial \mathbf{u}_k} \tag{2.73}$$

$$\frac{\partial^2 \phi_N}{\partial \mathbf{v}_{k+1} \partial \mathbf{v}_{k+1}} = -\mathbf{\Xi}_{k+1,k} + \mathbf{\Xi}_{\mathrm{r}k+1} - i\Delta t \frac{\partial^2 \bar{H}_{k+1,k}}{\partial \mathbf{v}_{k+1} \partial \mathbf{v}_{k+1}} \tag{2.74}$$

$$\frac{\partial^2 \phi_N}{\partial \mathbf{u}_k \partial \mathbf{v}_k} = \frac{\partial^2 \phi_N}{\partial \mathbf{v}_k \partial \mathbf{u}_k} = -\mathbf{\Xi}_{\mathrm{r}k}. \tag{2.75}$$

To make notation simple, we define $D \times D$ matrices $\mathbf{A}_{k,ij}(1 \leq k \leq N, \ i,j = 1,2)$ as

$$\mathbf{A}_{k,11} = i\mathbf{\Xi}_{\mathrm{r}k}^{-1} \frac{\partial^2 \phi_N}{\partial \mathbf{u}_k \partial \mathbf{u}_k} \tag{2.76}$$

$$\mathbf{A}_{k,12} = i\mathbf{\Xi}_{\mathrm{r}k}^{-1} \frac{\partial^2 \phi_N}{\partial \mathbf{u}_k \partial \mathbf{v}_{k+1}} \tag{2.77}$$

$$\mathbf{A}_{k,21} = i\mathbf{\Xi}_{\mathrm{r}k+1}^{-1} \frac{\partial^2 \phi_N}{\partial \mathbf{v}_{k+1} \partial \mathbf{u}_k} \tag{2.78}$$

$$\mathbf{A}_{k,22} = i\mathbf{\Xi}_{\mathrm{r}k+1}^{-1} \frac{\partial^2 \phi_N}{\partial \mathbf{v}_{k+1} \partial \mathbf{v}_{k+1}} \tag{2.79}$$

and define $(2ND) \times (2ND)$ matrix $\mathbf{M}_N$ as

$$\mathbf{M}_N = \begin{pmatrix} \mathbf{A}_{1,11} & \mathbf{A}_{1,12} & & & & & \mathbf{O} \\ \mathbf{A}_{1,21} & \mathbf{A}_{1,22} & -i\mathbf{E} & & & & \\ & -i\mathbf{E} & \mathbf{A}_{2,11} & \mathbf{A}_{2,12} & & & \\ & & \mathbf{A}_{2,21} & \mathbf{A}_{2,22} & -i\mathbf{E} & & \\ & & & -i\mathbf{E} & \mathbf{A}_{3,11} & & \\ & & & & & \ddots & \\ \mathbf{O} & & & & & & \mathbf{A}_{N,22} \end{pmatrix}. \tag{2.80}$$

Then, Eq. (2.15) becomes

$$
\begin{aligned}
K(\mathbf{x}, t, \mathbf{x}', 0) &= \int \frac{d\mathbf{u}_N d\mathbf{v}_0}{(2\pi\hbar)^{D(N+1)}} \prod_{k=0}^{N} \{\det(i\boldsymbol{\Xi}_{\mathrm{r}k})\} \prod_{k=0}^{N-1} \left\{ \frac{\det(\boldsymbol{\Gamma}_{\mathrm{r}k+1})^{1/4} \det(\boldsymbol{\Gamma}_{\mathrm{r}k})^{1/4}}{\det(\boldsymbol{\Gamma}_{k+1,k})^{1/2}} \right\} \\
&\qquad \frac{\pi^{DN}}{\det(-\frac{1}{2\hbar}\phi'')^{1/2}} \frac{\det(\boldsymbol{\Gamma}_{\mathrm{r}N})^{1/4} \det(\boldsymbol{\Gamma}_{\mathrm{r}0})^{1/4}}{(\pi\hbar)^{D/2}} \exp\left[\frac{1}{\hbar}\phi_N \right] \\
&= \int \frac{d\mathbf{u}_N d\mathbf{v}_0}{(2\pi\hbar)^{D}} \, i^D \det(\boldsymbol{\Xi}_{\mathrm{r}N})^{1/2} \det(\boldsymbol{\Xi}_{\mathrm{r}0})^{1/2} \prod_{k=0}^{N-1} \left\{ \frac{\det(\boldsymbol{\Gamma}_{\mathrm{r}k+1})^{1/4} \det(\boldsymbol{\Gamma}_{\mathrm{r}k})^{1/4}}{\det(\boldsymbol{\Gamma}_{k+1,k})^{1/2}} \right\} \\
&\qquad \times \frac{1}{\det(\mathbf{M}_N)^{1/2}} \frac{\det(\boldsymbol{\Gamma}_{\mathrm{r}N})^{1/4} \det(\boldsymbol{\Gamma}_{\mathrm{r}0})^{1/4}}{(\pi\hbar)^{D/2}} \exp\left[\frac{1}{\hbar}\phi_N \right].
\end{aligned}
\tag{2.81}
$$

Next, we make the variables continuous, namely consider the limit $N \to \infty$. Here we define ΔY_k as $\Delta Y_k = Y_{k+1} - Y_k$ where Y_k is an arbitrary variable and we only leave the first-order terms with respect to Δ in following calculation. Relation for regular matrix $\mathbf{A}$,

$$
(\mathbf{A} + \Delta\mathbf{B})^{-1} = \mathbf{A}^{-1} - \mathbf{A}^{-1}\Delta\mathbf{B}\mathbf{A}^{-1}
$$

is useful for following argument. Further, using the relations

$$
\begin{aligned}
\boldsymbol{\Xi}_{k+1,k} &= 2(\boldsymbol{\Gamma}_{k+1}^{*-1} + \boldsymbol{\Gamma}_k^{-1})^{-1} = 2(\boldsymbol{\Gamma}_k^{*-1} + \boldsymbol{\Gamma}_k^{-1} + \Delta\boldsymbol{\Gamma}_k^{*-1})^{-1} \\
&= \boldsymbol{\Xi}_{\mathrm{r}k} - \frac{1}{2}\boldsymbol{\Xi}_{\mathrm{r}k}\Delta\boldsymbol{\Gamma}_k^{*-1}\boldsymbol{\Xi}_{\mathrm{r}k} \tag{2.82} \\
&= \boldsymbol{\Xi}_{\mathrm{r}k+1} + \frac{1}{2}\boldsymbol{\Xi}_{\mathrm{r}k+1}\Delta\boldsymbol{\Gamma}_k^{-1}\boldsymbol{\Xi}_{\mathrm{r}k+1} \tag{2.83}
\end{aligned}
$$

and consider the limit $N \to \infty$, Eqs. (2.69) and (2.70) become

$$
\dot{\mathbf{u}} - \frac{1}{2}\dot{\boldsymbol{\Gamma}}^{-1}\boldsymbol{\Xi}_{\mathrm{r}}(\mathbf{u} - \mathbf{v}) = -i\boldsymbol{\Xi}_{\mathrm{r}}^{-1}\frac{\partial\bar{H}}{\partial\mathbf{v}} \tag{2.84}
$$

$$
\dot{\mathbf{v}} + \frac{1}{2}\dot{\boldsymbol{\Gamma}}^{*-1}\boldsymbol{\Xi}_{\mathrm{r}}(\mathbf{u} - \mathbf{v}) = i\boldsymbol{\Xi}_{\mathrm{r}}^{-1}\frac{\partial\bar{H}}{\partial\mathbf{u}} \tag{2.85}
$$

with boundary conditions

$$
\mathbf{v}(0) = \mathbf{v}_i, \quad \mathbf{u}(t) = \mathbf{u}_f .
$$

Then, we consider the exponent of Eq. (2.81). Here we change the notation as following:

$$
\frac{\det(\boldsymbol{\Gamma}_{\mathrm{r}N})^{1/4} \det(\boldsymbol{\Gamma}_{\mathrm{r}0})^{1/4}}{(\pi\hbar)^{D/2}} \exp\left[\frac{1}{\hbar}\phi_N\right] = \exp\left[\frac{1}{\hbar}\tilde{\phi}_N\right] \langle\mathbf{x}|g_N\rangle\langle g_0|\mathbf{x}'\rangle, \tag{2.86}
$$

where

$$
\begin{aligned}
\tilde{\phi}_N = \sum_{k=0}^{N-1} \Big\{ &-\frac{1}{2}(\mathbf{v}_{k+1} - \mathbf{u}_k)^{\mathrm{T}}\boldsymbol{\Xi}_{k+1,k}(\mathbf{v}_{k+1} - \mathbf{u}_k) \\
&+\frac{1}{4}(\mathbf{u}_{k+1} - \mathbf{v}_{k+1})^{\mathrm{T}}\boldsymbol{\Xi}_{\mathrm{r}k+1}\boldsymbol{\Gamma}_{k+1}^{*-1}\boldsymbol{\Xi}_{\mathrm{r}k+1}(\mathbf{u}_{k+1} - \mathbf{v}_{k+1}) \\
&+\frac{1}{4}(\mathbf{u}_k - \mathbf{v}_k)^{\mathrm{T}}\boldsymbol{\Xi}_{\mathrm{r}k}\boldsymbol{\Gamma}_k^{-1}\boldsymbol{\Xi}_{\mathrm{r}k}(\mathbf{u}_k - \mathbf{v}_k) - i\Delta t\bar{H}_{k+1,k} \Big\}. \tag{2.87}
\end{aligned}
$$

Using Eq. (2.82), Eq. (2.83) and the relation

$$
\begin{aligned}
\Xi_{k+1,k} &= \Xi_{k+1,k}\Xi_{k+1,k}^{-1}\Xi_{k+1,k} \\
&= \frac{1}{2}\Xi_{k+1,k}(\Gamma_{k+1}^{*-1} + \Gamma_k^{-1})\Xi_{k+1,k},
\end{aligned}
\tag{2.88}
$$

$\tilde{\phi}_N$ becomes

$$
\begin{aligned}
\tilde{\phi}_N &= \sum_{k=0}^{N-1}\Bigg\{ -\frac{1}{4}(\mathbf{v}_{k+1} - \mathbf{u}_k)^{\mathrm{T}}\Xi_{k+1,k}\Gamma_{k+1}^{*-1}\Xi_{k+1,k}(\mathbf{v}_{k+1} - \mathbf{u}_k) \\
&\quad -\frac{1}{4}(\mathbf{v}_{k+1} - \mathbf{u}_k)^{\mathrm{T}}\Xi_{k+1,k}\Gamma_k^{-1}\Xi_{k+1,k}(\mathbf{v}_{k+1} - \mathbf{u}_k) \\
&\quad +\frac{1}{4}(\mathbf{u}_{k+1} - \mathbf{v}_{k+1})^{\mathrm{T}}\Xi_{rk+1}\Gamma_{k+1}^{*-1}\Xi_{rk+1}(\mathbf{u}_{k+1} - \mathbf{v}_{k+1}) \\
&\quad +\frac{1}{4}(\mathbf{u}_k - \mathbf{v}_k)^{\mathrm{T}}\Xi_{rk}\Gamma_k^{-1}\Xi_{rk}(\mathbf{u}_k - \mathbf{v}_k) - i\Delta t\bar{H}_{k+1,k}\Bigg\} \\[4pt]
&= \frac{1}{2}\sum_{k=0}^{N-1}\Delta t(\mathbf{u} - \mathbf{v})^{\mathrm{T}}\Xi_r\Gamma^{-1}\Xi_r\left\{\frac{\Delta\mathbf{v}}{\Delta t} + \frac{1}{2}\frac{\Delta\Gamma^{*-1}}{\Delta t}\Xi_r(\mathbf{u} - \mathbf{v})\right\} \\
&\quad +\frac{1}{2}\sum_{k=0}^{N-1}\Delta t(\mathbf{u} - \mathbf{v})^{\mathrm{T}}\Xi_r\Gamma^{*-1}\Xi_r\left\{\frac{\Delta\mathbf{u}}{\Delta t} - \frac{1}{2}\frac{\Delta\Gamma^{-1}}{\Delta t}\Xi_r(\mathbf{u} - \mathbf{v})\right\} \\
&\quad -i\sum_{k=0}^{N-1}\Delta t\bar{H}_{k+1,k} \\[4pt]
&= \frac{i}{2}\sum_{k=0}^{N-1}\Delta t(\mathbf{u} - \mathbf{v})^{\mathrm{T}}\Xi_r\left(\Gamma^{-1}\frac{\partial\bar{H}}{\partial\mathbf{u}} - \Gamma^{*-1}\frac{\partial\bar{H}}{\partial\mathbf{v}}\right) - i\sum_{k=0}^{N-1}\Delta t\bar{H}_{k+1,k}.
\end{aligned}
\tag{2.89}
\tag{2.90}
$$

In the transformation from Eq. (2.89) to Eq. (2.90), we used Eq. (2.84) and Eq. (2.85). Then, in the limit $N \to \infty$, $\tilde{\phi}_N$ becomes

$$
\tilde{\phi}_N \to i\int_0^t d\tau\left\{\frac{1}{2}(\mathbf{u} - \mathbf{v})^{\mathrm{T}}\Xi_r\left(\Gamma^{-1}\frac{\partial\bar{H}}{\partial\mathbf{u}} - \Gamma^{*-1}\frac{\partial\bar{H}}{\partial\mathbf{v}}\right) - \bar{H}\right\}.
\tag{2.91}
$$

Before calculating $\det(\mathbf{M}_N)$, we need to examine the time derivative of Eq. (2.26). By use of Eq. (2.84) and Eq. (2.85), we obtain

$$
\begin{aligned}
\frac{d}{dt}\begin{pmatrix} \mathbf{U_u} & \mathbf{U_v} \\ \mathbf{V_u} & \mathbf{V_v} \end{pmatrix} &= \begin{pmatrix} \frac{1}{2}\dot{\Gamma}^{-1}\Xi_r - i\Xi_r^{-1}\frac{\partial^2\bar{H}}{\partial\mathbf{v}\partial\mathbf{u}} & -\frac{1}{2}\dot{\Gamma}^{-1}\Xi_r - i\Xi_r^{-1}\frac{\partial^2\bar{H}}{\partial\mathbf{v}\partial\mathbf{v}} \\ -\frac{1}{2}\dot{\Gamma}^{*-1}\Xi_r + i\Xi_r^{-1}\frac{\partial^2\bar{H}}{\partial\mathbf{u}\partial\mathbf{u}} & \frac{1}{2}\dot{\Gamma}^{*-1}\Xi_r + i\Xi_r^{-1}\frac{\partial^2\bar{H}}{\partial\mathbf{u}\partial\mathbf{v}} \end{pmatrix}\begin{pmatrix} \mathbf{U_u} & \mathbf{U_v} \\ \mathbf{V_u} & \mathbf{V_v} \end{pmatrix} \\
&= \begin{pmatrix} \mathbf{B}_{11} & \mathbf{B}_{12} \\ \mathbf{B}_{21} & \mathbf{B}_{22} \end{pmatrix}\begin{pmatrix} \mathbf{U_u} & \mathbf{U_v} \\ \mathbf{V_u} & \mathbf{V_v} \end{pmatrix}.
\end{aligned}
\tag{2.92}
$$

We introduce $\mathbf{B}$ for simple notation and we note $\mathbf{B}_k$ as $\mathbf{B}(t_k) = \mathbf{B}_k$. Then, $\mathbf{A}_k$ can be expressed as

$$
\mathbf{A}_k = \begin{pmatrix} \mathbf{A}_{k,11} & \mathbf{A}_{k,12} \\ \mathbf{A}_{k,21} & \mathbf{A}_{k,22} \end{pmatrix} = \begin{pmatrix} \mathbf{O} & i\mathbf{E} \\ i\mathbf{E} & \mathbf{O} \end{pmatrix} + i\Delta t\begin{pmatrix} -\mathbf{B}_{k,21} & -\mathbf{B}_{k,22} \\ \mathbf{B}_{k,11} & \mathbf{B}_{k,12} \end{pmatrix}.
\tag{2.93}
$$

In general, the relation

$$
\det \begin{pmatrix} \mathbf{L}_{11} & \mathbf{L}_{12} \\ \mathbf{L}_{21} & \mathbf{L}_{22} \end{pmatrix} = \det \begin{pmatrix} \mathbf{E} & \mathbf{O} \\ -\mathbf{L}_{21}\mathbf{L}_{11}^{-1} & \mathbf{E} \end{pmatrix} \det \begin{pmatrix} \mathbf{L}_{11} & \mathbf{L}_{12} \\ \mathbf{L}_{21} & \mathbf{L}_{22} \end{pmatrix}
$$

$$
= \det \begin{pmatrix} \mathbf{L}_{11} & \mathbf{L}_{12} \\ \mathbf{O} & \mathbf{L}_{22} - \mathbf{L}_{21}\mathbf{L}_{11}^{-1}\mathbf{L}_{12} \end{pmatrix}
$$

$$
= \det(\mathbf{L}_{11}) \det(\mathbf{L}_{22} - \mathbf{L}_{21}\mathbf{L}_{11}^{-1}\mathbf{L}_{12}) \tag{2.94}
$$

holds if $\mathbf{L}_{11}^{-1}$ exist,where $\mathbf{L}_{11}$ and $\mathbf{L}_{22}$ is $n_1 \times n_1$ and $n_2 \times n_2$ matrix respectively. Therefore, using the matrices $\tilde{\mathbf{A}}_k$ defined recursively as

$$
\tilde{\mathbf{A}}_{k+1} = \mathbf{A}_{k+1} - \begin{pmatrix} \mathbf{O} & -i\mathbf{E} \\ \mathbf{O} & \mathbf{O} \end{pmatrix} \tilde{\mathbf{A}}_k^{-1} \begin{pmatrix} \mathbf{O} & \mathbf{O} \\ -i\mathbf{E} & \mathbf{O} \end{pmatrix}
$$

$$
= \mathbf{A}_{k+1} + \begin{pmatrix} (\tilde{\mathbf{A}}_k^{-1})_{22} & \mathbf{O} \\ \mathbf{O} & \mathbf{O} \end{pmatrix} \tag{2.95}
$$

with

$$
\tilde{\mathbf{A}}_1 = \mathbf{A}_1. \tag{2.96}
$$

Then $\det(\mathbf{M}_N)$ can be expressed as

$$
\det(\mathbf{M}_N) = \prod_{k=1}^{N} \det(\tilde{\mathbf{A}}_k). \tag{2.97}
$$

Now we calculate $\tilde{\mathbf{A}}_k$. Because of Eq. (2.95), the submatrix of $\tilde{\mathbf{A}}_k$ except for $\tilde{\mathbf{A}}_{k,11}$ are identical to that of $\mathbf{A}_k$, namely

$$
\tilde{\mathbf{A}}_{k,12} = \mathbf{A}_{k,12}, \quad \tilde{\mathbf{A}}_{k,21} = \mathbf{A}_{k,21}, \quad \tilde{\mathbf{A}}_{k,22} = \mathbf{A}_{k,22} \tag{2.98}
$$

and we can express $\tilde{\mathbf{A}}_k$ as

$$
\tilde{\mathbf{A}}_k = \begin{pmatrix} \tilde{\mathbf{A}}_{k,11} & i\mathbf{E} \\ i\mathbf{E} & \mathbf{O} \end{pmatrix} + i\Delta t \begin{pmatrix} \mathbf{O} & -\mathbf{B}_{k,22} \\ \mathbf{B}_{k,11} & \mathbf{B}_{k,12} \end{pmatrix}. \tag{2.99}
$$

By substituting Eq. (2.99) into Eq. (2.95), we obtain

$$
\tilde{\mathbf{A}}_{k+1,11} = \tilde{\mathbf{A}}_{k,11} + \Delta t(-i\mathbf{B}_{k+1,21} + \mathbf{B}_{k,22}\tilde{\mathbf{A}}_{k,11} - \tilde{\mathbf{A}}_{k,11}\mathbf{B}_{k,11} - i\tilde{\mathbf{A}}_{k,11}\mathbf{B}_{k,12}\tilde{\mathbf{A}}_{k,11}) \tag{2.100}
$$

for $k \geq 1$. Eq. (2.100) also holds when $k = 0$ if we set $\tilde{\mathbf{A}}_{0,11}$ as

$$
\tilde{\mathbf{A}}_{0,11} = \mathbf{O} .
$$

Therefore, the continuous limit of $\tilde{\mathbf{A}}_{k,11}$ becomes

$$
\dot{\tilde{\mathbf{A}}}_{11} = -i\mathbf{B}_{21} + \mathbf{B}_{22}\tilde{\mathbf{A}}_{11} - \tilde{\mathbf{A}}_{11}\mathbf{B}_{11} - i\tilde{\mathbf{A}}_{11}\mathbf{B}_{12}\tilde{\mathbf{A}}_{11} \tag{2.101}
$$

with

$$\tilde{\mathbf{A}}_{11}(0) = \mathbf{O}$$

and $\tilde{\mathbf{A}}_{11}$ becomes

$$\tilde{\mathbf{A}}_{11} = -i\mathbf{V_u}\mathbf{U_u}^{-1}. \tag{2.102}$$

It can be shown easily by Eq. (2.92). As a result, $\tilde{\mathbf{A}}$ becomes

$$\tilde{\mathbf{A}} = \begin{pmatrix} -i\mathbf{V_u}\mathbf{U_u}^{-1} & i\mathbf{E} \\ i\mathbf{E} & \mathbf{O} \end{pmatrix} + i\Delta t \begin{pmatrix} \mathbf{O} & -\mathbf{B}_{22} \\ \mathbf{B}_{11} & \mathbf{B}_{12} \end{pmatrix} \tag{2.103}$$

and $\det(\mathbf{M}_N)$ becomes in the continuous limit

$$\begin{aligned}
\det(\mathbf{M}_N) &\rightarrow \exp\left[\int_0^t d\tau\,\mathrm{Tr}\left[\begin{pmatrix} -i\mathbf{V_u}\mathbf{U_u}^{-1} & i\mathbf{E} \\ i\mathbf{E} & \mathbf{O} \end{pmatrix}^{-1}\begin{pmatrix} \mathbf{O} & -\mathbf{B}_{22} \\ \mathbf{B}_{11} & \mathbf{B}_{12} \end{pmatrix}\right]\right] \\
&= \exp\left[\int_0^t d\tau\,\mathrm{Tr}(\mathbf{B}_{11} - \mathbf{B}_{22} + \mathbf{B}_{12}\mathbf{V_u}\mathbf{U_u}^{-1})\right]. \tag{2.104}
\end{aligned}$$

Next, we simplify Eq. (2.104) by the relation obtained from Eq. (2.92) as

$$\mathbf{B}_{12}\mathbf{V_u} = -\mathbf{B}_{11}\mathbf{U_u} + \dot{\mathbf{U}}_{\mathbf{u}} \ . \tag{2.105}$$

Then, $\det(\mathbf{M}_N)$ becomes

$$\begin{aligned}
\det(\mathbf{M}_N) &\rightarrow \exp\left[\int_0^t d\tau\,\mathrm{Tr}(-\mathbf{B}_{22} + \dot{\mathbf{U}}_{\mathbf{u}}\mathbf{U_u}^{-1})\right] \\
&= \exp\left[-\int_0^t d\tau\,\mathrm{Tr}(\mathbf{B}_{22})\right]\cdot\det(\mathbf{U_u}). \tag{2.106}
\end{aligned}$$

We simplify $\det(\mathbf{M}_N)$ more. Since $\mathbf{B}_{22}$ is expressed as

$$\mathbf{B}_{22} = \frac{1}{2}\dot{\boldsymbol{\Gamma}}^{*-1}\boldsymbol{\Xi}_{\mathrm{r}} + i\boldsymbol{\Xi}_r^{-1}\frac{\partial^2 \bar{H}}{\partial\mathbf{u}\partial\mathbf{v}} \tag{2.107}$$

and $\mathrm{Tr}(\dot{\boldsymbol{\Gamma}}^{*-1}\boldsymbol{\Xi}_{\mathrm{r}})$ can be transformed as

$$\begin{aligned}
\mathrm{Tr}(\dot{\boldsymbol{\Gamma}}^{*-1}\boldsymbol{\Xi}_{\mathrm{r}}) &= \mathrm{Tr}(-\boldsymbol{\Gamma}^{*-1}\dot{\boldsymbol{\Gamma}}^{*}\boldsymbol{\Gamma}^{*-1}\cdot 2\boldsymbol{\Gamma}^{*}(\boldsymbol{\Gamma}+\boldsymbol{\Gamma}^{*})^{-1}\boldsymbol{\Gamma}) \\
&= -2\mathrm{Tr}(\dot{\boldsymbol{\Gamma}}^{*}(\boldsymbol{\Gamma}+\boldsymbol{\Gamma}^{*})^{-1}\boldsymbol{\Gamma}\boldsymbol{\Gamma}^{*-1}) \\
&= -2\mathrm{Tr}(\dot{\boldsymbol{\Gamma}}^{*}(\boldsymbol{\Gamma}+\boldsymbol{\Gamma}^{*})^{-1}(\boldsymbol{\Gamma}+\boldsymbol{\Gamma}^{*}-\boldsymbol{\Gamma}^{*})\boldsymbol{\Gamma}^{*-1}) \\
&= -2\mathrm{Tr}(\dot{\boldsymbol{\Gamma}}^{*}\boldsymbol{\Gamma}^{*}) + \mathrm{Tr}(\dot{\boldsymbol{\Gamma}}^{*}\boldsymbol{\Gamma}_{\mathrm{r}}^{-1}), \tag{2.108}
\end{aligned}$$

$\det(\mathbf{M}_N)$ becomes

$$\begin{aligned}
\det(\mathbf{M}_N) &\rightarrow \exp\left[-\int_0^t d\tau\,\mathrm{Tr}\left(\frac{1}{2}\dot{\boldsymbol{\Gamma}}^{*}\boldsymbol{\Gamma}_{\mathrm{r}}^{-1} + i\boldsymbol{\Xi}_r^{-1}\frac{\partial^2 \bar{H}}{\partial\mathbf{u}\partial\mathbf{v}}\right)\right] \tag{2.109} \\
&\quad\times\det(\boldsymbol{\Gamma}_t^{*})\det(\boldsymbol{\Gamma}_0^{*})^{-1}\det(\mathbf{U_u}) \ . \tag{2.110}
\end{aligned}$$

Finally, by use of the relations

$$\mathbf{\Gamma}_{\mathrm{r}k+1} = \mathbf{\Gamma}_{k+1,k} + \frac{1}{2}\Delta\mathbf{\Gamma}_k, \quad \mathbf{\Gamma}_{\mathrm{r}k} = \mathbf{\Gamma}_{k+1,k} - \frac{1}{2}\Delta\mathbf{\Gamma}_k^*, \tag{2.111}$$

we can calculate the continuous limit of the following term as

$$\prod_{k=0}^{N-1} \left\{ \frac{\det(\mathbf{\Gamma}_{\mathrm{r}k+1})^{1/4}\det(\mathbf{\Gamma}_{\mathrm{r}k})^{1/4}}{\det(\mathbf{\Gamma}_{k+1,k})^{1/2}} \right\} \to \exp\left[\frac{1}{8}\int_0^t d\tau\,\mathrm{Tr}(\dot{\mathbf{\Gamma}}\mathbf{\Gamma}_{\mathrm{r}}^{-1} - \dot{\mathbf{\Gamma}}^*\mathbf{\Gamma}_{\mathrm{r}}^{-1})\right]. \tag{2.112}$$

Since the following term appearing in the rest of the procedure can be calculated as

$$\exp\left[\frac{1}{8}\int_0^t d\tau\,\mathrm{Tr}(\dot{\mathbf{\Gamma}}\mathbf{\Gamma}_{\mathrm{r}}^{-1} - \dot{\mathbf{\Gamma}}^*\mathbf{\Gamma}_{\mathrm{r}}^{-1})\right]\exp\left[\frac{1}{4}\int_0^t d\tau\,\mathrm{Tr}(\dot{\mathbf{\Gamma}}^*\mathbf{\Gamma}_{\mathrm{r}}^{-1})\right]$$

$$= \exp\left[\frac{1}{4}\int_0^t d\tau\,\mathrm{Tr}(\dot{\mathbf{\Gamma}}_{\mathrm{r}}\mathbf{\Gamma}_{\mathrm{r}}^{-1})\right] = \det(\mathbf{\Gamma}_{\mathrm{r}t})^{1/4}\det(\mathbf{\Gamma}_{\mathrm{r}0})^{-1/4}, \tag{2.113}$$

on account of the result obtained above, Eq. (2.81) becomes in the continuous limit

$$\begin{aligned}
K(\mathbf{x},t,\mathbf{x}',0) &= \int \frac{d\mathbf{u}_f d\mathbf{v}_i}{(2\pi\hbar)^D}\, i^D \det(\mathbf{\Xi}_{\mathrm{r}t})^{1/2}\det(\mathbf{\Xi}_{\mathrm{r}0})^{1/2}\det(\mathbf{\Gamma}_{\mathrm{r}t})^{1/4}\det(\mathbf{\Gamma}_{\mathrm{r}0})^{-1/4} \\
&\quad \times \det(\mathbf{\Gamma}_t^*)^{-1/2}\det(\mathbf{\Gamma}_0^*)^{1/2}\det(\mathbf{U_u})^{-1/2} \\
&\quad \times \exp\left[\frac{i}{\hbar}\int_0^t d\tau\left\{\frac{1}{2}(\mathbf{u}-\mathbf{v})^{\mathrm{T}}\mathbf{\Xi}_{\mathrm{r}}(\mathbf{\Gamma}^{-1}\frac{\partial\bar{H}}{\partial\mathbf{u}} - \mathbf{\Gamma}^{*-1}\frac{\partial\bar{H}}{\partial\mathbf{v}}) - \bar{H}\right.\right. \\
&\quad \left.\left. +\frac{\hbar}{2}\mathrm{Tr}\left(\mathbf{\Xi}_{\mathrm{r}}^{-1}\frac{\partial^2\bar{H}}{\partial\mathbf{u}\partial\mathbf{v}}\right)\right\}\right]\langle\mathbf{x}|g_N\rangle\langle g_0|\mathbf{x}'\rangle, \tag{2.114}
\end{aligned}$$

which is Eq.(2.22).

Reference

[1] J. Van. Vleck, Proc. Natl. Acad. Sci. U.S.A. **14**, 178 (1928).

[2] L. Schulman, *Techniques and applications of path integration*, (Wiley, New York, 1981).

[3] W. H. Miller, J. Chem. Phys. **53**, 3578 (1970)

[4] E. Heller, J. Chem. Phys. **62**, 1544 (1975).

[5] E. Heller, J. Chem. Phys. **75**, 2923 (1981).

[6] M. Herman and E. Kluk, Chem. Phys. **91**, 27 (1984).

[7] E. Kluk, M. Herman, and H. Davis, J. Chem. Phys. **84**, 326 (1986).

[8] M. Herman, J. Chem. Phys. **85**, 2069 (1986).

[9] K. Kay, J. Chem. Phys. **100**, 4377 (1994).

[10] K. Kay, J. Chem. Phys. **100**, 4432 (1994).

[11] K. Kay, J. Chem. Phys. **101**, 2250 (1994).

[12] A. Walton and D. Manolopoulos, Chem. Phys. Lett. **244**, 448 (1995).

[13] S. Garashchuk and D. Tannor, Chem. Phys. Lett. **262**, 447 (1996).

[14] G. Stock and M. Thoss, Phys. Rev. Lett. **78**, 578 (1997).

[15] X. Sun and W. Miller, J. Chem. Phys. **110**, 6635 (1999).

[16] M. Ovchinnikov, V. Apkarian, and G. Voth, J. Chem. Phys. **114**, 7130 (2001).

[17] F. Grossmann and A. Xavier, Jr., Phys. Lett. A **243**, 243 (1998).

[18] M. Baranger, M. de Aguiar, F. Keck, H. Korsch, and B. Schellhaaß, J. Phys. A **34**, 7227 (2001).

[19] M. Baranger, M. de Aguiar, F. Keck, H. Korsch, and B. Schellhaaß, J. Phys. A **35**, 9493 (2002).

[20] F. Grossmann and M. Herman, J. Phys. A **35**, 9489 (2002).

[21] B. Hu, Q. Jie, B. Li, and S. Wang, Phys. Rev. A **63**, 44102 (2001).

[22] W. Miller, Mol. Phys. **100**, 397 (2002).

[23] W. Miller, J. Phys. Chem. B **106**, 8132 (2002).

[24] M. Child and D. Shalashilin, J. Chem. Phys. **118**, 2061 (2003).

[25] K. Kay, Chem. Phys. **322**, 3 (2006).

[26] T. Swart and V. Rousse, Comm. Math. Phys. **286**, 725 (2009).

[27] C. Harabati, J. Rost, and F. Grossmann, J. Chem. Phys. **120**, 26 (2004).

[28] D. Kosloff and R. Kosloff, J. Comput. Phys. **52**, 35 (1983).

[29] H. Yoshida, Phys. Lett. A **150**, 262, (1990); K. Takahashi and K. Ikeda, J. Chem. Phys. **99**, 8680 (1993).

Part II

Theory for excitation energy transfer in light-harvesting dendrimers and its application

Chapter 3

Equivalence between a generalized dendritic network and a set of small one-dimensional networks as a ground of linear dynamics

abstract

Dynamics on networks, or graphs composed of nodes and edges give profound insights about the relation between geometrical structure and functions of the modeled objects. In this chapter, we study linear dynamical systems defined on dendritic graphs, which include classical mechanics with quadratic potential energy function, quantum mechanics and other mechanics represented in linear operators. It has been known that, in some special cases, linear dynamical systems defined on a dendritic graph can be equivalently transformed into those defined on a set of small one-dimensional graphs and the transformation, which we call linear chain (LC) decomposition, is of great importance in understanding the relation between structure and functions. Unfortunately, the systems known to be LC decomposable are limited. We therefore clarify general conditions that determine the feasibility of LC decomposition in terms of the group theory, which enable us to understand the known LC decomposable cases in a unified way. As a result of the discussion about the general conditions, the class of LC decomposable systems is expanded in three aspects: (i) the class of dendritic graphs on which linear operators are defined; (ii) the class of symmetry groups under which linear operators are invariant; (iii) the type of linear operators, which includes Laplacians, normalized Laplacians, quantum Hamiltonians, real symmetry matrices representing quadratic potential in classical dynamics. In addition, even though the usefulness of LC decomposition have been shown in the special cases in the literatures, we examine coherent quantum dynamics

on a dendritic graph in terms of excitation energy transfer as another example where the result can be well explained in terms of the simple picture of LC decomposition. By numerical calculations, it is found that too strong intra-generation (a layer consisting of a dendritic graph) interactions disrupt the transfer of population over generations. The reason for this fact is clearly explained with the help of LC decomposition.

3.1 Introduction

Dendrimers are molecules with hyper-branched structure composed of small molecules and they are expected to be used as functional molecules in various fields such as drug delivery molecules in medical chemistry [1], antenna system in the artificial photosynthetic system and so on [2,3]. Especially, light-harvesting dendrimers, which absorb photons at pigment molecules embedded in the peripheral parts and transfer the light energy to the core molecule (molecule bonded to the root of a dendrimer), have attracted much attention not only as a potential devise in artificial photosynthetic systems but also as an example that the geometric structure strongly affects the properties or functions, since experimental studies showed that the efficiency of the excitation energy transfer (EET) in light-harvesting dendrimers highly depends on their geometric structure [4–6]. This fact is a typical example suggesting that there is certain relation between the geometric structure and the function of dendrimers.

It is quite often the case that large-size molecules or molecular aggregates composed of many small molecules show their unique properties or functions that the each single small molecules does not. To reveal the relation between the geometric structure of the large molecules and their properties or functions, a number of theoretical studies have adopted models that extract the structural features and ignore inessential aspects. For example, dynamics that is (or can be interpreted as) defined on graphs composed of nodes and edges have been intensively studied in various fields such as quantum walk on graphs [7,8], relaxation process of macromolecules [9], and other transfer dynamics [10].

These dynamics on graphs is often described in the picture of linear dynamics. For example, there have been studies based on linear dynamics described by classical mechanics with quadratic potential energy function, where a real symmetric matrix is used to denote the quadratics [11–22] or by other mechanics with a linear operator including Laplacian [23–31], normalized Laplacian [32], quantum Hamiltonian [33–42] and other types of linear operator [43–47]. In such cases, the dynamics is mainly characterized by eigenvalues and/or eigenvectors of the matrix or the linear operators. Therefore, finding ways to determine the eigenvalues and the eigenvectors is of importance. Actually, the ways have been revealed in some classes of graphs including regular hypercubic lattices [9,23], dual Sierpinski gaskets [24,25], Vicsek fractals [26,27], other fractal

graphs [31, 32] and dendritic graphs known as Cayley trees [11] and Husimi cacti [16, 30].

Turning now to the topic about dendrimers, there have also been many theoretical studies using the linear dynamical system defined on graphs [11–22, 28–30, 32–48]. However, only a few studies directly focus on the symmetry of dendrimers. For example, Cai and Chen have obtained all eigenmodes of Laplacian defined on Cayley trees [11] and Galiceanu and Blumen have obtained that of Husimi cacti [16, 30].

The linear operators defined on the dendritic graphs in these studies have a common remarkable property: with proper change of basis, they can be equivalently transformed into a block diagonalized matrix (in the matrix representation) where each block matrix is in a triple diagonal form. In other words, the linear dynamical systems are transformed into those defined on a set of small one-dimensional graphs. For example, in the studies by Galiceanu and Blumen [16, 30], it is shown that the characteristic equation of the linear operator defined on a Husimi cactus can be decomposed into a product of determinants of some triple diagonal matrices. In this chapter, we refer to such transformations as linear chain (LC) decomposition. The meaning of LC decomposition is that the dynamics on a dendritic graph is nothing but a superposition of some one-dimensionally-linked modes of motion although it is originally defined on a complicated dendritic graph. Such simplification may be helpful to understand the relation between the structure and the functions of dendritic systems. Actually, the past studies have fully utilized this simple picture of LC decomposition.

In spite of the advantage of LC decomposition in understanding dendritic systems, the systems shown to be LC decomposable are unfortunately limited in the studies mentioned above [11, 16, 30]. In addition, since the main aim of these studies is not investigating LC decomposition itself in detail, little is known about general conditions that determine whether a given system is LC decomposable.

In this chapter, we therefore aim at clarifying the general conditions for LC decomposition. We discuss the conditions in terms of the group theory to make the discussion rigorous. Firstly, we preliminarily define a general class of dendritic graphs and its notation. After the definition, symmetry groups representing the symmetry of the systems defined on the general dendritic graphs are introduced. Then, we propose two sufficient conditions for LC decomposition, one of which is imposed on the symmetry group and another is imposed on the linear operator of the system. It turns out that, if the sufficient conditions are satisfied, the linear operator which is invariant under the action of the symmetry group becomes LC decomposable. LC decomposition is realized by changing the basis of the linear operator into that composed of the irreducible representation of the symmetry group.

We also examine coherent quantum dynamics modeling EET in light-harvesting dendrimers as another example in which LC decomposition can provide clear explanations

for the result even though the past studies [11, 16, 30] have shown the usefulness of LC decomposition. With respect to coherent quantum dynamics on dendritic graphs, there have been several studies in the context of the quantum walk [28, 29]. In these studies, magnitude of all interactions are set to be identical. However, this assumption is less realistic as the model for EET because the magnitude of interactions can differ by types of interactions in real systems of EET. In this chapter, we therefore distinguish intra-generation (a layer composed of a dendrimer) interactions from inter-generation interactions and separately investigate the role of these types of interactions. Additionally, we analyze the result utilizing LC decomposition.

This chapter is organized as follows. In Sec. II, we define a class of general dendritic graphs, their notation and the symmetry groups representing the symmetry of linear operators defined on the dendritic graphs. Then, in Sec. III, we propose the sufficient conditions for LC decomposition after clarifying the notion of LC decomposition in detail. Sec. III also shows that LC decomposition is realized by the change of basis of linear operators. In Sec. IV, some examples of LC decomposable linear operators and corresponding dendritic graphs are shown. In Sec. V, the coherent quantum dynamics are numerically examined and we analyze the result based on LC decomposition. Finally, we make concluding remarks in Sec. VI.

3.2   System and its symmetry

In this section, we first briefly review the Frenkel exciton Hamiltonian [10] as an example of the linear operators that describes dynamics on graphs composed of nodes and edges. Next, we define a general class of dendritic graphs and its notation. Lastly, symmetry groups representing the symmetry of the dendritic graphs are defined.

3.2.1   The Frenkel exciton Hamiltonian and the corresponding graph

In this chapter, we adopt the Frenkel exciton Hamiltonian as an example of linear operator describing dynamics on graphs composed of nodes and edges. We review the Hamiltonian first and clarify the correspondence between the Hamiltonian and graphs.

The Frenkel exciton Hamiltonian is a Hamiltonian that is frequently used for modeling the quantum dynamics of the EET in molecular aggregates. We here assume that the system to be consider has n pigment molecules and each of these pigment molecules has only two states, i.e. the ground state and an excited state. Under this assumption, the total coupled system has 2^n states. The Frenkel exciton Hamiltonian is defined on

these 2^n states and has the form

$$\hat{H} = \sum_i E_i \hat{a}_i^\dagger \hat{a}_i + \sum_{i,j \ (i \neq j)} J_{ij} \hat{a}_i^\dagger \hat{a}_j \ , \qquad (3.1)$$

where $\hat{a}_i^\dagger$ $(\hat{a}_i)$ is the creation (annihilation) operator for excitation of the i th molecule, E_i is the excitation energy of the i th molecule and J_{ij} is the interaction energy between the i th and the j th molecules, which satisfies $J_{ij} = J_{ji}^*$.

In the dynamics described by Eq. (3.1), the number of excited molecules $\langle \sum_i \hat{a}_i^\dagger \hat{a}_i \rangle$ is conserved. Therefore, in many cases, it is convenient to restrict the Hamiltonian so that it acts only on a subset of 2^n states where all states in it have same number of excited molecules. For example, by restricting the action of Eq. (3.1) to n states $|i\rangle (\equiv \hat{a}_i^\dagger |0\rangle$ for $i = 1, 2, \cdots, n)$, which represent the states where only the i th molecule is excited and other molecules are at their ground state ($|0\rangle$ is the ground state of the total system), Eq. (3.1) is rewritten as

$$\hat{H} = \sum_i E_i |i\rangle\langle i| + \sum_{i,j \ (i \neq j)} J_{ij} |i\rangle\langle j| \ . \qquad (3.2)$$

In this chapter, we use the latter restricted Hamiltonian for simplicity.

The Hamiltonians mentioned above can be applied not only to the EET but also to other transference phenomena. Therefore, we use general terms aside from EET hereafter by replacing the term "molecule" with "site". For example, E_i and J_{ij} is called the site energy of the i th site and the interaction energy between the i and the j th site respectively. In addition, we simply refer to the one-exciton state $|i\rangle$ as the state of the i th site.

In the second place, we clarify the way to represent the Hamiltonian Eq. (3.2) by a graph composed of nodes and edges. Firstly, assume that the sites in the system are represented by nodes in the graph: the node with the index i means that there exist the site i and the state $|i\rangle$ in the system. Secondly, assume that the non-zero interactions between two states are represented by edges linking two corresponding nodes. Under this assumption, there is no interaction between two states not linked by an edge in the graph. Note that the magnitude of the site energy and the interaction energy of each sites are not determined here. These quantities are to be determined properly in the next section. Fig. 3.1 shows an example of graph representing a Frenkel exciton Hamiltonian. It can be read from this graph that the system represented by this graph is composed of the three states $|1\rangle, |2\rangle, |3\rangle$ and the non-zero interaction energy exists only between the site 1 and the site 2.

3.2.2 Definition and notation of general dendritic graphs

We define a general class of dendritic graphs here. Firstly, the configuration of nodes in the graph is defined together with its notation. We also define the index of each sites

Figure 3.1: An example of graphs composed of nodes and edges on which a Frenkel exciton Hamiltonian is defined. Nodes represent the states of the system. Edges represent non-zero interactions between corresponding two sites.

in the graph.

The geometric structure of dendrimers is characterized in terms of the iteration of branching. Namely, starting from the innermost sites, which can generally be more than one, several branches emerge from inner sites to outer sites. Then, the layers of sites are formed over the iteration of branching. The layer of sites is often called generation. Dendrimers are composed as a result of the branching over many generations.

Focusing on the iteration of branching, we denote the configuration of nodes in a dendritic graph with L generations by a set of L integers $(n_1, n_2, \cdots, n_L)$, where n_1 is the number of sites in the first (innermost) generation and n_l $(l > 1)$ means that each site in the $(l-1)$th generation is linked to n_l sites in the lth generation without duplication. As an example, Fig. 3.2 shows a graph whose configuration of nodes is represented by $(1, 2, 2)$. Note that the sites in Fig. 3.2 are linked with dotted lines because we have not determined the magnitude of the interactions between two sites yet.

The configuration of sites in the typical class of dendritic graphs can also be represented by this notation. That of the Cayley tree with f branches and corresponding Husimi cactus are denoted by $(1, f, f-1, f-1, \cdots)$ and $(f, f-1, f-1, \cdots)$, respectively. In the case of the graph modeling the light-harvesting dendrimer known as D127 [4], which is made up of phenyl acetylenes, its configuration is represented by $(1, 3, 1, 1, 1, 2, 1, 1, 2, 1, 2, 2)$.

An important feature of the dendritic graphs defined here is that the number of branching n_l can differ from each generations. This freedom expands the class of dendritic graphs. For example, by setting $n_l = 1$, one can readily extend the length of branches between two branching nodes as is shown in the example of D127.

Next, we define the index of each site or node in the dendritic graph whose configuration of sites is $(n_1, n_2, \cdots, n_L)$. The index for the sites in the lth generation is
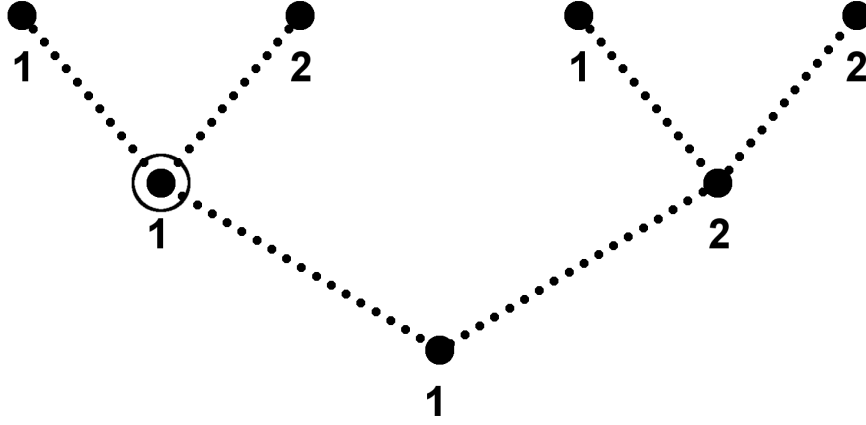
46

Figure 3.2: A dendritic graph whose configuration of nodes is represented by $(1, 2, 2)$. The circled node is represented by an index $(1, 1)$. Dotted lines means that magnitudes of interaction terms between two sites have not been determined.

denoted by a set of l integer $\mathbf{b}^{(l)} = (b_1, b_2, \cdots, b_l)$, where

$$1 \leq b_k \leq n_k \ (1 \leq k \leq l) . \tag{3.3}$$

Each site in the dendritic graph is represented by the index in the following recursive way. Firstly, the b_1th site in the first generation is represented by

$$\mathbf{b}^{(1)} = (b_1) . \tag{3.4}$$

Then, the b_kth site in the n_k sites emerging from the site $\mathbf{b}^{(k-1)}$ in the $(k-1)$th generation is represented by

$$\mathbf{b}^{(k)} = (\mathbf{b}^{(k-1)}, b_k) . \tag{3.5}$$

In other words, the site $\mathbf{b}^{(k)}$ is the site that can be reached by starting from the b_1th site in the first generation and following the b_kth branch from the $(k-1)$th generation to the kth generation. For example, the circled site in Fig. 3.2 is represented by the index $(1, 1)$.

We denote the set of all indexes for sites in the lth generation by B_l. In addition, terms used for relatively specifying a site from another site are introduced. If the first l_1 elements in the index for the node $\mathbf{b}^{(l_2)} \in B_{l_2}$ $(l_1 < l_2)$ are equal to the index for the node $\mathbf{b}^{(l_1)} \in B_{l_1}$, we refer to the node $\mathbf{b}^{(l_2)}$ as a descendant node of the node $\mathbf{b}^{(l_1)}$ and the node $\mathbf{b}^{(l_1)}$ as an ancestor node of the node $\mathbf{b}^{(l_2)}$. Especially in the case that these two nodes are in adjacent generations (i.e. $|l_2 - l_1| = 1$), we refer to these nodes as a child node and a parent node.

3.2.3 Definition of symmetry groups representing the symmetry of dendritic graphs

Next, we define symmetry operations acting on the dendritic graph. Suppose that the dendritic graph is represented by $(n_1, n_2, \cdots, n_L)$ and $(G_1, G_2, \cdots, G_L)$ is a set of groups, where G_l is a subgroup of the symmetric (permutation) group S_{n_l}. The portion of the dendritic graph composed of all the descendant nodes of $\mathbf{b}^{(k)} \in B_k$ has a n_{k+1}-fold structure, each of which is originated from one of the n_{k+1} branches emerging from $\mathbf{b}^{(k)}$. Then, we define a symmetry operation that transforms (permutates, rotates or inverts) only this portion by a element in G_{k+1} ($\subset S_{n_{k+1}}$) and does not change the remaining part. To be specific, the symmetry operation $\sigma^{(k+1)}[\mathbf{b}^{(k)}]$ with respect to $\sigma^{(k+1)} \in G_{k+1}$ and the node $\mathbf{b}^{(k)} \in B_k$ is defined as follows. If the first k elements in $\mathbf{b}^{(k)}$ and $\tilde{\mathbf{b}}^{(l)} \in B_l$ are identical, $\tilde{\mathbf{b}}^{(l)}$ is mapped by $\sigma^{(k+1)}[\mathbf{b}^{(k)}]$ as

$$\sigma^{(k+1)}[\mathbf{b}^{(k)}](\tilde{\mathbf{b}}^{(l)}) = (\tilde{b}_1, \cdots, \tilde{b}_k, \sigma^{(k+1)}(\tilde{b}_{k+1}), \tilde{b}_{k+2}, \cdots, \tilde{b}_l) \ , \tag{3.6}$$

and otherwise,

$$\sigma^{(k+1)}[\mathbf{b}^{(k)}](\tilde{\mathbf{b}}^{(l)}) = \tilde{\mathbf{b}}^{(l)} \ . \tag{3.7}$$

By this symmetry operation, n_{k+1} peripheral parts emerging from the node $\mathbf{b}^{(k)}$ are permutatated. For instance, if $\sigma^{(k+1)}$ is the transposition of 1 and 2, $\sigma^{(k+1)}[\mathbf{b}^{(k)}]$ transpose the first and the second peripheral parts. Figure 3.3 gives a schematic explanation of this symmetry operation.

Lastly, we define a group that is generated from $(G_1, G_2, \cdots, G_L)$, which represents the symmetry of the dendritic graph. By regarding all symmetry operations with respect to all nodes defined above as generators, a symmetry group acting on the dendritic graph is obtained. We denote this group as $G[G_1, G_2, \cdots, G_L]$. For instance, the symmetry of Cayley tree with f branches and corresponding Husimi cactus are represented by $G[I, S_f, S_{f-1}, S_{f-1}, \cdots]$ and $G[S_f, S_{f-1}, S_{f-1}, \cdots]$, respectively. The symmetry of the dendritic graph modeling D127 is represented by $G[I, S_3, I, I, I, S_2, I, I, S_2, I, S_2, S_2]$ (I is the group with only the identity element).

3.3 Irreducible representation and Linear chain decomposition

In this section, the notion of LC decomposition, which can be seen in the literatures [11,16,30], is reviewed. Then, we propose two sufficient conditions for LC decomposition. The procedure of the change of basis realizing LC decomposition is also shown. The new basis gives the irreducible representations of the group $G[G_1, G_2, \cdots, G_L]$. In this
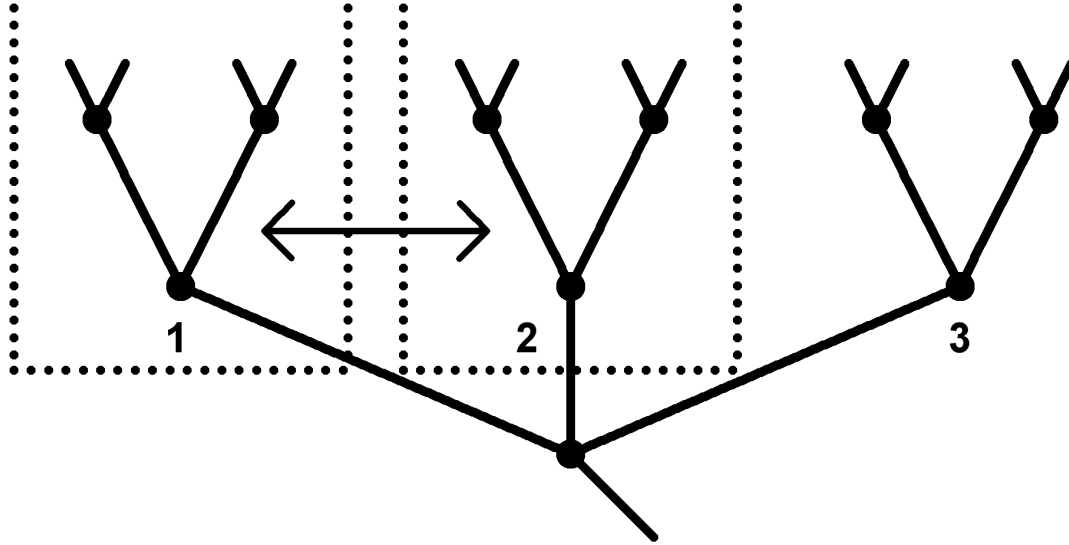
Figure 3.3: A schematic drawing of a symmetry operation. This drawing illustrate a portion of an dendritic graph composed of one node and its descendant nodes. The descendant nodes form a three-fold structure and two parts that originate from the first and the second brunch of the central node are individually surrounded by dotted lines. The example of symmetry operation permutate these two part.

change of basis, basis vectors belonging to each generation are transformed within their generation. Finally, we draw a new graph whose nodes correspond to the new basis vectors and show that the new graph is decomposed into several one-dimensionally-linked graphs like a linear chain.

3.3.1 Notion of linear chain decomposition

In order to show an example of LC decomposition, we use the Hamiltonian defined by the graph shown in Fig. 3.4. For simplicity, we assume that all site energies and non-zero interaction energies in the Hamiltonian Eq. (3.2) are unity. Under this assumption, $\hat{H}$ is written in a matrix form with respect to the basis
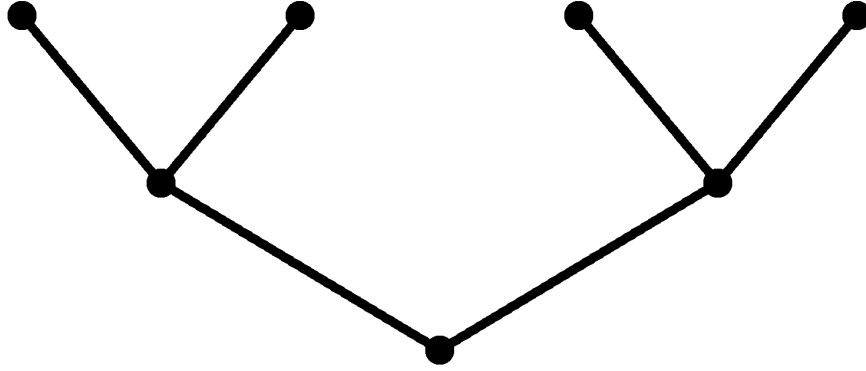
Figure 3.4: An example of dendritic graphs, whose configuration of nodes is $(1, 2, 2)$.

$\{|1\rangle, |1, 1\rangle, |1, 2\rangle, |1, 1, 1\rangle, |1, 1, 2\rangle, |1, 2, 1\rangle, |1, 2, 2\rangle\}$ as

$$\hat{H} = \begin{pmatrix} 1 & 1 & 1 & 0 & 0 & 0 & 0 \\ 1 & 1 & 0 & 1 & 1 & 0 & 0 \\ 1 & 0 & 1 & 0 & 0 & 1 & 1 \\ 0 & 1 & 0 & 1 & 0 & 0 & 0 \\ 0 & 1 & 0 & 0 & 1 & 0 & 0 \\ 0 & 0 & 1 & 0 & 0 & 1 & 0 \\ 0 & 0 & 1 & 0 & 0 & 0 & 1 \end{pmatrix} . \tag{3.8}$$

Next, we change the basis as follows;

$$
\begin{align}
|A_1^1\rangle &= |1\rangle \, , \tag{3.9a} \\
|A_1^2\rangle &= 2^{-1/2}(|1, 1\rangle + |1, 2\rangle) \, , \tag{3.9b} \\
|A_1^3\rangle &= 2^{-1}(|1, 1, 1\rangle + |1, 1, 2\rangle + |1, 2, 1\rangle + |1, 2, 2\rangle) \, , \tag{3.9c} \\
|B_1^2\rangle &= 2^{-1/2}(|1, 1\rangle - |1, 2\rangle) \, , \tag{3.9d} \\
|B_1^3\rangle &= 2^{-1}(|1, 1, 1\rangle + |1, 1, 2\rangle - |1, 2, 1\rangle - |1, 2, 2\rangle) \, , \tag{3.9e} \\
|C_1^3\rangle &= 2^{-1/2}(|1, 1, 1\rangle - |1, 1, 2\rangle) \, , \tag{3.9f} \\
|C_2^3\rangle &= 2^{-1/2}(|1, 2, 1\rangle - |1, 2, 2\rangle) \, . \tag{3.9g}
\end{align}
$$

The reason why we change the basis in this manner is clarified in later discussions. With

respect to the newly obtained basis, $\hat{H}$ is rewritten as

$$\hat{H} = \begin{pmatrix} 1 & \sqrt{2} & 0 & & & & \mathbf{O} \\ \sqrt{2} & 1 & \sqrt{2} & & & & \\ 0 & \sqrt{2} & 1 & & & & \\ & & & 1 & \sqrt{2} & & \\ & & & \sqrt{2} & 1 & & \\ & & & & & 1 & \\ \mathbf{O} & & & & & & 1 \end{pmatrix}. \qquad (3.10)$$

Notice that this matrix is decomposed into several triple diagonal submatrices.

Consequently, if we draw a new graph by assuming each new basis vectors as a node in the graph, we get the graph as illustrated in Fig. 3.5. The sets of nodes aligned vertically correspond to the sets of basis vectors $\{|A_1^l\rangle\ |l = 1, 2, 3\}, \{|B_1^l\rangle\ |l = 2, 3\}, \{|C_1^3\rangle\}, \{|C_2^3\rangle\}$ from left to right. A remarkable feature of this graph is that the total graph is composed of several segments of small graphs, each of which is one-dimensionally linked without branching like a linear chain. Compared with the original dendritic graph, this graph is far more simplified. This simplification is what we call LC decomposition, which can be seen in the literatures [11, 16, 30]. Although they do not explicitly visualize the LC decomposition as we have done here with the graph composed of nodes and edges, the simplifications in their studies are equivalent to the simplification introduced here.

As is already mentioned in the introduction, the problem of the LC decomposition, however, is that general conditions for LC decomposability are not known. The systems in the literatures [11, 16, 30] are defined specially for their studies and the general conditions for LC decomposability have not been clarified. We therefore seek the general conditions for LC decomposition in the following discussion.

3.3.2 Conditions for LC decomposition

We first propose two sufficient conditions for LC decomposition. The procedure realizing LC decomposition is shown later. The sufficient conditions are following. (LC1) The Hamiltonian $\hat{H}$ defined on a dendritic graph with its configuration $(n_1, n_2, \cdots, n_L)$ is invariant under the action of $G[G_1, G_2, \cdots, G_L]$, where the multiplicity of each irreducible representation included in the permutation representation of G_l is 1 for any l. (LC2) Non-zero interactions in $\hat{H}$ exist only in a same generation or between adjacent generations. If these two conditions are satisfied, $\hat{H}$ becomes LC decomposable. Remind that the permutation representation of G_l ($\subset S_{n_l}$) is the representation in which the action of σ ($\in G_l$) on the basis $\{|1\rangle, |2\rangle, \cdots, |n_l\rangle\}$ is defined by $|i\rangle \rightarrow |\sigma(i)\rangle$ (this action can be written in a matrix form using permutation matrices). For example, the
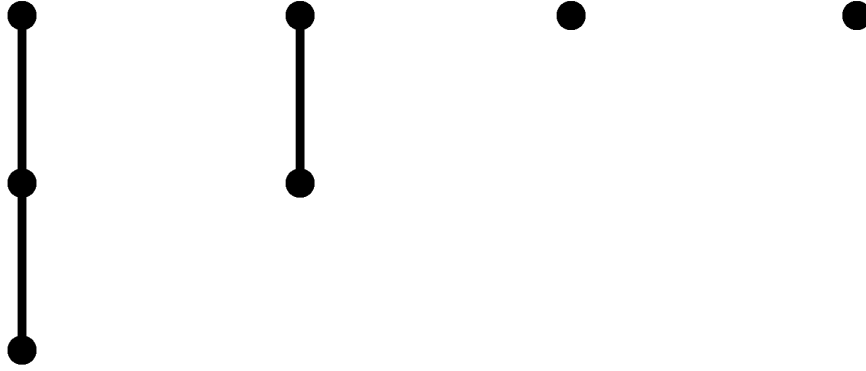
Figure 3.5: The newly obtained graph by the change of basis (see text). The segments of one-dimensional graphs correspond to the sets of basis vectors $\{|A_1^l\rangle\}, \{|B_1^l\rangle\}, \{|C_1^l\rangle\}, \{|C_2^l\rangle\}$ from left to right. The nodes that align on a same horizontal level correspond to the basis vectors belonging to a same generation.

symmetric group S_{n_l} and the group isomorphic to the point groups C_{n_l} or $C_{n_l v}$ are suitable for the components of $G[G_1, G_2, \cdots, G_L]$ in the condition (LC1).

Note that, in the condition (LC1), we have mentioned the magnitude of matrix elements of $\hat{H}$ for the first time (except for the example in the former subsection). The only condition imposed on $\hat{H}$ is the invariance under the action of $G[G_1, G_2, \cdots, G_L]$. Thus, one can arbitrarily set $\hat{H}$ as long as the condition holds. The restriction on the linear operators in this chapter is considerably less than that in the other studies related to LC decomposition.

3.3.3 Change of basis for irreducible representations of $G[G_1, G_2, \cdots, G_L]$

We show that, under the conditions (LC1) and (LC2), LC decomposition is realized by changing the basis of $\hat{H}$ so that new basis gives irreducible representations of $G[G_1, G_2, \cdots, G_L]$.

For later discussion, we first set some notations about irreducible representations of G_l (not $G[G_1, G_2, \cdots, G_L]$). We denote the series of orthonormal bases of irreducible representations included in the permutation representation of G_l as $\{|A_1^l\rangle\}, \{|B_1^l\rangle, |B_2^l\rangle, \cdots\}, \{|C_1^l\rangle, |C_2^l\rangle, \cdots\}, \cdots$. In this notation, different irreducible representations are distinguished by different alphabetic characters. We especially as-

sign the irreducible representation denoted by A to the totally symmetric irreducible representation, which is invariant under all the symmetry operations in G_l. Owing to the condition (LC1), the original basis of the permutation representation of G_l, $\{|1\rangle, |2\rangle, \cdots, |n_l\rangle\}$, can be transformed into these bases of irreducible representations of G_l without duplication. Then, we denote the transformation matrix that transforms the original basis into one of the bases of the irreducible representations $\{|X_1^l\rangle, |X_2^l\rangle, \cdots\}$ ($X = A, B, \cdots$) as x_{ij}^l ($x = a, b, \cdots$). These matrices satisfy

$$|X_j^l\rangle = \sum_{i=1}^{n_l} |i\rangle x_{ij}^l . \tag{3.11}$$

Especially, because $|A_1^l\rangle$ is a superposition of $|1\rangle, |2\rangle, \cdots, |n_l\rangle$ with equal weight, a_{i1} ($i = 1, 2, \cdots, n_l$) satisfy

$$a_{i1} = n_l^{-1/2} . \tag{3.12}$$

We now turn to the discussion about $G[G_1, G_2, \cdots, G_L]$ apart from each G_l. We first change the basis associated with sites or nodes in the dendritic graph in the following way. With respect to n_l sites in the lth ($l > 1$) generation emerging from a site $\mathbf{b} \in B_{l-1}$ (hereafter, superscript of $\mathbf{b}$ is omitted for simplicity), we transform the corresponding basis vectors $|\mathbf{b}, 1\rangle, |\mathbf{b}, 2\rangle, \cdots, |\mathbf{b}, n_l\rangle$ into new orthonormal vectors $|X_{j,\mathbf{b}}^l\rangle$ ($X = A, B, \cdots$; $j = 1, 2, \cdots$) using the transformation matrix Eq. (3.11) as

$$|X_{j,\mathbf{b}}^l\rangle = \sum_{i=1}^{n_l} |\mathbf{b}, i\rangle x_{ij}^l . \tag{3.13}$$

For the case $l = 1$, n_1 vectors in the first generation are transformed into $|X_j^1\rangle$ ($X = A, B, \cdots$; $j = 1, 2, \cdots$) in the same way as Eq. (3.11).

What is important in the new basis defined above is that basis vectors in the set $\{|A_{1,\mathbf{b}}^l\rangle | \mathbf{b} \in B_{l-1}\}$ are transformed in the exactly same manner as those in $\{|\mathbf{b}\rangle | \mathbf{b} \in B_{l-1}\}$ under the action of symmetry operations of $G[G_1, G_2, \cdots, G_L]$. This can be checked as follows. Figure 3.6 schematically shows $|\mathbf{b}\rangle$ and $|A_{1,\mathbf{b}}^l\rangle$. In Fig. 3.6, the node in a white circle is the site $\mathbf{b}$ and the nodes included in $|A_{1,\mathbf{b}}^l\rangle$ are in a white ellipse. A gray circle and an ellipse correspond to other basis vectors $|\mathbf{b}'\rangle$ and $|A_{1,\mathbf{b}'}^l\rangle$, respectively. Then, by equating the circle with the ellipse, it can be readily checked that the transformation of basis vectors in the two sets $\{|\mathbf{b}\rangle | \mathbf{b} \in B_{l-1}\}$ and $\{|A_{1,\mathbf{b}}^l\rangle | \mathbf{b} \in B_{l-1}\}$ coincide. For example, the permutation of the left side and the right side of Fig. 3.6 permutates the white circle and the gray circle and, in the same way, it permutates the white ellipse and the gray ellipse. For another example, under the permutation of the descendant nodes of a circled node, this circled node is invariant while each node in the ellipse is permutated within the ellipse. However, because all the coefficients
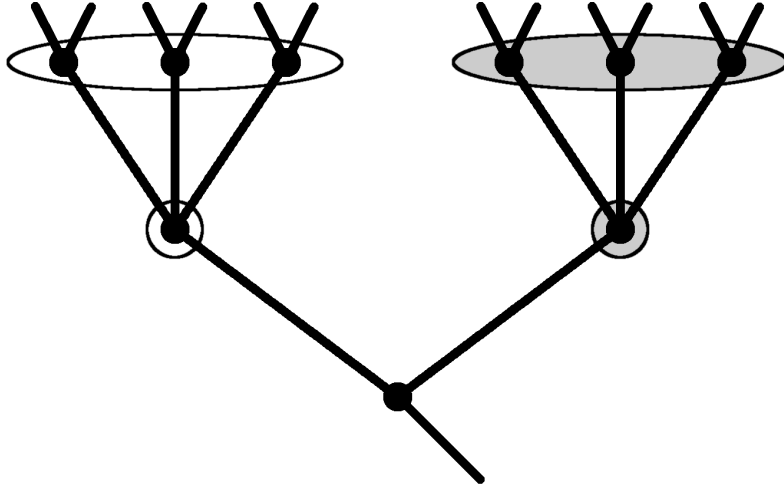
Figure 3.6: A schematic drawing of the basis vectors $|\mathbf{b}\rangle$ and $|A_{1,\mathbf{b}}^l\rangle$. The nodes surrounded by a circle corresponds to $|\mathbf{b}\rangle$ and $|\mathbf{b}'\rangle$ and the nodes surrounded by a ellipse corresponds to $|A_{1,\mathbf{b}}^l\rangle$ and $|A_{1,\mathbf{b}'}^l\rangle$. Under the operation of $G[G_1, G_2, \cdots]$, these two ellipses are transformed in the same way of the two circles as is explained in the text.

of superposition of $|A_{1,\mathbf{b}}^l\rangle$ are identical, $|A_{1,\mathbf{b}}^l\rangle$ as well as $|\mathbf{b}\rangle$ is invariant under the permutation. This is due to the fact that $|A_{1,\mathbf{b}}^l\rangle$ is originated from the totally symmetric irreducible representation of G_l. In this way, it can be checked that the transformation of the two sets $\{|\mathbf{b}\rangle|\mathbf{b} \in B_{l-1}\}$ and $\{|A_{1,\mathbf{b}}^l\rangle|\mathbf{b} \in B_{l-1}\}$ is identical. This coincidence is fully utilized later in the construction of irreducible representation of $G[G_1, G_2, \cdots, G_L]$.

Next, we decompose the basis of the system defined on the dendritic graph into the direct sum of bases of the irreducible representations of $G[G_1, G_2, \cdots, G_L]$. The procedure of this decomposition is expressed recursively with respect to generations. In the case of the first generation, the bases of the irreducible representations of $G[G_1, G_2, \cdots, G_L]$ are given by $\{|A_1^1\rangle\}, \{|B_1^1\rangle, |B_2^1\rangle, \cdots\}, \{|C_1^1\rangle, |C_2^1\rangle, \cdots\}, \cdots$, which are defined in Eq. (3.13). In the case of the lth generation, some of the bases of the irreducible representation of $G[G_1, G_2, \cdots, G_L]$ belonging to the lth generation are obtained from those belonging to the $(l-1)$th generation. Assume that $\{|Y_1^{l-1}\rangle, |Y_2^{l-1}\rangle, \cdots\}$ is one of the bases of such irreducible representations made from $\{|\mathbf{b}\rangle|\mathbf{b} \in B_{l-1}\}$ and is represented with a transformation matrix $y_{\mathbf{b}j}^{l-1}$ as

$$|Y_j^{l-1}\rangle = \sum_{\mathbf{b} \in B_{l-1}} |\mathbf{b}\rangle y_{\mathbf{b}j}^{l-1} \ (j = 1, 2, \cdots) . \tag{3.14}$$

Then, we construct a set of basis vectors $\{|Y_1^l\rangle, |Y_2^l\rangle, \cdots\}$ made from $\{|\mathbf{b}\rangle | \mathbf{b} \in B_l\}$ by using the basis vectors $\{|A_{1,\mathbf{b}}^l\rangle | \mathbf{b} \in B_{l-1}\}$ defined in Eq. (3.13) and the transformation matrix $y_{\mathbf{b}j}^{l-1}$ in Eq. (3.14) as

$$|Y_j^l\rangle = \sum_{\mathbf{b} \in B_{l-1}} |A_{1,\mathbf{b}}^l\rangle y_{\mathbf{b}j}^{l-1} \ (j = 1, 2, \cdots) . \tag{3.15}$$

Newly constructed $\{|Y_1^l\rangle, |Y_2^l\rangle, \cdots\}$ becomes a basis of the irreducible representation of $G[G_1, G_2, \cdots, G_L]$. As is mentioned above, $\{|A_{1,\mathbf{b}}^l\rangle | \mathbf{b} \in B_{l-1}\}$ and $\{|\mathbf{b}\rangle | \mathbf{b} \in B_{l-1}\}$ are transformed in a same manner under the action of $G[G_1, G_2, \cdots, G_L]$. Therefore, $\{|Y_1^l\rangle, |Y_2^l\rangle, \cdots\}$ and $\{|Y_1^{l-1}\rangle, |Y_2^{l-1}\rangle, \cdots\}$ are also transformed in a same manner. Consequently, $\{|Y_1^l\rangle, |Y_2^l\rangle, \cdots\}$ gives the irreducible representation that is isomorphic to that represented by $\{|Y_1^{l-1}\rangle, |Y_2^{l-1}\rangle, \cdots\}$.

Then, we implement this procedure to all the bases of the irreducible representations belonging to the $(l-1)$th generation and obtain corresponding bases of the irreducible representations belonging to the l th generation. Note that, for each of the irreducible representations included in the $(l-1)$th generation, there is one and only one irreducible representation in the lth generation that is isomorphic to the irreducible representation in the $(l-1)$th generation.

Next, we consider the rest of the bases of the irreducible representations of $G[G_1, G_2, \cdots, G_L]$ belonging to the lth generation. Because the number of the elements in $\{|\mathbf{b}\rangle | \mathbf{b} \in B_{l-1}\}$ is equal to that in $\{|A_{1,\mathbf{b}}^l\rangle | \mathbf{b} \in B_{l-1}\}$, the vector space spanned by all the bases of the irreducible representations in the lth generation constructed above becomes identical with the vector space spanned by $\{|A_{1,\mathbf{b}}^l\rangle | \mathbf{b} \in B_{l-1}\}$. Therefore, the remaining bases of the irreducible representations do not contain $\{|A_{1,\mathbf{b}}^l\rangle | \mathbf{b} \in B_{l-1}\}$ and are made only from $\{|B_{j,\mathbf{b}}^l\rangle, |C_{j,\mathbf{b}}^l\rangle, \cdots | \mathbf{b} \in B_{l-1}, j \geq 1\}$. Actually, the sets of basis vectors with an common alphabetic character in their index, which are written as

$$\{|X_{j,\mathbf{b}}^l\rangle | \mathbf{b} \in B_{l-1}, j \geq 1\} \ (X = B, C, \cdots) , \tag{3.16}$$

gives the remaining bases of the irreducible representations. The rigorous proof of this fact is shown in Appendix. A. However, it can be intuitively understood because each subset of basis vectors $\{|X_{j,\mathbf{b}}^l\rangle | j \geq 1\}$ of $\mathbf{b}$ $(\in B_{l-1})$ is originated from a irreducible representation of G_l.

3.3.4 A graph based on the new basis and LC decomposition

We rewrite the Hamiltonian with the new basis (i.e. the direct sum of all the bases of the irreducible representations of $G[G_1, G_2, \cdots, G_L]$ constructed above). To visualize the matrix elements of the Hamiltonian, we introduce a new graph whose nodes and edges correspond to the basis vectors and non-zero interactions between two of them, respectively.

What is important in drawing the graph is the theorem of group theory for selection rule [49]: unless two basis vectors are in a same irreducible representation and their indexes are also identical in the irreducible representation, the interaction between two basis vectors vanishes. We utilize this theorem in the following discussion.

The graph based on the new basis is drawn recursively. Firstly, we put $|B_1|$ nodes corresponding to the basis vectors in the first generation. Owing to the condition (LC1) for LC decomposition, the permutation representation of G_1 dose not contain duplicated irreducible representation and the irreducible representations of $G[G_1, G_2, \cdots, G_L]$ in the first generation do not duplicate either. Therefore, there is no intra-generation interaction. This means that no edge links two nodes in the first generation in the graph.

After we have drawn the graph until the $(l-1)$th generation, we put $|B_l|$ nodes in the graph corresponding to the basis vectors in the lth generation. As in the case of the first generation, there is no intra-generation interaction and no edge linking two nodes in the l th generation owing to the condition (LC1) for LC decomposition.

Next, we consider inter-generation interactions between the $(l-1)$th and the lth generations. As a result of the former subsection, for each irreducible representation in the $(l-1)$th generation, there is one and only one isomorphic irreducible representation in the lth generation. Therefore, there can be non-zero inter-generation interactions between two basis vectors that are in a common irreducible representation and indexes in it are also identical each other. In terms of the graph, one and only one edge emerge from each node in the $(l-1)$th generation toward the lth generation. Note that, because of the condition (LC2) for LC decomposition, inter-generation interactions exist only between adjacent generations. Figure 3.7 represents a portion of the graph composed of the nodes in the $(l-1)$th and the lth generations and the edges between them. Each node in the $(l-1)$th generation is linked to one node in the lth generation, forming an one-to-one corresponding from the $(l-1)$th generation to the lth generation. By continuing this procedure until the outermost generation, the Lth generation, we obtain a graph that is decomposed into several segments of small graphs, each of which has at most L nodes and is one-dimensionally linked like a linear chain. This means that LC decomposition is realized.

Before concluding this section, we make a remark about the two sufficient conditions for LC decomposition. Through the discussion about the realization of LC decomposition, we used the condition (LC2) only to prohibit the inter-generation interaction between non-adjacent generations. Thus, this condition has nothing to do with the irreducible representation of $G[G_1, G_2, \cdots, G_L]$. Therefore, even if we do not impose the condition (LC2), the new graph is decomposed into several small graphs and each of them has at most L nodes even though each of them no longer has a shape of a linear
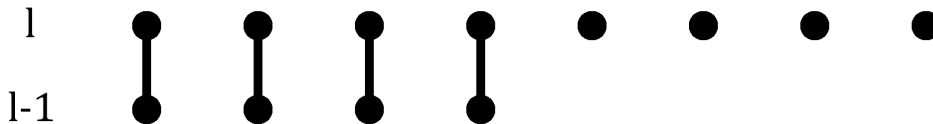
Figure 3.7: Nodes in the $l-1$ or l th generation of the new graph. Each node in the $l-1$ th generation is linked to just one node in the l th generation.

chain. The only essential condition for the decomposition of dendritic graphs is the condition (LC1). The study by Fürstenberg *et al.* [18] can be regarded as an example of the case without the condition (ii). They have shown that the matrix representing the quadratic potential energy function can be transformed into a block diagonalized form. In their study, each block diagonal matrix is not in a one-dimensionally-linked form because the semiflexibility of the dendrimer gives non-zero interaction to all pairs of two sites, which violates the condition (LC2) for LC decomposition. In their study, they have heuristically found this simplification based on an analogy from the study by Cai and Chen [11]. On the other hand, the result of this chapter can give an immediate prediction for the simplification, because the potential energy function V_{STP} in the literature [18] is apparently invariant under the symmetry operations for the dendrimer and the condition (LC1) is satisfied.

3.4 Examples of LC decomposable systems

In this section, some examples of LC decomposable Hamiltonians and corresponding graphs are shown. We also show in an example how the matrix elements of the Hamiltonian are actually transformed by LC decomposition.

3.4.1 Systems with intra-generation interactions

Figure 3.8 exhibits a graph with its configuration of nodes $(1, 2, 2)$. We define a Hamiltonian as follows: all site energies in the lth generation are E_l; all non-zero inter-generation interactions between the $l-1$ and l th generations are $J_{l-1,l}$; all non-zero intra-generation interactions in the l th generation are K_l. This Hamiltonian is invariant under the action of $G[I, S_2, S_2]$ and, according to the result of the previous section, is LC decomposable. Note that this graph is a portion of a Husimi cactus. Husimi cacti
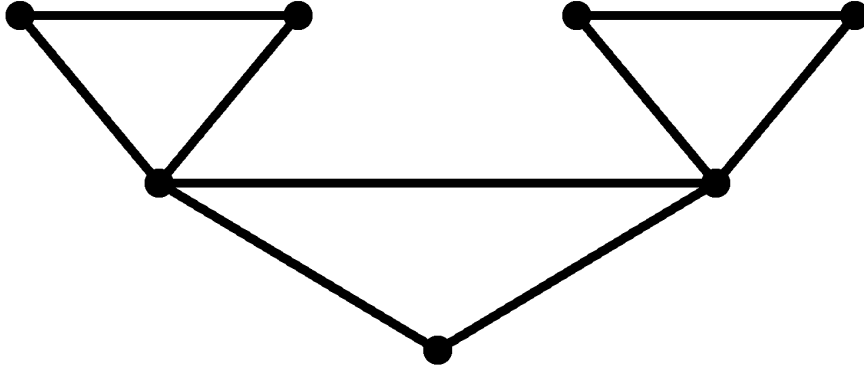
Figure 3.8: A dendritic graph, whose configuration of nodes is $(1, 2, 2)$. This can be regarded as a portion of a Husimi cactus.

are shown to be LC decomposable by Galiceanu and Blumen [16, 30] in the limiting case where all the non-zero interaction terms of the linear operator (i.e. non-diagonal elements in the corresponding matrix) are identical. On the other hand, we have shown that LC decomposition can be realized if the conditions (LC1) and (LC2) are satisfied. Therefore the interaction terms can differ from generation to generation or depend on the types of interactions (i.e. intra- or inter-generation interaction) like the Hamiltonian defined above.

Additionally, we investigate how the matrix elements of the Hamiltonian are transformed by LC decomposition. For this purpose, we change the basis vectors in each generation into the bases of the irreducible representations of $G[I, S_2, S_2]$. This change of basis is carried out along with the procedure shown in the previous section. Although the result coincides with Eqs. (3.9) after this change of basis, we actually demonstrate it as an example of the procedure to realize LC decomposition.

In the first generation, $|1\rangle$ is already a basis of the irreducible representations of $G[I, S_2, S_2]$. In order to show explicitly that $|1\rangle$ gives an irreducible representation, we denote $|1\rangle$ as $|A_1^1\rangle$:

$$|A_1^1\rangle = |1\rangle \ . \tag{3.17a}$$

In the second generation, the irreducible representation labeled by the alphabet A (recall that alphabetic characters distinguish the type of irreducible representations) is obtained by replacing $|1\rangle$ in Eq. (3.17a) with $2^{-1/2}(|1, 1\rangle + |1, 2\rangle)$, which is $|A_{1,\mathbf{b}}^1\rangle$ ($\mathbf{b} = (1)$) defined in Eq. (3.11). We denote the basis of this irreducible representation

belonging to the second generation as $\{|A_1^2\rangle\}$. Namely,

$$|A_1^2\rangle = 2^{-1/2}(|1,1\rangle + |1,2\rangle) \ . \tag{3.17b}$$

Another basis of the irreducible representation in the second generation is obtained from the antisymmetric irreducible representation of $G_2 \ (= S_2)$. We denote this basis as $\{|B_1^2\rangle\}$ and it is represented as

$$|B_1^2\rangle = 2^{-1/2}(|1,1\rangle - |1,2\rangle) \ . \tag{3.17c}$$

In the third generation, the irreducible representations labeled by A and B are obtained by replacing $|1,1\rangle$ and $|1,2\rangle$ in Eqs. (3.17b) and (3.17c) with $2^{-1/2}(|1,1,1\rangle + |1,1,2\rangle)$ and $2^{-1/2}(|1,2,1\rangle + |1,2,2\rangle)$ respectively, which are $|A_{1,\mathbf{b}}^2\rangle$ ($\mathbf{b} = (1,1), (1,2)$) defined in Eq. (3.11). We denote these bases as $\{|A_1^3\rangle\}$ and $\{|B_1^3\rangle\}$. These bases are written as

$$
\begin{aligned}
|A_1^3\rangle &= 2^{-1}(|1,1,1\rangle + |1,1,2\rangle + |1,2,1\rangle + |1,2,2\rangle) \ , \tag{3.17d} \\
|B_1^3\rangle &= 2^{-1}(|1,1,1\rangle + |1,1,2\rangle - |1,2,1\rangle - |1,2,2\rangle) \ . \tag{3.17e}
\end{aligned}
$$

Likewise, another basis of the irreducible representation in the third generation is obtained from the antisymmetric irreducible representation of $G_3 \ (= S_2)$. We denote this basis as $\{|C_1^3\rangle, |C_2^3\rangle\}$ and it is given by

$$
\begin{aligned}
|C_1^3\rangle &= 2^{-1/2}(|1,1,1\rangle - |1,1,2\rangle) \ , \tag{3.17f} \\
|C_2^3\rangle &= 2^{-1/2}(|1,2,1\rangle - |1,2,2\rangle) \ . \tag{3.17g}
\end{aligned}
$$

Next, we examine how the matrix elements are transformed by the change of basis for LC decomposition. With simple calculation of the elements using the transformed basis, we find that (i) all non-zero inter-generation interaction between the $(l-1)$th and the lth generations become $\sqrt{2}J_{l-1,l}$; (ii) the site energy of the innermost site in each linear chain becomes $E_l - K_l$, where l is the generation of the innermost sites and, exceptionally in the longest linear chain, the site energy of the innermost site becomes E_1; (iii) rest of the site energies become $E_l + K_l$, where l is the generation of the corresponding site. The result of this transformation is also true in the partial Husimi cacti with higher generation represented by $(1,2,2,2,2,\cdots)$.

Note that, while the inter-generation interactions $J_{l-1,l}$ in the original dendritic graph give the inter-generation interactions in the LC decomposed graph again, the intra-generation interactions K_l in the original dendritic graph are included in the site energies in the LC decomposed graph. Thus, it is found that the role of inter- and intra-generation interactions are apparently different in the LC decomposed picture although both of these are the interaction between two sites in the original dendritic picture. This difference in the type of interactions cannot be clearly visualized, if one assumes that all

interaction terms are identical as Galiceanu and Blumen did [16,30]. The effects of these two types of interaction in the dynamics on the dendritic graph should be separately examined and we do in the following section.

In order to make a model system realistic, it is inevitable that the magnitudes of parameters in the model system like E_l, $J_{l-1,l}$ and K_l are determined by taking values from the real systems or fitting them so that the behavior of the model system coincide with that of the real system. In both cases, parameters in the model system would depend on the generation or the types of the parameters. Even in such cases, LC decomposition can be realized if the two conditions for LC decomposition are satisfied. This freedom of the parameters may help to construct more realistic model systems.

3.4.2 Systems with ring-shaped intra-generation interactions

We show an example of the graphs where G_l in $G[G_1, G_2, \cdots, G_L]$ is not S_{n_l}. Figure 3.9 shows an example graph, whose configuration of nodes is $(1, 4, 4)$. The non-zero interactions between two sites are also shown in the graph as edges. For simplicity, we assume that all the non-zero parameters of the Hamiltonian are identical.

A noteworthy feature of this graph is that sites in a same generation are linked like a ring. Two edges emerge from one node toward two adjacent nodes and there is no diagonal edge within a same generation. In this case, G_2 and G_3 are isomorphic to the point group C_{4v} and not to S_4. Therefore, the group representing the symmetry of this graph becomes $G[I, C_{4v}, C_{4v}]$ and the Hamiltonian of this graph is LC decomposable.

3.4.3 Systems with interactions between a node and an other's child node

In all the graphs that have been shown so far, all inter-generation edges exist only between a pair of child and its parent nodes. For example, the site $(1, 1)$ in the graph shown in Fig. 3.8 is linked to only its parent node (1) and its child nodes $(1, 1, 1)$ and $(1, 1, 2)$ by edges. However, LC decomposition can be realized even in the graphs that have interactions between a node and an other's child node as long as the conditions (LC1) and (LC2) for LC decomposition are satisfied. We show some examples of such graphs. We assume all the non-zero parameters of the Hamiltonian of examples are identical for simplicity. Figures 3.10 and 3.11 represent graphs whose configuration of nodes are $(1, 2, 2)$ and $(1, 2, 1, 2, 1)$, respectively. These graphs have the interactions between a node and an other's child node. For example, the node $(1,1)$ in Fig. 3.10 is linked to the nodes $(1, 2, 1)$ and $(1, 2, 2)$, which are neither the child nodes nor the parent node of $(1, 1)$. Even in these examples, it can be readily checked that the Hamiltonian defined on these graphs are invariant under the action of $G[I, S_2, S_2]$ and $G[I, S_2, I, S_2, I]$
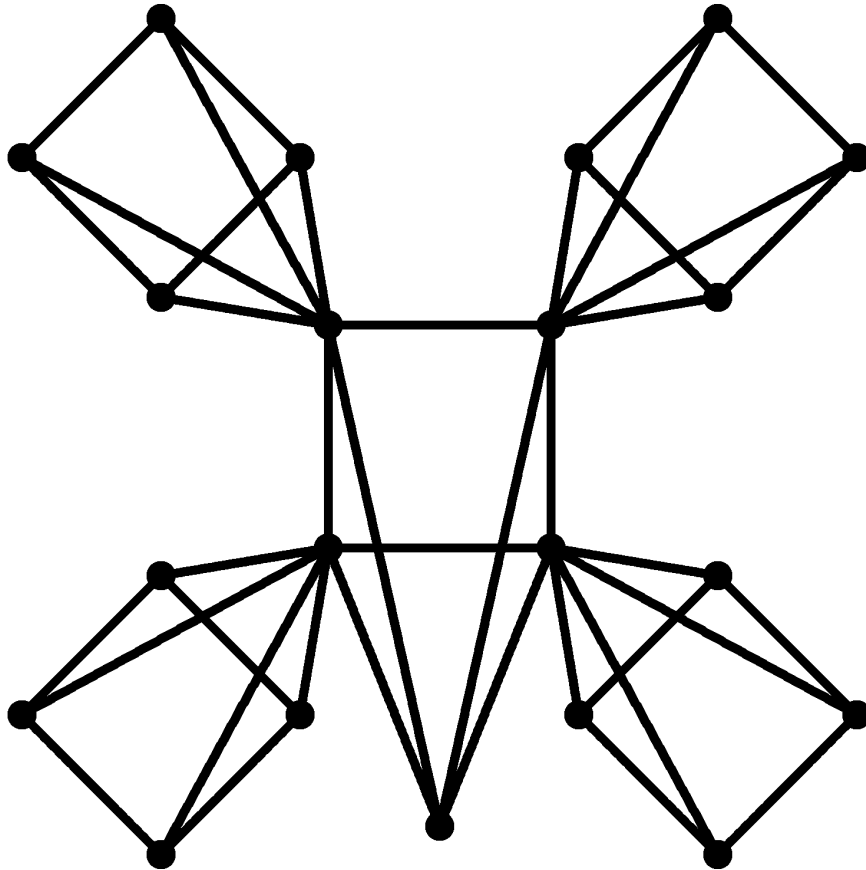
Figure 3.9: A dendritic graph, whose configuration of nodes is $(1, 4, 4)$. Within the four sites emerging from a same parent node, edges exist between pairs of adjacent nodes and there is no diagonal edge. The symmetry of this graph is represented by the group $G[I, C_{4v}, C_{4v}]$.

and are LC decomposable.

3.5 Role of intra-generation interaction in coherent dynamics on the partial Husimi cacti

In this section, we examine coherent quantum dynamics on the partial Husimi cactus, the first example in the previous section, in terms of EET. Through this study we demonstrate the usefulness of LC decomposition in analyzing phenomena on dendritic graphs.

It should be noted that Blumen *et al.* have already studied coherent quantum dynamics on Husimi cacti (not partial Husimi cacti) in terms of the continuous-time quantum walk [28, 29], where a classical transfer matrix is used as the quantum Hamiltonian to describe the dynamics. In their studies, the linear operators are restricted so that all the non-zero interactions are identical. However, as we remarked in the previous section, the role of the inter-generation interactions and the intra-generation interactions should be distinguished. Therefore, in order to reveal the effects of this difference on the coherent dynamics, we study the dynamics with various magnitudes of intra-generation interactions (and with fixed inter-generation interactions).

3.5.1 System

The system to be examined in this section is the partial Husimi cactus, which is presented in the previous section as an example of LC decomposable graph. We especially adopt the graph with 5 generations. In this section, site energies E_l, inter-generation interactions $J_{l-1,l}$ and intra-generation interaction K_l for all generation l are set at following values:

$$E_l = 0, \ J_{l-1,l} = -1, \ K_l = \alpha \ . \tag{3.18}$$

We examine the effect of the intra-generation interactions by setting α at various values.

In order to analyze the dynamics by LC decomposition, we define some notations: After changing the basis for LC decomposition, we define a set of basis vectors $L_{\mathbf{b}}$ by gathering the basis vectors that consist of each linear chain. The subscript $\mathbf{b}$ means that the innermost basis vector in $L_{\mathbf{b}}$ is $|B_{1,\mathbf{b}}^{l(\mathbf{b})+1}\rangle$ defined in Eq. (3.13), where $l(\mathbf{b})$ is the generation to which $\mathbf{b}$ belongs. In addition, because this definition of $L_{\mathbf{b}}$ does not include the longest linear chain, we exceptionally denote the set of the basis vectors of the longest linear chain by $\mathbf{b} = 0$. Note that the length of each linear chain is given by $|L_{\mathbf{b}}| = L - l(\mathbf{b})$, where L is the highest generation of the partial Husimi cactus (and $L = 5$ in the present system). According to the result of the previous section, by
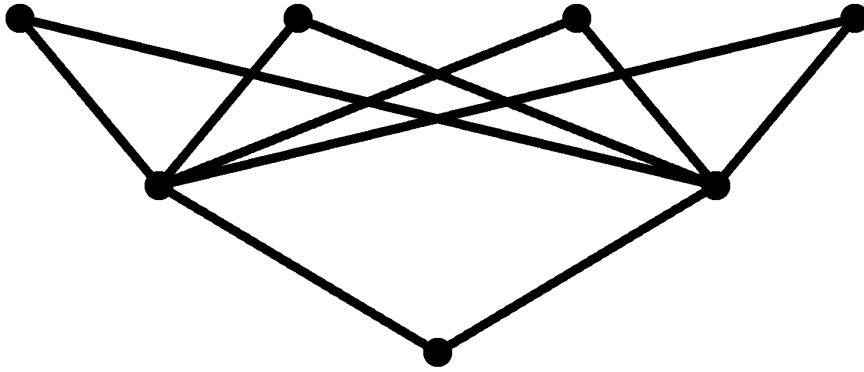
Figure 3.10: An example of dendritic graphs with edges linking a node and other's child node. In this graph, the nodes $(1, 1)$ and $(1, 2, 1)$ are linked, for example, although each of them is not the parent or child of another's.
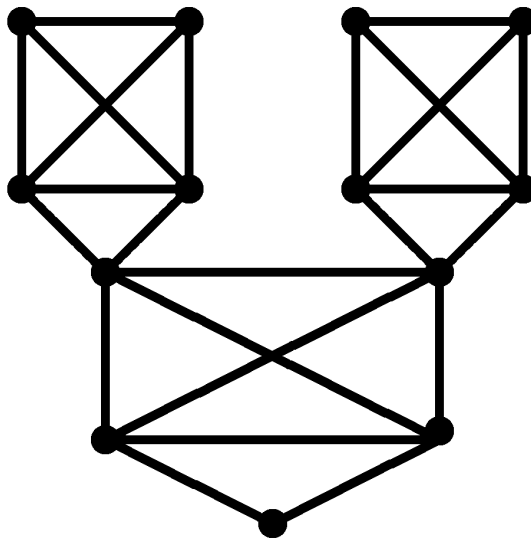

Figure 3.11: An example of dendritic graphs with edges linking a node and other's child node. In this graph, the nodes $(1, 1, 1, 1)$ and $(1, 1, 1, 2, 1)$ are linked, for example, although each of them is not the parent or child of another's.

restricting the basis to $L_{\mathbf{b}}$, the Hamiltonian is represented in a $l \times l$ matrix H^l as

$$
H^l = \begin{pmatrix}
-(1-\delta_{l,L})\alpha & -\sqrt{2} & & & \mathbf{O} \\
-\sqrt{2} & \alpha & -\sqrt{2} & & \\
& -\sqrt{2} & \alpha & \ddots & \\
& & \ddots & \ddots & -\sqrt{2} \\
\mathbf{O} & & & -\sqrt{2} & \alpha
\end{pmatrix} ,
\tag{3.19}
$$

when the length of the corresponding linear chain $|L_{\mathbf{b}}| = l$.

3.5.2 Long time average of transition probabilities

In this subsection, we present long time average of transition probabilities in a similar manner to the studies on the quantum coherent dynamics on the Husimi cacti [28, 29]. Although the definitions of quantities that characterize the dynamics are shown in their studies [28, 29] or elsewhere [7], we briefly review these definition as follows. Coherent quantum dynamics is represented by the time evolution of each state $|\mathbf{b}'\rangle$ starting at time 0, which is represented as $\exp(-it\hat{H}/\hbar)|\mathbf{b}'\rangle$ This time evolution is characterized by the transition amplitudes $\alpha_{\mathbf{b},\mathbf{b}'}(t)$, which are defined as

$$
\alpha_{\mathbf{b},\mathbf{b}'}(t) = \langle \mathbf{b}| \exp(-it\hat{H}/\hbar)|\mathbf{b}'\rangle .
\tag{3.20}
$$

Next, the transition probabilities $\pi_{\mathbf{b},\mathbf{b}'}(t)$ are defined as

$$
\pi_{\mathbf{b},\mathbf{b}'}(t) = |\alpha_{\mathbf{b},\mathbf{b}'}(t)|^2 .
\tag{3.21}
$$

In coherent quantum dynamics, the transition probabilities $\pi_{\mathbf{b},\mathbf{b}'}(t)$ never converge with any value as $t \to \infty$ in general because of their oscillation. Thus, it is convenient to consider the long-time average of the transition probabilities (LPs) $\chi_{\mathbf{b},\mathbf{b}'}$, which is defined as

$$
\chi_{\mathbf{b},\mathbf{b}'} = \lim_{T\to\infty} \frac{1}{T} \int_0^T dt \, \pi_{\mathbf{b},\mathbf{b}'}(t) .
\tag{3.22}
$$

Note that $\chi_{\mathbf{b},\mathbf{b}'}$ can be written in another form. Assume that $|E_i\rangle$ are orthonormal eigenvectors of the Hamiltonian with the eigenvalue E_i. Then, by representing the time propagator of the system as $\exp(-it\hat{H}/\hbar) = \sum_i |E_i\rangle \exp(-iE_it/\hbar)\langle E_i|$, $\chi_{\mathbf{b},\mathbf{b}'}$ is expressed as

$$
\chi_{\mathbf{b},\mathbf{b}'} = \sum_{ij} \delta_{E_i,E_j} c_{\mathbf{b}i} c^*_{\mathbf{b}j} c^*_{\mathbf{b}'i} c_{\mathbf{b}'j} ,
\tag{3.23}
$$

where $c_{\mathbf{b}i} = \langle \mathbf{b}|E_i\rangle$.

3.5.3 Simplification of $\chi_{\mathbf{b},\mathbf{b}'}$ by LC decomposition

In the case of the present system, $\chi_{\mathbf{b},\mathbf{b}'}$ can be simplified more. Since every vector space spanned by $L_{\mathbf{b}}$ (we denote this vector space as $V_{\mathbf{b}}$) is invariant under the action of $\hat{H}$, the eigenvectors of $\hat{H}$ can be composed so that each eigenvector are contained in one of $V_{\mathbf{b}}$. Consequently, the time propagator of the system can be divided into some parts $\hat{G}_{\mathbf{b}}(t)$ each of which acts only on $V_{\mathbf{b}}$. Namely,

$$\hat{G}_{\mathbf{b}}(t) = \sum_{|E_i\rangle \in V_{\mathbf{b}}} |E_i\rangle \exp(-iE_i t/\hbar)\langle E_i| \tag{3.24}$$

and $\exp(-it\hat{H}/\hbar) = \sum_b \hat{G}_{\mathbf{b}}(t)$, where $\mathbf{b}$ run through 0 and the sites in the graph without those in the outermost generation. In this representation, the transition probability $\pi_{\mathbf{b},\mathbf{b}'}(t)$ is written as

$$\pi_{\mathbf{b},\mathbf{b}'}(t) = \sum_{\mathbf{b}_1,\mathbf{b}_2} \langle\mathbf{b}|\hat{G}_{\mathbf{b}_1}(t)|\mathbf{b}'\rangle\langle\mathbf{b}'|\hat{G}_{\mathbf{b}_2}^{\dagger}(t)|\mathbf{b}\rangle \ . \tag{3.25}$$

The term $\langle\mathbf{b}|\hat{G}_{\mathbf{b}_1}(t)|\mathbf{b}'\rangle$ vanishes unless $\mathbf{b}_1$ is an ancestor of both $\mathbf{b}$ and $\mathbf{b}'$ (regard $\mathbf{b}=0$ is an ancestor of all nodes in the graph). Thus, it is sufficient to consider that, in the sum in Eq. (3.25), $\mathbf{b}_1$ and $\mathbf{b}_2$ run only through the set of common ancestors of $\mathbf{b}_1$ and $\mathbf{b}_2$. We denote this set as $B_a[\mathbf{b},\mathbf{b}']$. Then, we simplify $\chi_{\mathbf{b},\mathbf{b}'}$ in the present system. Since any two eigenvalues in those of H^{l_1} or H^{l_2} do not coincide in general if $l_1 \neq l_2$, the long time average of the term $\langle\mathbf{b}|\hat{G}_{\mathbf{b}_1}(t)|\mathbf{b}'\rangle\langle\mathbf{b}'|\hat{G}_{\mathbf{b}_2}^{\dagger}(t)|\mathbf{b}\rangle$ in the case $\mathbf{b}_1, \mathbf{b}_2 \in B_a[\mathbf{b},\mathbf{b}']$ and $\mathbf{b}_1 \neq \mathbf{b}_2$. Therefore, $\chi_{\mathbf{b},\mathbf{b}'}$ can be expressed as

$$\chi_{\mathbf{b},\mathbf{b}'} = \sum_{\mathbf{b}_1 \in B_a[\mathbf{b},\mathbf{b}']} \chi_{\mathbf{b},\mathbf{b}'}(\mathbf{b}_1) \ , \tag{3.26}$$

where

$$\chi_{\mathbf{b},\mathbf{b}'}(\mathbf{b}_1) = \lim_{T\to\infty} \frac{1}{T}\int_0^T dt \ |\langle\mathbf{b}|\hat{G}_{\mathbf{b}_1}(t)|\mathbf{b}'\rangle|^2 \ . \tag{3.27}$$

In addition, since eigenvalues of each H^l never degenerate, $\chi_{\mathbf{b},\mathbf{b}'}(\mathbf{b}_1)$ can be expressed as

$$\chi_{\mathbf{b},\mathbf{b}'}(\mathbf{b}_1) = \sum_{|E_i\rangle \in V_{\mathbf{b}_1}} |\langle\mathbf{b}|E_i\rangle|^2|\langle E_i|\mathbf{b}'\rangle|^2 \ . \tag{3.28}$$

Note that $\chi_{\mathbf{b},\mathbf{b}'}$ is decomposed into the sum of the contribution from each linear chain that contains both $\mathbf{b}$ and $\mathbf{b}'$. Therefore the behavior of $\chi_{\mathbf{b},\mathbf{b}'}$ can be examined through examinations about each $\chi_{\mathbf{b},\mathbf{b}'}(\mathbf{b}_1)$. This means that, although the original dendritic graph has a rather complicated geometrical structure, $\chi_{\mathbf{b},\mathbf{b}'}$ can be reduced to the LPs of simple one-dimensional systems, owing to LC decomposition.

A remark: In the discussion above, we assumed that any eigenvalues of H^l and those of $H^{l'}$ do not coincide if $l \neq l'$. However, at some values of α, degeneracy of eigenvalues can occur accidentally. Thus, in such case, we ignore or avoid the accidental degeneracy by considering a infinitesimally small deviation of α (See also Appendix B, which summarizes the α dependency of the eigenvalues).

3.5.4 Intra-generation interaction dependency of $\chi_{\mathbf{b},\mathbf{b}'}$

Next, we illustrate $\chi_{\mathbf{b},\mathbf{b}'}$ obtained from the numerical calculation with various values of the intra-generation interaction α. The results of the calculation are illustrated in Fig. 3.12. Panels (a) to (e) correspond to the case of $\alpha = 0, 1, 2, 4, 8$, respectively. In these panels, both vertical and horizontal axes indicate the sites in the partial Husimi cacti. We here label the sites by sequential serial numbers that increase as the sites go from left to right and as the generation of the sites grow. More explicitly, the site $\mathbf{b}$ is labeled by a number $2^{l(\mathbf{b})-1} + \sum_{k=1}^{l(\mathbf{b})}(b_k - 1) \cdot 2^{l(\mathbf{b})-k}$, where $l(\mathbf{b})$ is the generation of $\mathbf{b}$.

Note that in all the cases, $\chi_{\mathbf{b},\mathbf{b}'}$ in 2×2 blocks on the diagonal line and $\chi_{1,1}$ are larger than 0.1. These magnitudes are considerably larger than those of other non-diagonal terms. Therefore, these diagonal terms are colored in a same color (yellow online) in Fig. 3.12 (a) to (e) and the precise vales of them are alternatively shown in Fig. 3.12 (f).

In Fig. 3.12 (a), two distinct ridge lines are shown around the line with slope 0.5 or 2. In addition, other two ridge lines, which have lower height than the formers, also stand around the line with slope 0.25 or 4. This pattern of the map is remarkably similar to the results of the studies on the full Husimi cactus [28, 29]. This pattern means that population in the system can be transferred over generations along edges in the graph of interactions, which visualizes the Hamiltonian of the system.

However, as the intra-generation interaction α increases, this pattern in non-diagonal region becomes quite weak and, correspondingly, diagonal terms become bigger. Actually, the ridge lines mentioned above are lowered and almost disappear in Fig. 3.12 (e). On the other hand, in Fig. 3.12 (f), the diagonal terms increase in all generation as α increases. This fact means that intra-generation interactions cause localization of the population within one generation. In other words, the population given initially tends to stay at the initial generation. LC decomposition gives clear explanation about this localization. As we have previously shown by Eq. (3.26) that $\chi_{\mathbf{b},\mathbf{b}'}$ can be decomposed into the contributions from each linear chain including $\mathbf{b}$ and $\mathbf{b}'$. Each system of these linear chains obeys the Hamiltonian Eq. (3.19). In this Hamiltonian, the first diagonal element (site energy) corresponding to the innermost site in the linear chain is 0 or $-\alpha$ and other diagonal elements are α. Thus, as α increases, the energy gap between the first site and other sites is broadened and this energy gap inhibits "resonance" between
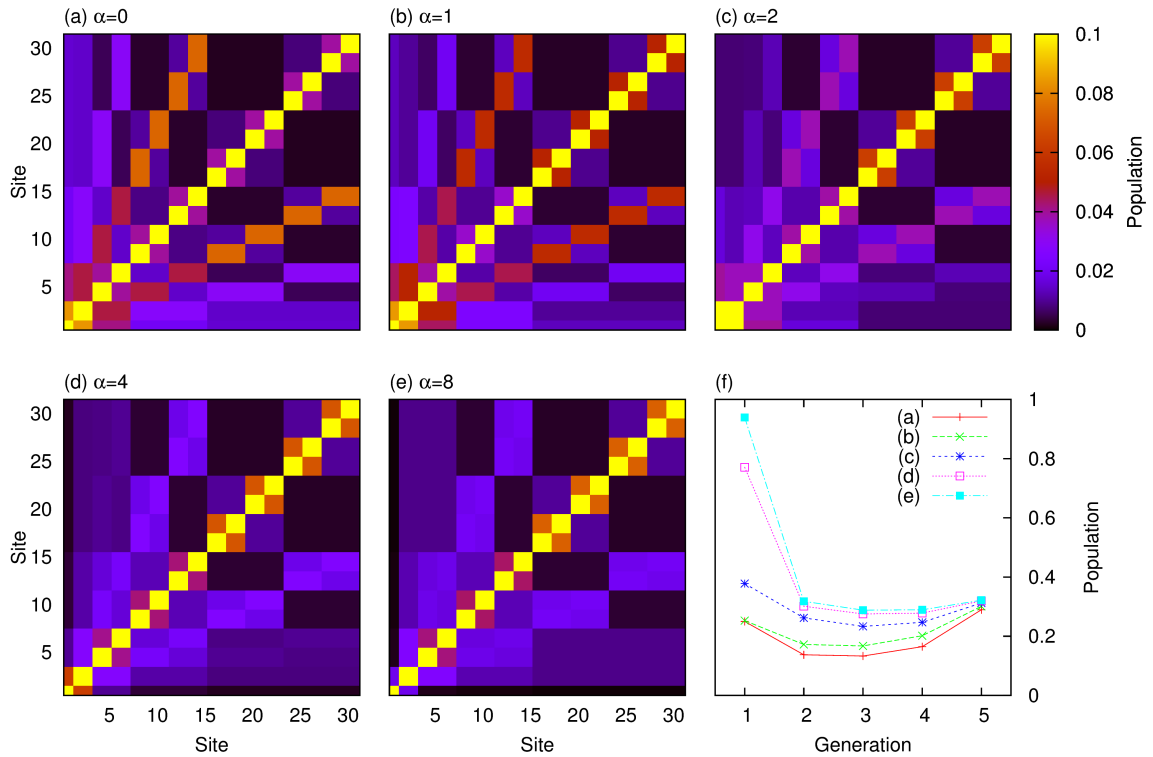
Figure 3.12: Intra-generation interaction dependency of LPs $\chi_{\mathbf{b},\mathbf{b}'}$: (a)-(e) $\chi_{\mathbf{b},\mathbf{b}'}$ with $\alpha = 0, 1, 2, 4, 8$, respectively. Both vertical axis and horizontal axis indicate sites $\mathbf{b}$ and $\mathbf{b}'$ by sequential serial numbers (the correspondence is written in the text). The magnitudes of $\chi_{\mathbf{b},\mathbf{b}'}$ on the diagonal line in (a)-(e) are alternatively shown in (f) by generations.

them. Consequently, the increase of α results in the formation of an eigenstate that localizes around the innermost site in the linear chain. This localized eigenstate causes the increase of diagonal terms of $\chi_{\mathbf{b},\mathbf{b}'}$ as is shown in Fig. 3.12.

3.6 Summary and Conclusion

In this chapter, we have discussed LC decomposition, which is a way that equivalently transforms linear dynamics on a dendritic graph into that on a set of small one-dimensional graphs. In other words, linear operators defined on a dendritic graph are transformed into a block diagonal form where each block matrix is triply diagonalized. While a dendritic graph looks complicated at a glance, a set of one-dimensional graphs is rather simplified. Thus, this simple picture help to understand the relation between the geometric structure and functions of dendritic systems.

This type of decomposition have been introduced in some special cases [11, 16, 30]. This chapter have focused on the common properties among these studies and have revealed the general conditions for the LC decomposability. We have proposed the sufficient conditions for LC decomposition and have shown that, under the conditions, LC decomposition is realized by the proper change of basis of the linear operators. Compared with the already-known examples, the LC decomposable linear operators that have been proposed in this chapter are generalized in the following three aspects: (i) the class of dendritic graphs on which linear operators are defined; (ii) the symmetry operations under which linear operators are invariant; (iii) the type of linear operators: Firstly, as the generalization of dendritic graphs, we have introduced the general class of dendritic graphs and its notation, where the number of branching can differ by generations and the configuration of nodes is denoted by $(n_1, n_2, \cdots, n_L)$. This class of dendritic graphs covers broader range of dendritic graphs including Cayley trees and Husimi cacti, which are used in the past studies [11, 16, 30]. Secondary, we have defined the symmetry groups $G[G_1, G_2, \cdots]$ that represent the symmetry of the linear operators defined on the dendritic graphs. $G[G_1, G_2, \cdots]$ means that every portion of the dendritic graph composed of all the descendant nodes of a given node in the $(l-1)$th generation are permutated by symmetry operations in G_l. We have imposed one of the two sufficient conditions on this symmetry group: (LC1) multiplicity of each irreducible representation included in the permutation representation of G_l is 1 for any l. Owing to this condition, proper subgroup G_l ($\subsetneqq S_{n_l}$) can be used in the construction of $G[G_1, G_2, \cdots]$. This freedom expands the class of symmetry operations acting on LC decomposable linear operator than before. The second case in Sec. IV is an example using proper subgroups of S_{n_l}. Lastly, we have adopted quantum Hamiltonians without restriction, i.e. Hermitian matrices, as linear operators defined on dendritic graphs.

Hence, the result of this chapter can be applied to linear operators represented by real symmetry matrices including Laplacians, normalized Laplacians, matrices representing quadratic potential energy in classical dynamics and other linear operators because real symmetry matrices are included in Hermitian matrices. Thus, the class of LC decomposable linear operators has been significantly expanded in these three aspects.

Next, we summarize the sufficient conditions for LC decomposition. In Sec. III, we have presented the procedure to realize LC decomposition. The key point of the realization of LC decomposition is that irreducible representations included in a generation are inherited to the next generation just once. Consequently, each node in a generation get to be linked to just one node in the next generation in the LC decomposed graph. The restriction for multiplicity of irreducible representations in the condition (LC1) results in the one-time inheritance of irreducible representation.

We have also impose the second sufficient condition for LC decomposition on linear operators only to prohibit inter-generation interactions between non-adjacent generations. This condition let the decomposed graphs to have one-dimensional form. However, even without the condition (LC2), a linear operator on a dendritic graph is decomposed into that defined on a set of small graphs each of which have at most L nodes. Therefore, the essential condition for the feasibility of decomposition is only the condition (LC1). The example of linear operators satisfying only the condition (LC1) can be seen in the literature [18].

We have also examined the coherent quantum dynamics on the partial Husimi cactus focusing on the role of intra-generation interactions to present another example of dynamics that can be well explained by LC decomposition even though the usefulness of LC decomposition have been already shown in the past studies [11, 16, 30]. According to the result of the numerical calculation, we have revealed that too intense intra-generation interaction reduces the transfer of population over generations. We have also found that this fact can be well explained in the picture of LC decomposition. This is because the excessive intra-generation interactions create eigenstates localized around the innermost sites in each linear chain because the energy gap in each linear chain provided by the intra-generation interaction prohibits the resonance of states with in the linear chain. Note that this analysis can be done based on LC decomposition.

As is shown in the analysis on the coherent dynamics, LC decomposition gives a simple and unified viewpoint for the study of dynamics on dendritic graphs. This simplicity may help to understand the relation between geometrical structure and properties or functions of dendritic systems even in other areas.

3.7 Appendix A: Proof that Eq. (3.16) gives the irreducible representations of $G[G_1, G_2, \cdots, G_L]$

In this section, we only prove that the sets defined by Eq. (3.16) belonging to the outermost (L th) generation give the irreducible representation of $G[G_1, G_2, \cdots, G_L]$ because it is easy to prove that these sets also gives the irreducible representation of expanded groups $G[G_1, G_2, \cdots, G_L, G_{L+1}, \cdots]$. Now, let $\chi(\sigma)$ be the character of the representation by one of the set in the L th generation. In order to prove that this representation is irreducible, we should show that

$$\sum_{\sigma \in G[G_1, G_2, \cdots, G_L]} |\chi(\sigma)|^2 = \left| G[G_1, G_2, \cdots, G_L] \right| . \tag{3.29}$$

3.7.1 Preliminary A

The number of elements in $G[G_1, G_2, \cdots, G_L]$ is explicitly expressed as follow. Because any element $\sigma \in G[G_1, G_2, \cdots, G_L]$ can be uniquely expressed by the generators of $G[G_1, G_2, \cdots, G_L]$ defined in Eqs. (3.6) and (3.7) in the following form:

$$\sigma = \sigma^{(1)} \cdot \left(\prod_{\mathbf{b}^{(1)} \in B_1} \sigma^{(2)}[\mathbf{b}^{(1)}] \right) \cdots \left(\prod_{\mathbf{b}^{(L-1)} \in B_{L-1}} \sigma^{(L)}[\mathbf{b}^{(L-1)}] \right) . \tag{3.30}$$

Hence, it is found that

$$\left| G[G_1, G_2, \cdots, G_L] \right| = \prod_{k=1}^{L} |G_k|^{|B_{k-1}|} . \tag{3.31}$$

Here we assign $|B_0| = 1$.

3.7.2 Preliminary B

Consider the representation of $G[G_1, G_2, \cdots, G_l]$ ($l \le L$) whose basis is the set of basis vectors in the l th generation $\{|\mathbf{b}\rangle | \mathbf{b} \in B_l\}$ and let $\tilde{\chi}^{(l)}(\sigma)$ ($\sigma \in G[G_1, G_2, \cdots, G_l]$) be the character of this representation. Because the action of σ on the basis results in a permutation within $\{|\mathbf{b}\rangle | \mathbf{b} \in B_l\}$, $\tilde{\chi}^{(l)}(\sigma)$ is the number of basis vectors that are invariant under the action of σ. Then, we define a set $B_l[\sigma]$ ($\subset B_l$) composed of the invariant basis vectors under the action of σ. Note that $\left| B_l[\sigma] \right| = \tilde{\chi}^{(l)}(\sigma)$.

$\tilde{\chi}^{(l)}(\sigma)$ can be written in the following expression. We count the invariant basis vectors every n_l vectors emerging from each sites in the $l - 1$ th generation. Suppose that $\sigma \in G[G_1, G_2, \cdots, G_l]$ is expressed as

$$\sigma = \sigma' \cdot \prod_{\mathbf{b}^{(l-1)} \in B_{l-1}} \sigma^{(l)}[\mathbf{b}^{(l-1)}] \tag{3.32}$$

where $\sigma' \in G[G_1, G_2, \cdots, G_{l-1}]$. Then, if a basis vector in the $l-1$ th generation $|\mathbf{b}_1^{l-1}\rangle$ is mapped to another basis vector $|\mathbf{b}_2^{l-1}\rangle$ ($\neq |\mathbf{b}_1^{l-1}\rangle$) by σ', each n_l basis vectors emerging from the site $\mathbf{b}_1^{l-1}$ is mapped to one of the n_l basis vectors emerging from the site $\mathbf{b}_2^{l-1}$. Thus, all of the former n_l basis vectors are not invariant. The invariant basis vectors in the l th generation, therefore, have the parent site in the $l-1$ th generation that is also invariant under the action of σ'. In addition, the invariant basis vectors in n_l basis vectors emerging from an invariant site $\mathbf{b} \in B_{l-1}[\sigma']$ can be counted by $\chi_p^{(l)}(\sigma^{(l)}[\mathbf{b}])$ where $\chi_p^{(l)}(\sigma^{(l)}[\mathbf{b}])$ is the character of the permutation representation of the group G_l which is given by the basis $\{|\mathbf{b}, 1\rangle \cdots |\mathbf{b}, n_l\rangle\}$ and $\sigma^{(l)}[\mathbf{b}]$ is the symmetry operation shown in Eq. (3.32). To sum up, $\tilde{\chi}^{(l)}(\sigma)$ can be expressed as

$$\tilde{\chi}^{(l)}(\sigma) = \sum_{\mathbf{b} \in B_{l-1}[\sigma']} \chi_p^{(l)}(\sigma^{(l)}[\mathbf{b}]) \; . \tag{3.33}$$

Lastly, we define the value of $A^{(l)}$ for the later proof by

$$A^{(l)} \equiv \sum_{\sigma \in G[G_1, G_2, \cdots, G_l]} \tilde{\chi}^{(l)}(\sigma) \; . \tag{3.34}$$

$A^{(l)}$ is expressed as

$$
\begin{aligned}
A^{(l)} &= \sum_{\sigma' \in G[G_1, G_2, \cdots, G_{l-1}]} \prod_{\mathbf{b} \in B_{l-1}} \sum_{\sigma^{(l)}[\mathbf{b}] \in G_l} \tilde{\chi}^{(l)}(\sigma) \\
&= \sum_{\sigma' \in G[G_1, G_2, \cdots, G_{l-1}]} \sum_{\mathbf{b}' \in B_{l-1}[\sigma']} \prod_{\mathbf{b} \in B_{l-1}} \sum_{\sigma^{(l)}[\mathbf{b}] \in G_l} \chi_p^{(l)}(\sigma^{(l)}[\mathbf{b}']) \; .
\end{aligned} \tag{3.35}
$$

For each $\mathbf{b}' \in B_{l-1}[\sigma']$,

$$\prod_{\mathbf{b} \in B_{l-1}} \sum_{\sigma^{(l)}[\mathbf{b}] \in G_l} \chi_p^{(l)}(\sigma^{(l)}[\mathbf{b}']) = |G_l|^{|B_{l-1}|-1} \sum_{\sigma^{(l)}[\mathbf{b}'] \in G_l} \chi_p^{(l)}(\sigma^{(l)}[\mathbf{b}']) \; . \tag{3.36}$$

Because $\chi_p^{(l)}$ is the character of the permutation representation of G_l and this representation includes the totally symmetric irreducible representation just once due to the condition (i) for LC decomposition,

$$\sum_{\sigma^{(l)}[\mathbf{b}'] \in G_l} \chi_p^{(l)}(\sigma^{(l)}[\mathbf{b}']) = |G_l| \; . \tag{3.37}$$

Thus,

$$
\begin{aligned}
A^{(l)} &= \sum_{\sigma' \in G[G_1, G_2, \cdots, G_{l-1}]} \sum_{\mathbf{b}' \in B_{l-1}[\sigma']} |G_l|^{|B_{l-1}|} \\
&= |G_l|^{|B_{l-1}|} A^{(l-1)} = \prod_{k=1}^{l} |G_k|^{|B_{k-1}|} \; .
\end{aligned} \tag{3.38}
$$

3.7.3 Proof

We now prove the claim. Let $\chi_X^{(L)}$ be the character of the irreducible representation of G_L that gives the set of basis vectors in Eq. (3.16) labeled by X. Then, in a similar fashion as the preliminary, $\chi(\sigma)$ can be expressed as

$$\chi(\sigma) = \sum_{\mathbf{b} \in B_{L-1}[\sigma']} \chi_X^{(L)}(\sigma^{(L)}[\mathbf{b}]) \ . \tag{3.39}$$

Consequently, we obtain

$$\sum_{\sigma \in G[G_1, G_2, \cdots, G_L]} |\chi(\sigma)|^2 = \sum_{\sigma' \in G[G_1, G_2, \cdots, G_{L-1}]} \sum_{\mathbf{b}', \mathbf{b}'' \in B_{L-1}[\sigma']}$$
$$\prod_{\mathbf{b} \in B_{L-1}} \sum_{\sigma^{(L)}[\mathbf{b}] \in G_L} \chi_X^{(L)}(\sigma^{(L)}[\mathbf{b}']) \chi_X^{(L)}(\sigma^{(L)}[\mathbf{b}''])^* \ . \tag{3.40}$$

Because $\chi_X^{(L)}$ is the character of one of the irreducible representations of G_L except for the totally symmetric irreducible representation,

$$\sum_{\sigma^{(L)} \in G_L} \chi_X^{(L)}(\sigma^{(L)}) = 0 \tag{3.41}$$

and

$$\sum_{\sigma^{(L)} \in G_L} |\chi_X^{(L)}(\sigma^{(L)})|^2 = |G_L| \ . \tag{3.42}$$

Hence, we find

$$\begin{aligned}
\sum_{\sigma \in G[G_1, G_2, \cdots, G_L]} |\chi(\sigma)|^2 &= \sum_{\sigma' \in G[G_1, G_2, \cdots, G_{L-1}]} |G_L|^{|B_{L-1}|-1} \sum_{\mathbf{b}' \in B_{L-1}[\sigma']} \sum_{\sigma^{(L)}[\mathbf{b}'] \in G_L} |\chi_X^{(L)}(\sigma^{(L)}[\mathbf{b}'])|^2 \\
&= \sum_{\sigma' \in G[G_1, G_2, \cdots, G_{L-1}]} |G_L|^{|B_{L-1}|} \\
&= |G_L|^{|B_{L-1}|} A^{(L-1)} = \prod_{k=1}^{L} |G_k|^{|B_{k-1}|} \\
&= \left| G[G_1, G_2, \cdots, G_L] \right| \tag{3.43}
\end{aligned}$$

and the claim is proven.

3.8   Appendix B: Eigenvalues of H^l

We examine the eigenvalues of the $N \times N$ matrix H^N in Eq. (3.19). For simplicity, consider another matrix A defined by

$$A = -\frac{1}{\sqrt{2}}(H^N - \alpha I) \ . \tag{3.44}$$

Furthermore, we invert the order of index of A. Then, A has the following form:

$$A = \begin{pmatrix} 0 & 1 & & & & \mathbf{O} \\ 1 & 0 & 1 & & & \\ & 1 & \ddots & \ddots & & \\ & & \ddots & 0 & 1 \\ \mathbf{O} & & & 1 & \gamma \end{pmatrix} . \tag{3.45}$$

In this appendix, we examine the eigenvalues of this matrix instead of H^l.

Suppose that $\mathbf{x}$ and λ are one of the eigenvectors and eigenvalues respectively. Namely, $\mathbf{x}$ and λ satisfy

$$A\mathbf{x} = \lambda\mathbf{x} . \tag{3.46}$$

By denoting this equation by each element, we get

$$x_2 = \lambda x_1 \tag{3.47}$$
$$x_{n-1} + x_{n+1} = \lambda x_n \tag{3.48}$$
$$x_{N-1} + \gamma x_N = \lambda x_N . \tag{3.49}$$

where the second equation is valid for $2 \le n \le N-1$.

$\mathbf{x}$ and λ that satisfy only Eqs. (3.47) and (3.48) is given with an arbitrary variable θ as

$$(x_n, \lambda) = \begin{cases} (\sin n\theta, 2\cos\theta) \\ (\sinh n\theta, 2\cosh\theta) \\ ((-1)^n \sinh n\theta, -2\cosh\theta) \end{cases} . \tag{3.50}$$

Then, we substitute Eq. (3.50) into Eq. (3.49) and determine θ that makes Eq. (3.49) valid. By the substitution, we get

$$\gamma x_N = x_{N+1} \tag{3.51}$$

in all cases of Eq. (3.50) because $x_{N-1} + x_{N+1} = \lambda x_N$ is valid in these cases. We, hence, get the equations for θ.

$$\gamma = \frac{x_{N+1}}{x_N} = \begin{cases} \frac{\sin(N+1)\theta}{\sin N\theta} \\ \frac{\sinh(N+1)\theta}{\sinh N\theta} \\ -\frac{\sinh(N+1)\theta}{\sinh N\theta} \end{cases} . \tag{3.52}$$

The roots of these equations of θ give the eigenvectors and the eigenvalues of A through Eq. (3.50).

To determine the roots of θ, it is sufficient to search the roots only in an interval $0 \leq \theta \leq \pi$ for the first equation in Eq. (3.52) and $0 \leq \theta \leq \infty$ for the second and the third equations. If θ^* is an root of the first equation, $\theta = \pm|\theta^* + 2m\pi|$ are also the roots for any integer m and all of these roots give a same eigenvector and eigenvalue in Eq. (3.50). Thus, searching in the $0 \leq \theta \leq \pi$ is sufficient for the first equation. In the cases of the second and the third equations, because $\theta = -\theta^*$ becomes another root and gives a same result, it is sufficient to search the roots in $0 \leq \theta \leq \infty$.

Next, we plot the right hand side of Eq. (3.52) only in the interval mentioned above. The roots of Eq. (3.52) are visualized as intersection points of the plot and the horizontal line whose level is γ. Fig. 3.13 is an example of the plot, where $N = 5$. The right hand side of Eq. (3.52) of the first case is represented by solid lines (blue online) and that of the second and the third cases are represented by dashed lines (purple online). It is found from this figure that, for any γ, there always exist just N unique intersection points. Thus, all of the eigenvectors of A are exhausted by these intersection points.

Lastly, we examine the behavior of the eigenvectors and the eigenvalues in the limit of $\gamma \to \infty$. This limit corresponds to the case of the large intra-generation interactions in the coherent dynamics examined in Sec. V. Firstly, the number of the roots of the first equation in Eq. (3.52) is $N - 1$ and these roots converge to $\theta = k\pi/N$ ($k = 1, 2, \cdots, N - 1$). The remaining one root is given by the second equation in Eq. (3.52). In this case, because $\gamma \simeq e^\theta$ and the eigenvalue $\lambda = 2\cosh\theta \simeq e^\theta$, λ asymptotically approaches to γ. The corresponding normalized eigenvector converges to $(0, 0, \cdots, 1)$. To sum up, in the limit of $\gamma \to \infty$, the eigenvectors and the eigenvalues of A approach to those of $\tilde{A}$, which is a block diagonal matrix obtained by vanishing the $(N - 1, N)$ and $(N, N - 1)$ matrix elements of A:

$$\tilde{A} = \begin{pmatrix} 0 & 1 & & & \mathbf{O} \\ 1 & 0 & \ddots & & \\ & \ddots & \ddots & 1 & \\ & & 1 & 0 & \\ \mathbf{O} & & & & \gamma \end{pmatrix}. \tag{3.53}$$

This separation is what we have called in Sec. V the "inhibition of resonance by energy gap".
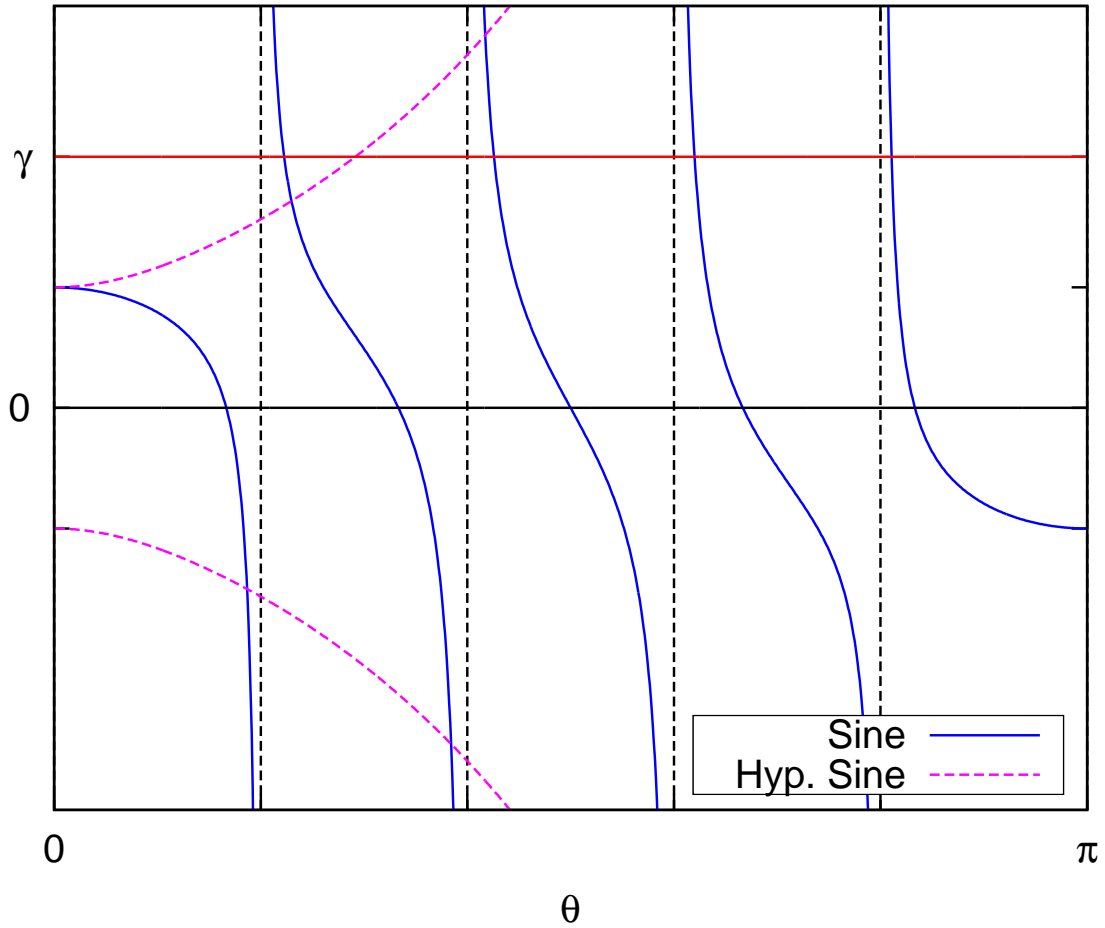
Figure 3.13: A plot of the right hand side of Eq. (3.52) with $N = 5$. Solid lines (blue online) are that of the first equation in Eq. (3.52), which is expressed by sine functions. Dashed lines (purple online) are that of the second and the third equations, which are expressed by hyperbolic sine functions. Horizontal solid line (red online) is located at horizontal level γ. Intersection points of the plots and the horizontal line represent θ that give the eigenvectors and the eigenvalues of the matrix A through Eq. (3.50).

Reference

[1] S. Svenson and D. a. Tomalia, Adv. Drug Deliv. Rev. **64**, 102 (2012).

[2] W.-S. Li and T. Aida, Chem. Rev. **109**, 6047 (2009).

[3] D. Astruc, E. Boisselier, and C. Ornelas, Chem. Rev. **110**, 1857 (2010).

[4] C. Devadoss, P. Bharathi, and J. S. Moore, J. Am. Chem. Soc. **118**, 9635 (1996).

[5] D.-L. Jiang and T. Aida, J. Am. Chem. Soc. **120**, 10895 (1998).

[6] M. Kimura, T. Shiba, T. Muto, K. Hanabusa, and H. Shirai, Macromolecules **32**, 8237 (1999).

[7] O. Mülken and A. Blumen, Phys. Rep. **502**, 37 (2011).

[8] S. Venegas-Andraca, Quantum Inf. Process. **11**, 1015 (2012).

[9] A. A. Gurtovenko and A. Blumen, Adv. Polym. Sci. **182**, 171 (2005).

[10] L. Valkunas, D. Abramavicius, and T. Mančal, *Molecular Excitation Dynamics and Relaxation*, Wiley, Weinheim, 2013.

[11] C. Cai and Z. Y. Chen, Macromolecules **30**, 5104 (1997).

[12] P. Biswas, R. Kant, and A. Blumen, J. Chem. Phys. **114**, 2430 (2001).

[13] M. Dolgushev and A. Blumen, J. Chem. Phys. **131**, 044905 (2009).

[14] M. Dolgushev and A. Blumen, Macromolecules **42**, 5378 (2009).

[15] M. Dolgushev and A. Blumen, J. Chem. Phys. **132**, 124905 (2010).

[16] M. Galiceanu, J. Phys. A Math. Theor. **43**, 305002 (2010).

[17] M. Dolgushev, G. Berezovska, and A. Blumen, Macromol. Theory Simulations **20**, 621 (2011).

[18] F. Fürstenberg, M. Dolgushev, and A. Blumen, J. Chem. Phys. **136**, 154904 (2012).

[19] D. A. Markelov, M. Dolgushev, Y. Y. Gotlib, and A. Blumen, J. Chem. Phys. **140**, 244904 (2014).

[20] A. Kumar and P. Biswas, Macromolecules **43**, 7378 (2010).

[21] A. Kumar and P. Biswas, J. Chem. Phys. **134**, 214901 (2011).

[22] A. Kumar and P. Biswas, J. Chem. Phys. **137**, 124903 (2012).

[23] A. I. M. Denneman, R. J. J. Jongschaap, and J. Mellema, J. Eng. Math. **34**, 75 (1998).

[24] M. Cosenza and R. Kapral, Phys. Rev. A **46**, 1850 (1992).

[25] U. M. B. Marconi and A. Petri, J. Phys. A. Math. Gen. **30**, 1069 (1997).

[26] C. Jayanthi, S. Wu, and J. Cocks, Phys. Rev. Lett. **69**, 1955 (1992).

[27] C. Jayanthi and S. Wu, Phys. Rev. B **50**, 897 (1994).

[28] A. Blumen, V. Bierbaum, and O. Mülken, Phys. A Stat. Mech. its Appl. **371**, 10 (2006).

[29] O. Mülken, V. Bierbaum, and A. Blumen, J. Chem. Phys. **124**, 124905 (2006).

[30] M. Galiceanu and A. Blumen, J. Chem. Phys. **127**, 134904 (2007).

[31] H. Liu and Z. Zhang, J. Chem. Phys. **138**, 114904 (2013).

[32] A. Julaiti, B. Wu, and Z. Zhang, J. Chem. Phys. **138**, 204116 (2013).

[33] K. Harigaya, Phys. Chem. Chem. Phys. **1**, 1687 (1999).

[34] T. Minami, S. Tretiak, V. Chernyak, and S. Mukamel, J. Lumin. **87-89**, 115 (2000).

[35] J. C. Kirkwood, C. Scheurer, V. Chernyak, and S. Mukamel, J. Chem. Phys. **114**, 2419 (2001).

[36] M. Nakano, M. Takahata, H. Fujita, S. Kiribayashi, and K. Yamaguchi, Chem. Phys. Lett. **323**, 249 (2000).

[37] M. Takahata, M. Nakano, H. Fujita, and K. Yamaguchi, Chem. Phys. Lett. **363**, 422 (2002).

[38] M. Nakano et al., J. Chem. Phys. **120**, 2359 (2004).

[39] M. Martín-Delgado, J. Rodriguez-Laguna, and G. Sierra, Phys. Rev. B **65**, 155116 (2002).

[40] O. Varnavski et al., J. Chem. Phys. **116**, 8893 (2002).

[41] V. Pouthier, J. Chem. Phys. **139**, 234111 (2013).

[42] V. Pouthier, Phys. Rev. E **90**, 022818 (2014).

[43] J. L. Bentz, F. Niroomand Hosseini, and J. J. Kozak, Chem. Phys. Lett. **370**, 319 (2003).

[44] D. Rana and G. Gangopadhyay, J. Chem. Phys. **118**, 434 (2003).

[45] D.-J. Heijs, V. a. Malyshev, and J. Knoester, J. Chem. Phys. **121**, 4884 (2004).

[46] J. K. Ochab and Z. Burda, Phys. Rev. E **85**, 021145 (2012).

[47] X. Peng and Z. Zhang, J. Chem. Phys. **140**, 234104 (2014).

[48] A. A. Gurtovenko, S. V. Lyulin, M. Karttunen, and I. Vattulainen, J. Chem. Phys. **124**, 94904 (2006).

[49] M. Hamermesh, *Group theory and its application to physical problems*, Dover, New York, 1989.

Chapter 4

Symmetry-origin unidirectional energy gradient in light-harvesting dendrimers

Abstract

In excitation energy transfer (EET) in molecular aggregates, it is preferable to transfer excitation energy directly to destination parts along with unidirectional energy flow, the direction of which is generally determined by the structure of energy gradient in the aggregates. In this chapter, based on a theoretical model, we show a possibility that symmetry of the repetitively branched structure of light-harvesting dendrimers creates the energy gradient descending toward inner generations (layers of pigment molecules) of the dendrimers. The model system is represented by the Frenkel exciton Hamiltonian and is defined on a dendritic graph composed of nodes and edges. We set the model to have only a portion of dendrimers without core molecules in order to focus on the role of symmetry. We show numerically that the energy distribution at a thermal equilibrium state of the model system collects more excitation energy at inner generations compared with the homogeneous energy distribution where excitation energy is distributed equally to all pigment molecules. In addition, we also propose two mechanisms that create energy gradient base on the theory of linear chain decomposition, general theory of which is presented in Chapter 3, and attribute the energy gradient in the model system to the symmetry of the system. The linear chain decomposition equivalently transforms the model system, which is defined on a dendritic graph, into a simple system defined on a set of one-dimensional graphs like linear chains by utilizing the symmetry of the dendritic model system. In the picture of the decomposition, we find that energy gradient is formed both in each linear chain and among linear chains. These mechanisms of the intra-chain and the inter-chain energy gradient well explain

the inclination of the energy distribution at the thermal equilibrium state of the model system.

4.1   Introduction

Light-harvesting dendrimers have attracted much attention for several decades because of their curious properties in the process of excitation energy transfer (EET) [1, 2]. Dendrimers have repetitively branched structure and, in particular, light-harvesting dendrimers have many pigment molecules, which absorb photons of light, in their peripheral part. Energy of photons absorbed by the pigment molecules is transferred to the core molecule bonded to the root of the light-harvesting dendrimers. While many of light-harvesting dendrimers show high quantum yield of EET, it is known from experimental studies [3–5] that this yield of EET is strongly relevant to morphology of light-harvesting dendrimers. These experimental facts suggest that there is a certain mechanism enhancing EET originated from the morphology of the light-harvesting dendrimers. In this chapter, we focus on the role of morphology of dendrimers in EET.

To make the following discussion clear, we here recall the key points that determine the efficiency of general EET in molecular aggregates: magnitude of velocity of EET and unidirectionality of EET. In order to achieve high yield, excitation energy must be transferred to destination molecules before deactivation occurs. Hence, fast transfer is preferable in general. On the other hand, the unidirectionality is also important because EET promoted by stochastic (random-walk-like) transfer takes extra time while excitation energy is wandering. Therefore, excitation energy should be directly transferred to the destination molecules along with unidirectional energy flow.

The direction of energy flow is generally determined by the correlation between the structure of energy level of excited states and the spatial location of the excited states, or the energy gradient. Excitation energy is relaxed from excited states of higher energy levels to those of lower energy levels. In this process, excitation energy is spatially transferred from the region where the former states locate to the latter states' region.

While energy gradient can be formed by embedding several species of pigment molecules with various excitation energies, it can also be formed by interaction energy among pigment molecules. Even in aggregates composed of a single species of pigment molecules, many excited states delocalized around the components with various energy levels can be formed if the interaction among the components is significantly strong. These excited states give rich structures of energy level of the aggregates and particular spatial location of excited states. This results in the formation of energy gradient. In addition, it is often the case that connectivity of significantly large interaction among pigment molecules strongly affects the structure of energy level and spatial location of

excited states. Therefore, it is also important to investigate the relation between the connectivity of interaction and these properties of excited states for understanding the structure of energy gradient, or the direction of energy flow in EET.

We here investigate the EET in light-harvesting dendrimers in terms of the unidirectionality of energy flow in this chapter. In particular, we focus on the repetitive branched structure of dendrimers and its symmetry as they represent the connectivity of interaction among pigment molecules. To our knowledge, although there have been many theoretical studies on EET in light-harvesting dendrimers [6–24], there are few studies that focus mainly on the role of symmetry of dendrimers. In this chapter, we show a possibility that there exist symmetry-origin energy gradient descending toward core molecules in light-harvesting dendrimers. To do so, we firstly define a model system for EET in light-harvesting dendrimer based on the Frenke exciton Hamiltonian. Then, we compare the energy distribution at the thermal equilibrium state based on the model Hamiltonian with the energy distribution obtained from stochastic hopping picture. Through the comparison, we show that the excitation energy tends to gather at pigment molecules near the core in the former distribution.

We also explain how the light-harvesting ability is originated from the symmetry of the model system. This explanation is based on the theory of linear chain (LC) decomposition, a general theory of which has been proposed in Chapter 3. This theory visualize the symmetry of dendrimers in a simple picture by equivalently transforming a dendritic system into a set of small one-dimensional systems and it have been known that this simple picture gives profound insights for understanding of properties of the original dendritic system. In this chapter, applying the theory of LC decomposition, we propose two symmetry-origin mechanisms for the systems to create the energy gradient.

This chapter is organized as follows. In Sec. 4.2, we define the system modeling EET in light-harvesting dendrimer based on the Frenkel exciton Hamiltonian. Section 4.3 presents the energy distribution at the thermal equilibrium state of the model Hamiltonian and shows excitation energy tends to gather at inner pigment molecules. In Sec. 4.4, we explain how the light-harvesting ability arises from the symmetry of the dendritic model system based on the linear chain decomposition. Lastly, Sec. 4.5 concludes this chapter with some remarks.

4.2   System

In this section, we define a model system for EET in light-harvesting dendrimers using the Frenkel exciton Hamiltonian [25]. We visualize this Frenkel exciton Hamiltonian by a dendritic graph composed of nodes and edges. Notation for this graph is also defined in this section.

In order to focus on the role of symmetry of dendrimers, we set up the model Hamiltonian so that it has no special features other than the structure of the symmetry. We assume the model system is composed of single species of pigment molecules and does not have core molecules. Some light-harvesting dendrimers are synthesized with several species of pigment molecules to embed energy gradient by arranging these molecules in order of their magnitude of excitation energies [1, 2]. However, to focus on the role of symmetry, we avoid such situation by including only single species of pigment molecules in the model. In addition, we also exclude core molecules, which usually play a role to trap excitation energy, from the model system (we hereafter refer to the portion of dendrimer without core molecules as a dendron) in order to distinguish the light-harvesting ability of dendron itself from that of core molecules.

4.2.1   The Frenkel exciton Hamiltonian

The Frenkel exciton Hamiltonian is a model Hamiltonian that is frequently used for modeling the quantum dynamics of EET in molecular aggregates. Under the assumption that the model system is composed of n pigment molecules and each pigment molecule can be considered two-state system, the Frenkel exciton Hamiltonian is defined as follows,

$$\hat{H} = \sum_i E_i \hat{a}_i^\dagger \hat{a}_i + \sum_{i,j \ (i \neq j)} J_{ij} \hat{a}_i^\dagger \hat{a}_j \ , \tag{4.1}$$

where $\hat{a}_i^\dagger$ ($\hat{a}_i$) is the creation (annihilation) operator for excitation of the ith molecule, E_i is the excitation energy of the ith molecule and J_{ij} is the interaction energy between the ith and the jth molecules, which satisfies $J_{ij} = J_{ji}^*$. For simplicity, we refer to pigment molecules as sites hereafter.

The number of states in the system defined by Eq. (4.1) is 2^n. However, in many case of EET in molecular aggregates, it is not necessary to consider all these states. In this chapter, we adopt a Hamiltonian that acts only on one-exciton states. One-exciton state $|i\rangle$ ($= \hat{a}_i^\dagger |0\rangle$) is the state where only the ith site is excited and other sites are in their ground state. The restricted Hamiltonian becomes

$$\hat{H} = \sum_i E_i |i\rangle\langle i| + \sum_{i,j \ (i \neq j)} J_{ij} |i\rangle\langle j| \ . \tag{4.2}$$

We use this restricted Hamiltonian in the following discussion.

In this chapter, we visualize the Frenkel exciton Hamiltonian by a graph composed of nodes and edges in the following way. Node i in a graph corresponds to the ith site in the system under consideration and edge between the node i and j indicates that there is non-zero interaction energy J_{ij} between the corresponding two sites. Fig. 4.1 is an example of graph representing a Frenkel exciton Hamiltonian. The system represented
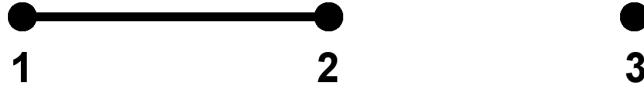
Figure 4.1: An example of graphs composed of nodes and edges on which a Frenkel exciton Hamiltonian is defined. Nodes represent the states of the system. Edges represent non-zero interactions between corresponding two sites.

by this graph is composed of three sites. The one-exciton states to be consider are $|1\rangle, |2\rangle, |3\rangle$. The non-zero interaction energy exists only between $|1\rangle$ and $|2\rangle$.

4.2.2 Model Hamiltonian for EET in light-harvesting dendrimers

Next, we define a Frenkel exciton Hamiltonian modeling EET in light-harvesting dendrimers. The model Hamiltonian used in this chapter is visualized by a dendritic graph. Fig. 4.2 shows only the configuration of nodes in the dendritic graph for the model Hamiltonian (edges will be added to the graph in the setting of interaction afterward). This dendritic graph has four generations (layers of sites). Note that this graph models only dendron and does not contain nodes corresponding to core molecules, which are usually linked to the site in the first generation and capture excitation energy in the process of EET. In general, core molecules have lower excitation energy than other molecules consisting of light-harvesting dendrimers and, thus, they also possess the light-harvesting ability. However, the aim of this chapter is to investigate a possibility that dendrons themselves have their own light-harvesting ability. Therefore, we exclude core molecules from the model system in order to distinguish the ability of dendron from that of core molecules.

Next, we give an index to each nodes in the graph in the same way as Chapter 3. Nodes in the lth generation are expressed by l integers $\mathbf{b} = (b_1, b_2, \cdots, b_l)$. We denote the set of indexes in the lth generation as B_l. Indexes are defined recursively. In the first place, the index of the node in the first generation in Fig. 4.2 is set to be (1). Then, the nodes in the lth generation linked to the node in the $(l-1)$th generation $\mathbf{b}'$ $(\in B_{l-1})$ by the b_lth branch emerging from $\mathbf{b}'$ is represented by $\mathbf{b}$ as

$$\mathbf{b} = (\mathbf{b}', b_l) . \tag{4.3}$$

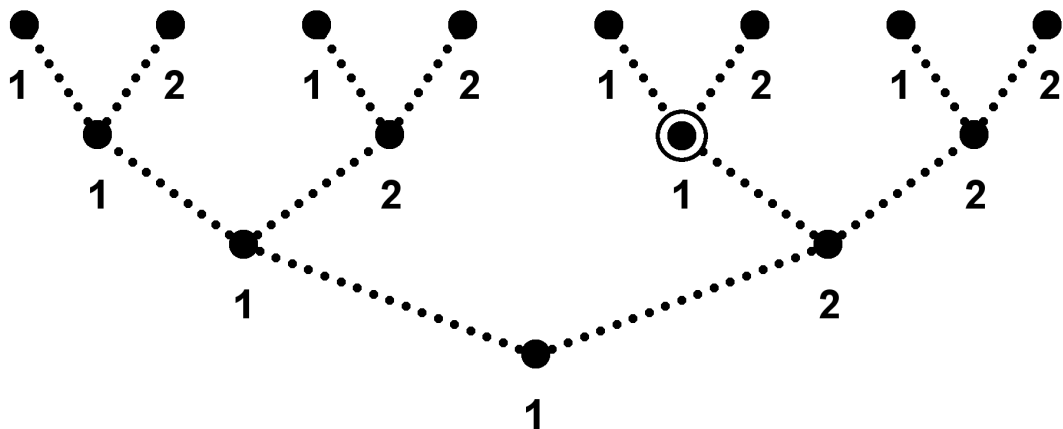For example, the circled node in Fig. 4.2 is represented by $(1, 2, 1)$.

Figure 4.2: Configuration of nodes of the dendritic graph for the model system. Index of a node is given by sequentially arranging the numbers attached to ancestor nodes and the node itself. For example, the index of the circled node is $(1, 2, 1)$.

Magnitude of the matrix elements are set so that modeled light-harvesting dendrimers are composed of single species of pigment molecules. This setting excludes all the features but the structure of symmetry from the model system. Firstly, all excitation energies E are set to be identical. For simplicity, we assume $E = 0$. Then, all inter-generation interaction energies (corresponding to the edges linking two adjacent generations) and all intra-generation interaction energies (corresponding to the edges linking two nodes in a same generation) are set to be $-J$ and αJ, respectively. These matrix elements are visualized in Fig. 4.3. Black nodes mean that the excitation energies of the node is 0. Black oblique edges and gray horizontal edges mean that corresponding interactions are $-J$ and αJ, respectively. The model Hamiltonian to be consider $\hat{H}$ can be also written in a matrix form as

$$\hat{H} = J\mathbf{A} \ , \tag{4.4}$$

where $\mathbf{A}$ is a matrix with following matrix elements

$$A_{\mathbf{b},\mathbf{b'}} = \begin{cases} -1 & \text{(inter-generation interaction)} \\ \alpha & \text{(intra-generation interaction)} \\ 0 & \text{(otherwise)} \end{cases} . \tag{4.5}$$

In this chapter, we mainly consider the case where both J and α are positive. These signs of interaction energies are consistent with the case where the interaction energies
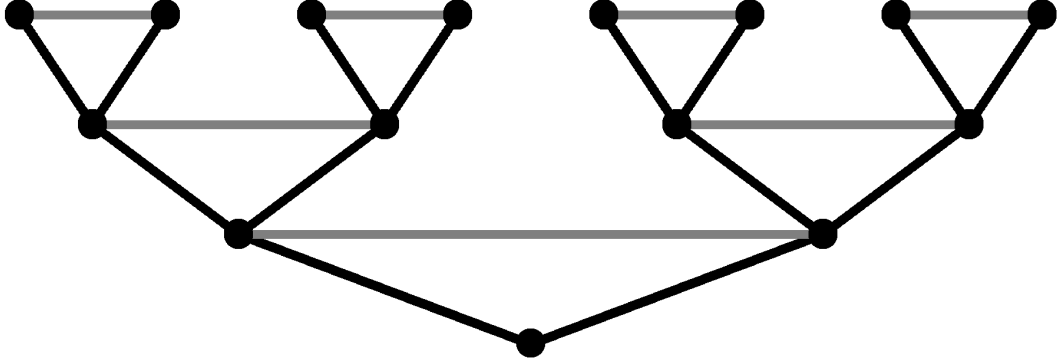
Figure 4.3: Connection of interaction of the model system. Black oblique edges represent inter-generation interactions with their magnitude $-J$. Gray horizontal edges represent intra-generation interactions with their magnitude αJ.

are determined by the dipole-dipole interaction and transition dipole moment of each site heads to outer generations.

4.3 Unidirectional energy gradient in light-harvesting dendrimers

One of possible ways to investigate the correlation between energy level and spatial location of eignestates of the model Hamiltonian is explicitly determining and observing eigenvalues and eigenstates of Eqs. (4.4) and (4.5). However, it is difficult to discuss the energy gradient quantitatively based only this observation. We therefore investigate the energy gradient in more quantitative way.

In this section, we examine the energy distribution at a thermal equilibrium state of the model system. We define the population of excitation energy of the lth generation $P_l(\beta J)$ by

$$P_l(\beta J) = \sum_{\mathbf{b} \in B_l} \langle \mathbf{b} | \rho_{\mathrm{eq}}(\beta J) | \mathbf{b} \rangle \,, \tag{4.6}$$

where $\rho_{\mathrm{eq}}(\beta J)$ is the density matrix of the thermal equilibrium state

$$
\begin{aligned}
\rho_{\mathrm{eq}}(\beta J) &= e^{-\beta \hat{H}} / \mathrm{Tr}[e^{-\beta \hat{H}}] \\
&= e^{-\beta J \mathbf{A}} / \mathrm{Tr}[e^{-\beta J \mathbf{A}}] \,.
\end{aligned}
\tag{4.7}
$$

At a thermal equilibrium state, the population generally tends to gather at eigenstates of lower eigenenergies. Therefore, if the population gathers at inner generations, it is found that eigenstates of lower energies locate mainly around inner generations and the energy gradient descending toward inner generation is formed. In this way, we can investigate the correlation between energy levels and spatial location of many eignestates at once and quantitatively. In this chapter, $P_l(\beta J)$ are calculated numerically. We calculate $P_l(\beta J)$ by diagonalizing the model Hamiltonian.

In addition, in order to estimate which generation strongly collects the population, we compare the energy distribution at the thermal equilibrium state P_l ($l = 1, 2, 3, 4$) with that obtained under the assumption that excitation energy is transferred by stochastic hopping. Since the present model system is defined so that the system models light-harvesting dendrimers composed of single species of pigment molecules, the magnitude of matrix elements in Eq. (4.5) does not vary by generation. Therefore, if stochastic hopping picture is applied, the population of excitation energy is distributed equally to each site. In this case, the population of excitation energy of each generation P_l^{hom} ($l = 1, 2, 3, 4$) becomes proportional to the number of sites in the corresponding generation; to write explicitly,

$$P_l^{\mathrm{hom}} = 2^{l-1} / \sum_{k=1}^{4} 2^{k-1} . \tag{4.8}$$

We refer to this distribution as the homogeneous distribution.

Fig. 4.4 (a)-(c) show parameter kT/J ($= 1/\beta J$) dependency of P_l at the intra-generation $\alpha = 0.0, 0.5, 1.0$, respectively. Red, green, blue and purple line correspond to the population from the first to the fourth generation, respectively. Note that right sides of these graphs correspond to the case with small value of the interaction energy J because J is in the denominator of the parameter kT/J. Fig. 4.4 (d)-(e) show the ratio $P_l(\beta J)/P_l^{\mathrm{hom}}$ in the case $\alpha = 0.0, 0.5, 1.0$, respectively. $P_l(\beta J)/P_l^{\mathrm{hom}}$ means how each generation collects the population of excitation energy compared with the homogeneous energy distribution by stochastic hopping. Therefore, if this value is bigger than 1, it can be said that the corresponding generation strongly collects excitation energy. It should be noted that any ratio in any case converges to 1 in the limit of $J \to 0$. This is because, in the case of the interaction energy is small, every sites in the system can be regarded to be almost independent of each other and the population is distributed to each site equivalently.

The most remarkable and common feature among Fig. 4.4 (a)-(c) is that the population of the outermost (fourth) generation sharply drops as the interaction energy J increase (see graphs from right to left). Correspondingly, the populations of other inner generations increase except the first generation in the case $\alpha = 1.0$ (Fig. 4.4 (c)). This tendency is obvious especially when $kT/J < 1$. According to Fig. 4.4 (d)-(e), it is
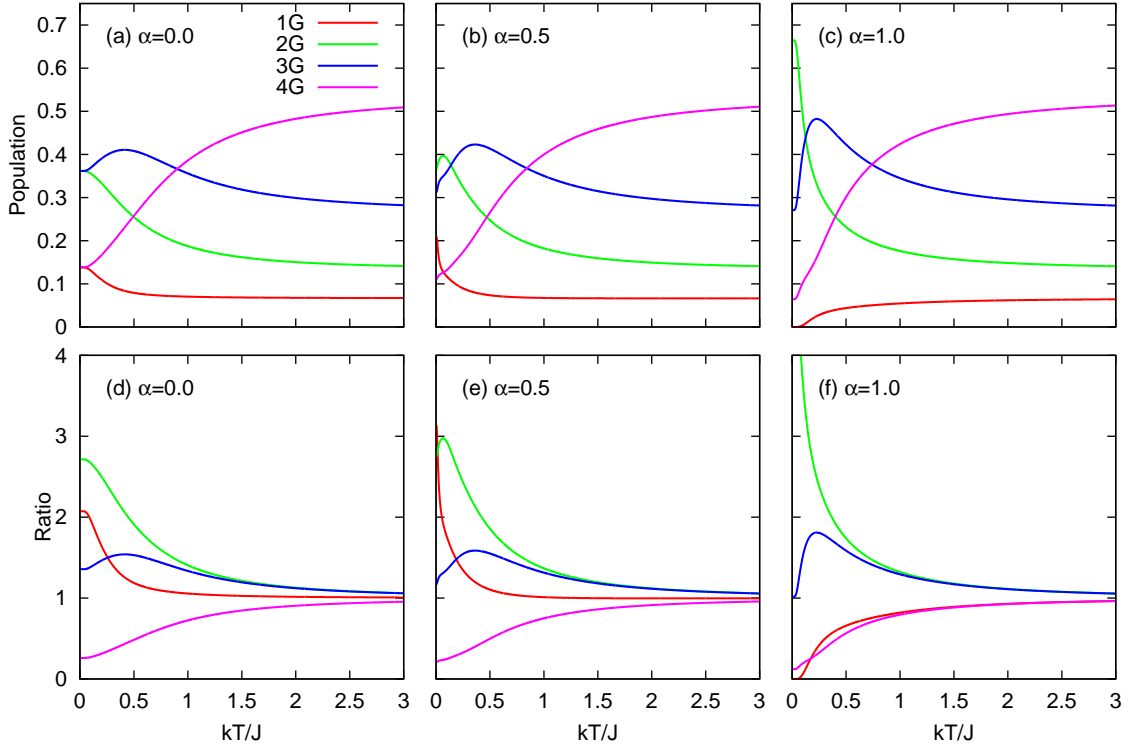
Figure 4.4: Parameter kT/J $(= 1/\beta J)$ dependency of the population $P_l(\beta J)$ by generations at the thermal equilibrium state (a)-(c) and that of the ratio $P_l(\beta J)/P_l^{\mathrm{rnd}}$ (d)-(f). (a) and (d) correspond to the case $\alpha = 0.0$, (b) and (e) is the case $\alpha = 0.5$ and (c) and (f) is the case $\alpha = 1.0$. In all graphs, red, green, blue and purple lines correspond to the population or ratio from the first to the fourth generation, respectively.

found that the second generation strongly collects excitation energy in all cases. The second generation collects excitation energy 2 to 3 times more than the homogeneous distribution. The first generation also shows remarkable ability to collect energy in the case $\alpha = 0.0$ and 0.5.

As a result of these observations, it is found that the model system has the ability to collect excitation energy at inner (first and second) generations. As is mentioned above, this inclination of the distribution of the population implies that there is the energy gradient descending from outer generations to inner generations. We next analyze the reason in the next section.

4.4 Mechanism for the light-harvesting ability

In this section, we investigate the mechanism of the light-harvesting ability of the model system, which is shown numerically in the previous section. For this purpose, we utilize the linear chain (LC) decomposition, which is the theory that simplifies linear operators including quantum Hamiltonians defined on dendritic graphs. LC decomposition can equivalently transform a linear operator on a dendritic graph into that on a set of small one-dimensional graphs with the help of the symmetry of the dendritic graph. This section firstly reviews the LC decomposition. Then, we propose two mechanism of the light-harvesting ability of the model system.

4.4.1 Linear chain decomposition

Overview of LC decomposition

Here we briefly review the LC decomposition. In Sec. 4.2, we defined the Frenkel exciton Hamiltonian on a dendritic graph by Eqs. (4.2) and (4.5) (or Fig. 4.3). The basis of the Hamiltonian is given by a set of one-exciton states of each site

$$\{|\mathbf{b}\rangle | \mathbf{b} \in B_l, l = 1, 2, 3, 4\} . \tag{4.9}$$

LC decomposition is realized by changing this basis (creating new states by superposition of these states). This change of basis is carried out within each generation; in other words, new states belonging to a given generation are represented by superposition of one-exciton states in this generation. Note that, even though each of the new states is delocalized within a generation, it still keep the property of generation to which the new state belongs.

We here show the result of LC decomposition first, before details of the change of basis are reviewed. After the change of basis for LC decomposition, the result of LC decomposition is clearly visualized by drawing new graph. In this new graph, nodes
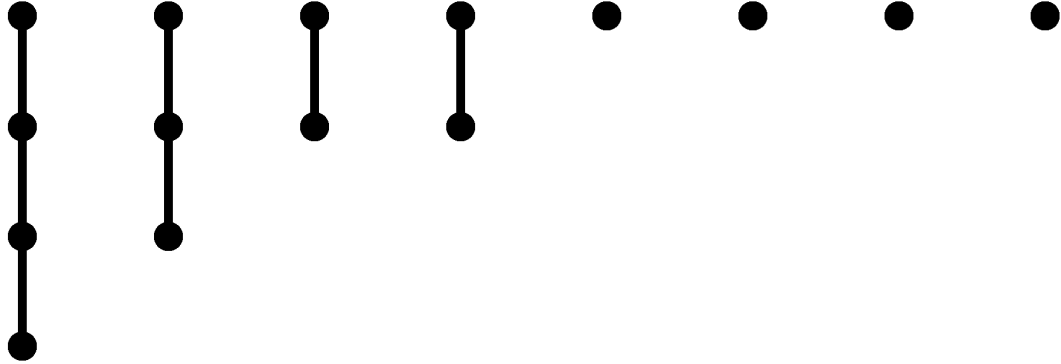
Figure 4.5: New graph visualizing the model Hamiltonian after LC decomposition. Horizontal level represents the generation of the modeled dendrimer.

correspond to the newly obtained states and edges correspond to non-zero interactions between two of the new states. The new graph for LC decomposition results in a set of one-dimensionally-linked graphs like Fig. 4.5 (horizontal level of Fig. 4.5 corresponds to generation of the dendrimer to which each node belongs). This graph means that the original system defined on the dendritic graph is equivalent to a set of one-dimensional systems. Compared with the original graph Fig. 4.3, this LC decomposed graph is far more simplified. This simplification is utilized elsewhere [26–28] to understand properties of various dendritic systems. Note that the nodes in the new graph no longer represent the spatial configuration of pigment molecules in the modeled dendrimer, because each of the new states is a superposition of original one-exciton states. However, the new graph remains useful to visualize the connectivity of non-zero interaction among the new states.

The change of basis for LC decomposition is done utilizing the symmetry of dendritic systems. General theory of LC decomposition is presented in Chapter 3 based on the group theory. In this chapter, we only apply the theory to the model Hamiltonian Eqs. (4.4) and (4.5).

Construction of the new basis

Before the construction of the new basis for the present model system, we define a procedure that creates a new state in the $(l + 1)$th generation from a given state in the lth generation. The construction of the new basis is achieved with the help of the

following procedure.

Assume that $|X_l\rangle$ is a superposition of one-exciton states in the lth generation with coefficients $c_\mathbf{b} \in B_l$,

$$|X_l\rangle = \sum_{\mathbf{b} \in B_l} c_\mathbf{b} |\mathbf{b}\rangle \ . \tag{4.10}$$

The procedure to create a new state in the $(l+1)$th generation $|X_{l+1}\rangle$ is given by replacing $|\mathbf{b}\rangle$ with $2^{-1/2}(|\mathbf{b}, 1\rangle + |\mathbf{b}, 2\rangle)$, where $2^{-1/2}$ is the normalized coefficient. Thus, $|X_{l+1}\rangle$ is represented as

$$|X_{l+1}\rangle = 2^{-1/2} \sum_{\mathbf{b} \in B_l} c_\mathbf{b}(|\mathbf{b}, 1\rangle + |\mathbf{b}, 2\rangle) \ . \tag{4.11}$$

Note that the node $(\mathbf{b}, 1)$ and $(\mathbf{b}, 2)$ are the child nodes of $\mathbf{b}$ in the original dendritic graph and they belong to the $(l+1)$th generation. In this procedure, the one-exciton states of these child nodes are summed with equal coefficients. Therefore, $|X_{l+1}\rangle$ shows same transformation as $|X_l\rangle$ under symmetry operations of the system like inversions of a portion of the dendritic graph. In other words, $|X_{l+1}\rangle$ inherits the symmetry of $|X_l\rangle$ by this procedure.

The new states for LC decomposition are constructed sequentially with the symmetry-inheriting procedure defined above. We start from the one-exciton state in the first generation $|1\rangle$. This state is also one of the new states and we rename $|1\rangle$ as $|A_1\rangle$. Next, we continue to construct other new states by applying the procedure to $|A_1\rangle$ repeatedly until a state in the outermost generation is obtained. Then, we obtain a set of new states $|A_l\rangle$ ($l = 1, 2, 3, 4$), which can be written explicitly as

$$|A_l\rangle = 2^{-(l-1)/2} \sum_{\mathbf{b} \in B_l} |\mathbf{b}\rangle \ . \tag{4.12}$$

Note that these four states have same symmetry under the symmetry operation of the system as a result of the symmetry-inheriting procedure. Therefore, interaction among them does not vanish and, in the new graph, the corresponding nodes are linked by edges. The series of $|A_l\rangle$ ($l = 1, 2, 3, 4$) are visualized in Fig. 4.5 as the longest linear chain.

In the same way, we construct new states starting from the following states repre-

sented as

$$|A_1\rangle = |1\rangle , \tag{4.13a}$$

$$|B_2\rangle = 2^{-1/2}(|1,1\rangle - |1,2\rangle) , \tag{4.13b}$$

$$|C_3\rangle = 2^{-1/2}(|1,1,1\rangle - |1,1,2\rangle) , \tag{4.13c}$$

$$|D_3\rangle = 2^{-1/2}(|1,2,1\rangle - |1,2,2\rangle) , \tag{4.13d}$$

$$|E_4\rangle = 2^{-1/2}(|1,1,1,1\rangle - |1,1,1,2\rangle) , \tag{4.13e}$$

$$|F_4\rangle = 2^{-1/2}(|1,1,2,1\rangle - |1,1,2,2\rangle) , \tag{4.13f}$$

$$|G_4\rangle = 2^{-1/2}(|1,2,1,1\rangle - |1,2,1,2\rangle) , \tag{4.13g}$$

$$|H_4\rangle = 2^{-1/2}(|1,2,2,1\rangle - |1,2,2,2\rangle) . \tag{4.13h}$$

By applying the symmetry-inheriting procedure repeatedly for each state in Eqs. (4.13), we obtain a series of new states linked one-dimensionally by non-zero interactions corresponding to the initial state in Eqs. (4.13). These series of new states are visualized in Fig. 4.5 and correspond to the linear chains from left to right. Note that the states in Eqs. (4.13) have different symmetry from each other (to be precise, they are the basis vectors in different irreducible representations in terms of the group theory). Therefore, interaction between any two series of states vanishes and the new graph is decomposed into the small one-dimensional graphs.

Matrix elements in the picture of LC decomposition

We then investigate the matrix elements. For example, we consider the series of the new states $\{|B_2\rangle, |B_3\rangle, |B_4\rangle\}$. Fig. 4.6 represents signs of the superposition coefficients of one-exciton states of these new states. Red and blue circles means that the signs of the coefficients are positive and negative, respectively. Dotted lines distinguish these new states each other. According to the actual calculation, it is found that (i) the inter-generation interactions among these new states become $-\sqrt{2}J$:

$$\langle B_l|\hat{H}|B_{l+1}\rangle = -\sqrt{2}J \quad (l = 2,3) , \tag{4.14}$$

and (ii) the intra-generation interactions in the original Hamiltonian αJ appear in the site energies (diagonal elements) in the LC decomposed Hamiltonian. The magnitude of these site energies are determined by the following rule: if the signs of the coefficients of the both ends of intra-generation interaction in the original dendritic graph are identical (opposite), the site energy in the new Hamiltonian becomes αJ $(-\alpha J)$. According to Fig. 4.6, the signs of the both ends of intra-generation interaction (gray horizontal edge) are opposite in $|B_2\rangle$ and are identical in other states. Therefore, the site energies
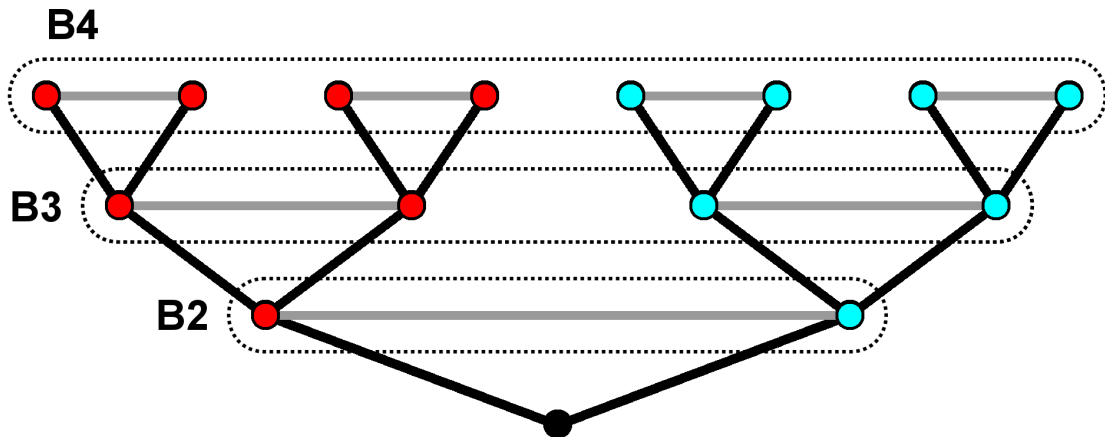
Figure 4.6: Signs of the superposition coefficients of original one-exciton states of $|B_2\rangle, |B_3\rangle$ and $|B_4\rangle$. Red and blue nodes means that corresponding coefficients are positive and negative, respectively.

of these states are summarized as

$$\langle B_2|\hat{H}|B_2\rangle = -\alpha J , \qquad (4.15\text{a})$$

$$\langle B_3|\hat{H}|B_3\rangle = \alpha J , \qquad (4.15\text{b})$$

$$\langle B_4|\hat{H}|B_4\rangle = \alpha J . \qquad (4.15\text{c})$$

This rule of the new matrix elements is also true for other series of new states consisting of linear chains. Thus, all non-zero inter-generation interactions are $-\sqrt{2}J$. The site energy of the innermost generation is $-\alpha J$ and those of other outer generations are αJ.

However, there is one exception in the longest linear chain. The site energy of the innermost generation of the longest linear chain remains 0 because there is no intra-generation in the original Hamiltonian in the first generation. Fig. 4.7 summarizes the result. All edges in Fig. 4.7 represent $-\sqrt{2}J$ and the site energies of the red, blue and black nodes are $\alpha J, -\alpha J$ and 0, respectively.

4.4.2 Mechanisms

Next, we propose two mechanisms of the light-harvesting ability of the model system in the picture of LC decomposition. These mechanisms explain why the eigenstates of lower energy tend to locate at inner generations and energy gradient is formed. One
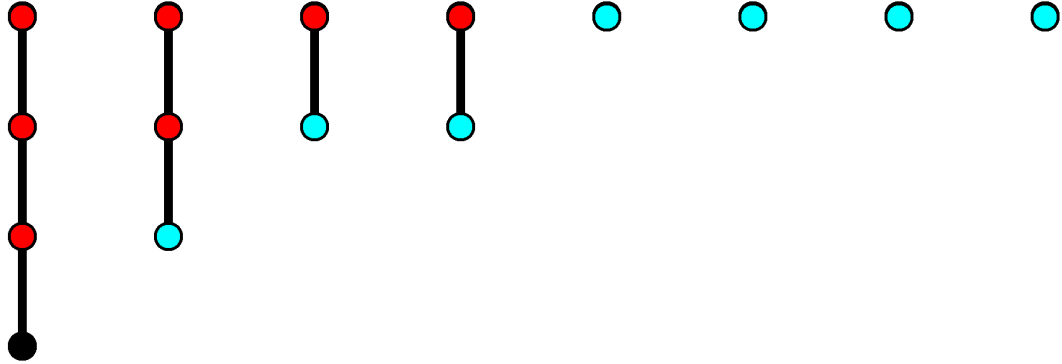
Figure 4.7: Matrix elements in the picture of LC decomposition. Red, blue and black nodes means that corresponding site energies (diagonal elements) are $\alpha J, -\alpha J$ and 0, respectively. In addition, all edges represents non-zero interactions with their magnitude $-\sqrt{2}J$.

of the mechanisms shows that energy gradient is formed with in each linear chain and another mechanism shows that energy gradient is also formed among linear chains.

Intra-chain energy gradient

According to the previous discussion about matrix elements in the picture of LC decomposition, it was found that the site energy of the innermost generation is $-\alpha J$ (or 0) and those of other outer generations are αJ in each linear chain as is shown in Fig. 4.7. If $\alpha J > 0$, the site energy of the innermost generation becomes lower than others. Consequently, an eigenstate of lower energy is formed around the innermost generation in each linear chain. In addition, other eigenstates, which have higher energy, are located at outer generations in the corresponding linear chain. This means that the energy gradient descending toward inner generations is formed in each linear chain. Note that, in the case $\alpha J < 0$, magnitude relation of eigenenergies is reversed and the energy gradient in this case prohibits excitation energy from gathering at inner generation.

Inter-chain energy gradient

According to Fig. 4.4 (a) and (d), although there is no mechanism of the intra-chain energy gradient in this case (because $\alpha = 0$), excitation energy gathers at inner generations when kT/J is small. This suggests another mechanism for the light-harvesting

ability.

We propose a mechanism creating inter-chain energy gradient. For simplicity, we consider the case $\alpha = 0$. In this case, all site energies in the picture of LC decomposition become 0 and all inter-generation interactions become $-\sqrt{2}J$. Therefore, the lowest eigenenergy in the linear chain whose length is l, $\tilde{E}_l$, is given by

$$\tilde{E}_l = -2\sqrt{2}|J|\cos\left(\frac{\pi}{l+1}\right) . \tag{4.16}$$

Then, it is found that the lowest eigenenergy in a linear chain is lowered as the length of the linear chain increases.

Next, we pay attention to the spatial location of linear chains. According to Fig. 4.5, many short linear chains are localized at outer generations while longer linear chains reach inner generations. Therefore, by combining these aspects of the energy level and the spatial location, it is found that energy gradient among linear chains is formed because short linear chains with higher energies are localized at outer generations and long linear chains with lower energies reach inner generations.

4.4.3 Discussion

Before closing this section, we again discuss the result of Sec. 4.3 (Fig. 4.4) in detail from the view point of the two mechanisms proposed above.

Firstly, as is mentioned above, in the case $\alpha = 0$ (Fig. 4.4 (a) and (d)), this result is attributed to the mechanism of the inter-chain energy gradient. It is noteworthy that this mechanism work well even without the intra-chain energy gradient.

Fig. 4.4 (b) and (e) show similar result to (a) and (d). This fact suggests that the main contribution for this result is the inter-chain energy gradient rather than the intra-chain energy gradient. The intra-chain energy gradient in this case enhances the light-harvesting ability of the first and second generations when kT/J is less than about 0.5.

On the other hand, in the case $\alpha = 1$ (Fig. 4.4 (c) and (f)), the population of the first generation almost vanishes as kT/J approaches 0. This is due to the weak intra-chain energy gradient in the longest chain. As is remarked above, the site energy of the first generation of the longest linear chain is 0 because of the lack of intra-generation interaction in the original dendritic system while site energies of the innermost generations of other linear chains are $-\alpha J$. Therefore, the intra-chain energy gradient is weak in the longest linear chain. In the former two case $\alpha = 0, 0.5$, the inter-chain energy gradient is dominant and this weakness of intra-chain energy gradient is less important. However, if α becomes too large, the contribution of the intra-chain energy gradient exceeds the inter-chain energy gradient. In this case, the ground state of the total system is switched from the eigenstate of the lowest energy in the longest linear chain to that

in the second longest linear chains. Consequently, the population of the first generation vanishes as kT/J approaches 0 because the second longest linear chain does not reach the first generation.

The mechanisms of both inter and intra-chain energy gradient generally give the system to the light-harvesting ability. However, too much intra-generation interaction may cause the energy barrier between the first and the second generations because of the weaker intra-chain energy gradient in the longest linear chain.

4.5   Concluding remarks

In this chapter, we have shown that the structure of energy gradient is formed in the model system for EET in light-harvesting dendrimers. For this purpose, we have investigated the energy distribution at a thermal equilibrium state of the model system and have compared that with the homogeneous energy distribution, which is obtained under the assumption of stochastic hopping transfer. Then, we have found that the population of excitation energy gathers at inner generations and have concluded that energy gradient is formed in the model system and causes the inclination of population. Note that the formation of the energy gradient is of importance in the sense that the energy gradient possibly cause the unidirectional energy flow from outer generations to inner generations and this unidirectional energy flow may enhance EET in light-harvesting dendrimers.

We have also proposed the two mechanisms that create energy gradient based on the picture of LC decomposition, general theory of which is presented in Chapter 3. Utilizing the symmetry of dendrimer's repetitively branched structure, the theory of LC decomposition equivalently transforms the model system on a dendritic graph into the system on a set of one-dimensional graphs, or linear chains. In the picture of LC decomposition, we have found that energy gradient is formed both in each of the linear chains and among these linear chains, which we call as the mechanisms of the intra-chain and the inter-chain energy gradient.

We here emphasize that the energy gradient can be attributed to the symmetry of dendrimers because LC decomposition cannot be realized without the symmetry. Owing to the repetitively branched structure, the symmetry-inheriting procedure can be defined as Eq. (4.11) and this procedure realize the LC decomposition. Therefore, it is concluded that the energy gradient formed in the model system is originated from the symmetry of the system. This means that the symmetry of light-harvesting dendrimers may have a role to enhance EET in the dendrimers.

Reference

[1] W.-S. Li and T. Aida, Chem. Rev. **109**, 6047 (2009).

[2] D. Astruc, E. Boisselier, and C. Ornelas, Chem. Rev. **110**, 1857 (2010).

[3] C. Devadoss, P. Bharathi, and J. S. Moore, J. Am. Chem. Soc. **118**, 9635 (1996).

[4] D.-L. Jiang and T. Aida, J. Am. Chem. Soc. **120**, 10895 (1998).

[5] M. Kimura, T. Shiba, T. Muto, K. Hanabusa, and H. Shirai, Macromolecules **32**, 8237 (1999).

[6] S. Tretiak, V. Chernyak, and S. Mukamel, J. Phys. Chem. B **102**, 3310 (1998).

[7] K. Harigaya, Phys. Chem. Chem. Phys. **1**, 1687 (1999).

[8] T. Minami, S. Tretiak, V. Chernyak, and S. Mukamel, J. Lumin. **87-89**, 115 (2000).

[9] M. Nakano, M. Takahata, H. Fujita, S. Kiribayashi, and K. Yamaguchi, Chem. Phys. Lett. **323**, 249 (2000).

[10] J. C. Kirkwood, C. Scheurer, V. Chernyak, and S. Mukamel, J. Chem. Phys. **114**, 2419 (2001).

[11] M. Martín-Delgado, J. Rodriguez-Laguna, and G. Sierra, Phys. Rev. B **65**, 155116 (2002).

[12] M. Takahata, M. Nakano, H. Fujita, and K. Yamaguchi, Chem. Phys. Lett. **363**, 422 (2002).

[13] O. Varnavski et al., J. Chem. Phys. **116**, 8893 (2002).

[14] J. L. Bentz, F. Niroomand Hosseini, and J. J. Kozak, Chem. Phys. Lett. **370**, 319 (2003).

[15] D. Rana and G. Gangopadhyay, J. Chem. Phys. **118**, 434 (2003).

[16] T. Tada, D. Nozaki, M. Kondo, and K. Yoshizawa, J. Phys. Chem. B **107**, 14204 (2003).

[17] D.-J. Heijs, V. a. Malyshev, and J. Knoester, J. Chem. Phys. **121**, 4884 (2004).

[18] M. Nakano et al., J. Chem. Phys. **120**, 2359 (2004).

[19] W. Ortiz, B. P. Krueger, V. D. Kleiman, J. L. Krause, and A. E. Roitberg, J. Phys. Chem. B **109**, 11512 (2005).

[20] S. Fernandez-Alberti, V. D. Kleiman, S. Tretiak, and A. E. Roitberg, J. Phys. Chem. A **113**, 7535 (2009).

[21] J. L. Palma et al., J. Phys. Chem. C **114**, 20702 (2010).

[22] S. Fernandez-Alberti, A. E. Roitberg, V. D. Kleiman, T. Nelson, and S. Tretiak, J. Chem. Phys. **137**, 22A526 (2012).

[23] V. Pouthier, J. Chem. Phys. **139**, 234111 (2013).

[24] V. Pouthier, Phys. Rev. E **90**, 022818 (2014).

[25] L. Valkunas, D. Abramavicius, and T. Mančal, *Molecular Excitation Dynamics and Relaxation*, Wiley, Weinheim, 2013.

[26] C. Cai and Z. Y. Chen, Macromolecules **30**, 5104 (1997).

[27] M. Galiceanu, J. Phys. A Math. Theor. **43**, 305002 (2010).

[28] M. Galiceanu and A. Blumen, J. Chem. Phys. **127**, 134904 (2007).

Chapter 5

General conclusion

This thesis has studied the two subjects: (I) quantum dynamics of nuclei (in Chapter 2) and (II) excitation energy transfer in light-harvesting dendrimers (in Chapters 3 and 4). In these studies, the theories for these subjects, semiclassical propagators for the subject (I) and linear chain (LC) decomposition for the subject (II), have been developed. This thesis has also studied the role of morphology of light-harvesting dendrimers in their functions in terms of excitation energy transfer (in Chapter 4). We have applied the theory of LC decomposition to this study. We here summarize the achievements in this thesis below.

In Chapter 2, we have shown the systematic derivation of various semiclassical propagators, which have been derived originally in independent and complicated ways. For the present systematic derivation, we have generalized one of the representations of quantum dynamics known as the coherent-state path integral by adding arbitrary parameters to the coherent-state path integral. Then, we have shown that, after evaluating the integral approximately, various semiclassical propagators are derived by choosing the arbitrary parameters properly.

What is important in Chapter 2 is the fact that a common theoretical ground among semiclassical propagators has been established owing to the present systematic derivation. The unified framework provided by this systematic derivation may give deeper understanding of semiclassical propagators. As an example, we have studied the accuracy of a series of Herman-Kluk propagators, which are the most popular semiclassical propagators, and have explained the result of the numerical calculations clearly based on the unified framework.

In Chapter 3, we have generalized the theory of LC decomposition, which equivalently transforms a linear operator defined on a dendritic graph into that defined on a set of one-dimensional graphs like linear chains. We have clarified that a dendritic system becomes LC decomposable if the linear operator of the system is invariant under the symmetry operations of the system (and the symmetry of the system satisfies the

condition described in Chapter 3).

In the discussion about LC decomposition, we have proposed the general class of dendritic graphs and the general symmetry groups for these graphs. In addition, we have not restricted the type of linear operators in the discussion. As a result, the class of LC decomposable systems has been expanded in the three aspect: the class of dendritic graphs, the class of symmetry groups and the type of linear operators.

In Chapter 4, we have shown a possibility that the ability to collect excitation energy at inner generations of light-harvesting dendrimers arises from their symmetry. For this purpose, we have set the model Hamiltonian that only extracts the feature of the symmetry of dendrimers and have numerically shown that the model system has the ability to collect energy. If there is no interaction among pigment molecules, excitation energy is equally distributed to each pigment molecule. On the other hand, the present numerical calculations have revealed that excitation energy can be collected at inner generation by only a dendritic network of interaction.

In addition, we have examined the result in detail in terms of the role of morphology of dendrimers in their functions. We have attributed the ability to collect energy to the symmetry of dendrimers by proposing the two mechanisms based on the theory of LC decomposition. In these mechanisms, it has been shown that the structure of energy gradient is formed both in each one-dimensional system of LC decomposition and among these one-dimensional systems. The fact that the explanation based on LC decomposition works well indicates that focusing on the symmetry is of great importance during studies on properties of dendrimers.

List of publications

[1] Shin-ichi Koda and Kazuo Takatsuka, Physical Review A **83**, 032117 (2011).
A generalization of the coherent state path integrals and systematic derivation of semi-classical propagators

[2] Shin-ichi Koda and Kazuo Takatsuka, in preparation for submission.
Equivalence between a generalized dendritic network and a set of small one-dimensional networks as a ground of linear dynamics

[3] Shin-ichi Koda and Kazuo Takatsuka, in preparation for submission.
Symmetry-origin unidirectional energy gradient in light-harvesting dendrimers

Acknowledgements

This thesis is the summary of my study at the Graduate School of Arts and Sciences, University of Tokyo from 2009 to 2014, under the guidance of Prof. Kazuo Takatsuka. I am sincerely grateful to Prof. Takatsuka for his invitation to theoretical molecular science, lesson on science and creation of the best environment for my study.

I am grateful to Dr. Satoshi Takahashi for his management for the environment of Takatsuka laboratory. I am greatful to Dr. Yasuki Arasaki for his management for the computer system of Takatsuka laboratory. I am greatful to Dr. Takehiro Yonehara for a lot of suggestions on my study. I am greatful to Mrs. Yukiko Kosaka for her support for all the members of Takatsuka laboratory. I also wish to acknowledge all the members of Takatsuka laboratory for their efforts to keep the research environment comfortable.

I am grateful to Kiyoko Shingai for her encouragement. Finally, I wish to express my gratitude to my parents for their long-term support.

<div align="right">

Tokyo, Japan, December 2014

Shin-ichi Koda

</div>